THE JOURNAL OF CHEMICAL PHYSICS

VOLUME 11 NUMBER 2

FEBRUARY, 1943

Published by the

AMERICAN INSTITUTE OF PHYSICS

Incorporated

LANCASTER, PA., AND NEW YORK, N. Y.

THE JOURNAL OF CHEMICAL PHYSICS

ADVISORY EDITORIAL BOARD

R. T. BIRGE
A. H. COMPTON
JAMES FRANCK
IRVING LANGMUIR
JOHN T. TATE
HAROLD C. UREY

BOARD OF EDITORS

JOSEPH E. MAYER, *Editor*

Associate Editors

Term ending December 31, 1943

SIMON FREED
MAURICE L. HUGGINS
J. G. KIRKWOOD
GEORGE SCATCHARD
J. H. VAN VLECK

Term ending December 31, 1944

CHARLES O. BECKMAN
BRYCE L. CRAWFORD, JR.
P. DEBYE
DAVID HARKER
FRANK H. WESTHEIMER

Term ending December 31, 1945

L. O. BROCKWAY
RONALD W. GURNEY
KENNETH S. PITZER
ALFRED L. SKLAR
E. W. R. STEACIE
HUGH S. TAYLOR

THE JOURNAL OF CHEMICAL PHYSICS is published monthly by the American Institute of Physics. Its purpose is to bridge a gap between journals of physics and journals of chemistry. The artificial boundary between physics and chemistry has now been in actual fact completely eliminated, and a large and active group is engaged in research which is as much the one as the other. It is to this group that the Journal is rendering its principal service and makes its greatest appeal, both as a prompt and efficient medium for publication of research and as a convenient and carefully edited assemblage of pertinent information.

Manuscripts for publication should be submitted to Joseph E. Mayer, Havemeyer Hall, Columbia University, New York, New York.

Proof and all correspondence concerning papers in the process of publication should be addressed to the Publications Manager, American Institute of Physics, 175 Fifth Avenue, New York, New York.

Subscriptions and orders for single copies should be addressed to Prince and Lemon Streets, Lancaster, Pennsylvania, or to the American Institute of Physics, 175 Fifth Avenue, New York, New York.

Changes of address should be addressed to the Publications Manager.

Subscription Price

The United States and Possessions, Canada and Mexico $10.00
Elsewhere 11.00

Back Numbers

Complete set: Vol 1, 1933—Vol 10, 1942 ..... $100.00
Yearly rate: $11.00.
Single copies: $1.00 each.

The Journal of Chemical Physics is published monthly at Prince and Lemon Streets, Lancaster, Pennsylvania.

Entered as second-class matter December 30, 1932, at the Post Office at Lancaster, Pa., under the Act of August 24, 1912. Acceptance for mailing at special rate of postage, provided for in the Act of February 28, 1925, embodied in paragraph 4, Section 538, P. L. & R.: authorized February 3, 1933.

THE JOURNAL
OF
CHEMICAL PHYSICS

VOLUME 11, NUMBER 2 FEBRUARY, 1943

Theory of Molecular Size Distribution and Gel Formation in Branched-Chain Polymers*

WALTER H. STOCKMAYER
Department of Chemistry, Columbia University, New York, New York

(Received October 22, 1942)

The most probable distributions of molecular sizes are calculated for certain types of branched-chain polymers. The results represent an extension of the previous work of Flory, who showed that very large polymeric molecules appear suddenly at a critical extent of reaction, which is predicted to occur very nearly at the experimentally observed gel point. This transition from liquid to gel is shown to be analogous to the condensation of a saturated vapor. It is believed that the size distributions obtained herein will aid in a study of viscosity-molecular weight relationships in branched-chain polymers.

I

HIGH polymeric substances may be divided according to their structure into two general classes, which exhibit distinctly different properties.[1] Reactions which can lead only to unbranched linear chains yield products which are always soluble in suitable media, regardless of the extent of reaction, and as the reaction proceeds the change from a fluid to a plastic material is gradual. On the other hand, if frequent branching of chains is structurally permissible, as for example in the glycerol-phthalic anhydride reaction, the material gels suddenly at a certain critical extent of reaction which appears to depend on the composition of the reacting mixture but not on the temperature at which the reaction is carried out.[2] The gels formed in these so-called three-dimensional polymerizations are insoluble in all solvents which do not cause degradation.

Recent theoretical and experimental studies by Flory[3,4] have furnished strong evidence that gel formation in three-dimensional polymerizations is caused by the appearance of macroscopic branched-chain molecules. More specifically, Flory showed statistically that such very large structures can appear only after a certain extent of reaction is reached. Experimentally, he observed that the gel point in several three-dimensional polyesterifications occurred very nearly at this extent of reaction as calculated by the statistical theory. In agreement with experiment, the theory indicates that the gel point should depend only on the functionality and proportions of the ingredients. At the same time, Flory also developed methods for calculating, in certain special cases, the actual distribution of molecular sizes during the course of a three-dimensional polymeric reaction.

* Publication assisted by the Ernest Kempton Adams Fund for Physical Research of Columbia University.

[1] For a general account, see H. Mark and R. Raff, *High Polymeric Reactions* (Interscience Publishers, Inc., New York, 1941), pp. 25–30.

[2] R. H. Kienle, P. A. van der Meulen, and F. E. Petke, J. Am. Chem. Soc. **61**, 2258 (1939), especially Table II.

[3] P. J. Flory, J. Am. Chem. Soc. **63**, 3083, 3091, and 3096 (1941).

[4] P. J. Flory, J. Phys. Chem. **46**, 132 (1942).

In this paper, molecular size distributions are studied by a different mathematical method, which confirms Flory's predictions of the gel point, but which has the advantage of somewhat greater generality. While Flory obtained distribution formulae for tri- or tetrafunctional branch units (in the latter case only for very long chains of uniform length), the present method permits calculations to be made for chains of any length and branch units of any functionality.

The treatment to be presented here has added interest in that its mathematical features resemble in some respects those of the theory of condensation developed by Mayer[5] and others. Because of the necessity of considering intermolecular action at varying distances of separation, the distribution of cluster sizes in the imperfect gas can be expressed only in terms of extremely difficult multiple integrals in coordinate space, which have thus far defied explicit evaluation. In three-dimensional polymerizations, however, all interactions may be adequately described in terms of the definite presence or absence of covalent bonds, so that the distribution laws may be written down algebraically. From this point of view, the formation of gels in such systems is a phase transition particularly well adapted to theoretical study.

It should be remarked at the outset that in the following presentation there are employed two assumptions which also characterized the work of Flory:

(a) Intramolecular reactions, leading to cyclic structures, are postulated not to occur. This assumption prevents exact agreement with experiment, since in three-dimensional polyesterifications about five percent of the reaction prior to gelation appears to be intramolecular.[3] It should be possible, however, to provide for this circumstance within the general framework of the present method, although no attempt to do so is made in this paper.

(b) At any stage during the reaction, all unreacted functional groups are considered to be equally reactive, regardless of the size of the molecule to which they are attached or of the fate of other functional groups on the same molecule. This assumption restricts application of the theory to systems with the proper structure and reaction mechanism. Kinetic studies[6] have demonstrated its validity for polyesterifications in which the functional groups on a unit are similar and sufficiently far apart. It should also hold for certain polymerizations proceeding by a chain mechanism, if the processes of chain growth and chain rupture are independent of chain length[3] (e.g., possibly the polymerization of olefins catalyzed by acids). Molecular size distributions in linear polystyrenes,[7] for example, are in good accord with this assumption. Reactions not conforming to this condition would include ethylene oxide polymerizations[8] (in which growth involves addition of monomers only) and polyesterifications involving glycerol (in which the secondary hydroxyl group is less reactive than the two primary hydroxyls). Again, it should be possible, though tedious, to extend the theory to reactions of the latter type.[3]

II

The first case to be considered is the simplest one of a system composed of N identical monomeric units, each carrying f (≥ 2) identical functional groups capable of reacting with each other. Examples are vinyl acetate ($f=2$), or divinyl ether ($f=4$). Let m_n be the number of polymeric molecules composed of n units (n-mers). The total number of units is then

$$\sum_{n\geq 1} nm_n = N, \tag{1}$$

and the number of molecules is

$$\sum_{n\geq 1} m_n = M. \tag{2}$$

The upper limit of the index n changes in a finite system as the reaction proceeds, but it can never exceed N. Since intramolecular reactions are excluded, an n-mer contains $(n-1)$ inter-unit bonds, corresponding to $(2n-2)$ reacted functional groups. Then the total number of reacted groups is

$$\sum_{n\geq 1} (2n-2)m_n = 2N-2M. \tag{3}$$

[5] J. E. Mayer and M. G. Mayer, *Statistical Mechanics* (John Wiley and Sons, Inc., New York, 1940), Chapters 13 and 14.

[6] P. J. Flory, J. Am. Chem. Soc. **61**, 3334 (1939).

[7] G. V. Schulz, A. Dinglinger, and E. Husemann, Zeits. f. physik. Chemie **B43**, 25, 47, 385 (1939).

[8] P. J. Flory, J. Am. Chem. Soc. **62**, 1561 (1940).

We seek the most probable distribution of molecular sizes for a chosen extent of reaction; that is, for given values of N and M. The total number of ways in which the N units may be formed into m_1 monomers, m_2 dimers, $\cdots$, m_n n-mers, $\cdots$ etc., is[9]

$$\Omega = N! \prod_n \left(\frac{w_n}{n!}\right)^{m_n} \frac{1}{m_n!}, \tag{4}$$

where w_n is the number of ways in which n units may form an n-mer, intramolecular reaction being excluded. Since all functional groups are equally reactive, the value of Ω for a given distribution (i.e., a given set of the numbers m_n) is a measure of its probability of occurrence. To find the most probable distribution, Ω must be maximized with respect to each m_n, subject to the conditions that N and M be constant. With the aid of Stirling's approximation for the logarithm of $(m_n!)$, differentiation yields the distribution law

$$m_n = A w_n \xi^n / n!, \tag{5}$$

where A and ξ, which have been introduced as Lagrangian multipliers, can be given a physical significance after the summations indicated by Eqs. (1) and (2) are performed.

It will be observed that the above process resembles one of maximizing an entropy at constant energy. It should therefore be valid for the polyesters, in which the size distribution is probably controlled by ester-interchange equilibria.[10] The resulting distribution law, however, is by no means restricted to cases of equilibrium, but should be equally applicable to unidirectional processes,[11] as long as assumption (b) is fulfilled. Furthermore, in a system of macroscopic size any alternative distribution has a negligible probability of occurrence. In support of this statement, it is shown in Appendix C that the distribution found in this section can be equally well derived from a set of differential equations defining the kinetic mechanism.

To proceed with the distribution law, the value of w_n is required, and in Appendix A this is shown to be

$$w_n = \frac{f^n (fn-n)!}{(fn-2n+2)!}. \tag{6}$$

The summations of Eqs. (1) and (2) may now be performed. The details are given in Appendix B, the results being

$$M/A = \frac{\alpha(1-\alpha f/2)}{f(1-\alpha)^2}, \tag{7}$$

$$N/A = \frac{\alpha}{f(1-\alpha)^2}, \tag{8}$$

where α is the lowest positive real root of the equation

$$f\xi = x = \alpha(1-\alpha)^{f-2}. \tag{9}$$

For $f>2$, Eqs. (7) and (8) are correct only in the range $0 \leq x \leq x_c$, where

$$x_c = (f-2)^{f-2}/(f-1)^{f-1}. \tag{10}$$

In this range, comparison of Eqs. (7) and (8) yields the relationship

$$\alpha = \frac{2N-2M}{fN}, \tag{11}$$

so that α is identified as the reacted fraction of the functional groups. Since the quantity A may then be expressed as

$$A = fN(1-\alpha)^2/\alpha, \tag{12}$$

the size-distribution law may be written

$$m_n = \frac{fN(1-\alpha)^2}{\alpha} \frac{(fn-n)!}{n!(fn-2n+2)!} x^n, \tag{13}$$

where x is defined in terms of the physical quantity α by Eq. (9). The weight fraction W_n of material bound into n-mers is then

$$W_n = nm_n/N$$

$$= \frac{f(1-\alpha)^2}{\alpha} \frac{(fn-n)!}{(n-1)!(fn-2n+2)!} x^n, \tag{14}$$

if the weight of material lost during reaction is negligible. Average molecular sizes are readily obtained. The number average is simply

$$\langle n_n \rangle_{Av} = N/M = 1/(1-\alpha f/2), \tag{15}$$

[9] J. E. Mayer and M. G. Mayer, reference 5, page 437.
[10] P. J. Flory, J. Am. Chem. Soc. **64**, 2205 (1942).
[11] B. Longtin, J. Chem. Phys. **10**, 546 (1942).

while the weight average is

$$\langle n_w \rangle_{Av} = \sum n W_n = (1+\alpha)/[1-(f-1)\alpha]. \quad (16)$$

It is to be noted that the latter average approaches an infinite value as α approaches $1/(f-1)$.

For the special case $f=2$ (linear polymers), Eq. (9) shows that α becomes identical with x, and the weight fractions reduce to the well-

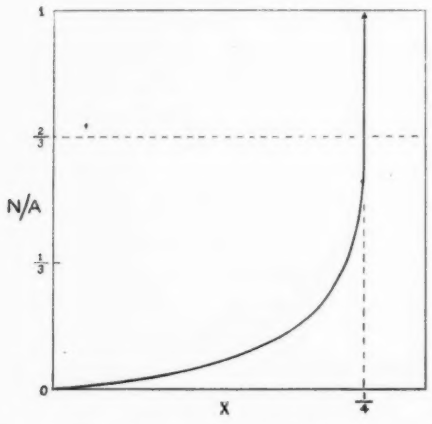

FIG. 1. Plot of N/A as a function of x for a system of trifunctional units. This resembles a plot of density against fugacity in vapor-liquid condensation theory. The gel point is indicated by dotted lines.

known relationship:[12]

$$W_n = (1-\alpha)^2 n \alpha^{n-1}, \quad (f=2). \quad (17)$$

For $f>2$, the lowest positive real root of Eq. (9) is necessarily less than

$$\alpha_c = 1/(f-1), \quad (18)$$

and it is not possible to retain Eqs. (11) through (16) after the fraction of reacted groups exceeds α_c. The behavior of the system after this point is reached, however, may be inferred from an argument similar to that employed by Mayer[13] in discussing the condensation of a saturated vapor. It is convenient to consider the dependence of the quantity

$$N/A = \sum n m_n/A = \sum_{n \geq 1} n x^n \frac{(fn-n)!}{n!(fn-2n+2)!} \quad (19)$$

on the value of the parameter x. Figure 1 shows a plot of N/A against x for the case $f=3$ (for which $x_c=\frac{1}{4}$, $\alpha_c=\frac{1}{2}$). As noted in Appendix B, the unlimited sum converges for $x \leq x_c$, but diverges for $x>x_c$. In a system of finite N, this sum never diverges, but undergoes a sudden increase as soon as x exceeds x_c, which is due almost entirely to an increase in the terms of high n. Low powers of x are changed only inappreciably when x just exceeds x_c, but for large n the asymptotic value of the terms is

$$n m_n/A \backsimeq \frac{(x/x_c)^n}{2\pi^{\frac{1}{2}}(f-2)^{5/2} n^{3/2}}, \quad (n \text{ large}). \quad (20)$$

For large values of n, such terms increase enormously as soon as x exceeds x_c by a small finite amount.

Since N is constant and finite, the sudden increase in the sum must be interpreted as a sudden decrease in the value of A. But conversely one may consider A as the independent variable, and say that x remains constant at the value x_c as soon as A becomes less than a critical value which may readily be found by substituting $1/(f-1)$ for α in Eq. (12). Strictly, x cannot be quite constant in a finite system; it increases to a value so very slightly above x_c that the low members of the sum, which describe the distribution of material in small molecules, appear to remain constant, but the very high terms become enormous, so that the weight fraction of very large molecules increases greatly. As A continues to decrease, the material gradually passes into the form of large molecules, although the value of x remains practically constant. This behavior resembles exactly that of a condensing vapor,[13] in which the fugacity (analagous to x) remains essentially constant while the total volume (analagous to A) is decreased, and during which process the material changes gradually from one composed predominantly of small clusters (vapor) to one of large clusters (liquid). If the gelation of a polymer is attributed to the sudden formation of very large molecules, which immobilize the entrapped remaining small molecules, then α_c, as defined in Eq. (18), is the extent of reaction at which the gel should appear. This is just the result obtained by Flory[3] in a different manner.

As the reaction continues beyond the gel point, the number of small molecules, which may be

[12] P. J. Flory, J. Am. Chem. Soc. **58**, 1877 (1936).
[13] J. E. Mayer and M. G. Mayer, reference 5, page 299.

said to constitute the "sol" phase,[3,4] decreases, but since small powers of x remain (almost) constant, their average size may be shown by substitution in Eq. (15) to retain the constant value

$$\langle n_n \rangle_{\text{Av(sol)}} = 2(f-1)/(f-2), \qquad (21)$$

and the fraction of reacted groups in this portion of the system remains at α_c. Also, since an n-mer possesses fn total groups, $(2n-2)$ of which have reacted, the extent of reaction in the very large molecules (which constitute the "gel" phase) is $2/f$. Therefore, if the symbol α be retained for the fraction of reacted groups in the entire system, the fraction of material in the gel form should be a linear function of α, proceeding from zero at $\alpha=\alpha_c$ to unity at $\alpha=2/f$. This may be written

$$W_g = [(f-1)\alpha - 1]/[1-2/f]. \qquad (22)$$

Since the sol may be extracted with suitable solvents, it is possible in principle to subject Eqs. (21) and (22) to experimental test, but the occurrence of intramolecular reaction, which would be especially prevalent in the gel, would render any conclusions doubtful, particularly with regard to Eq. (22).

Flory[3,4] calculates the gel fraction by a method which gives results in disagreement with Eqs. (21) and (22). He unfortunately did not treat the present case in detail, but his method may be readily applied. It amounts to retaining Eqs. (9) and (12) as definitions of x and A in terms of α even after the gel point has been passed. Then, when α is greater than α_c, the sum over all weight fractions W_n of Eq. (14) would be given by

$$W_s = \sum_{n=1}^{\infty} W_n = \frac{(1-\alpha)^2\alpha'}{(1-\alpha')^2\alpha}, \quad (\alpha > \alpha_c) \qquad (23)$$

where α' is the lower root of Eq. (9) corresponding to α. Since $\alpha' < \alpha$, W_s is less than unity, so that all the material is not accounted for. Flory takes the difference to represent the weight fraction of "infinite" molecules, i.e., of gel, and W_s to be the weight fraction of sol. For the special case $f=3$, the lower root is $\alpha'=1-\alpha$, and the gel fraction thus predicted becomes

$$W_g = 1 - W_s = 1 - (1-\alpha)^3/\alpha^3. \quad (f=3) \qquad (24)$$

In Fig. 2, the values of W_g calculated from this equation, and from Eq. (22) with $f=3$, are plotted for comparison.

An additional disagreement between the two methods is found in considering the average size of the sol molecules. According to the present method this quantity maintains the constant value given by Eq. (21), but the reasoning employed by Flory leads to

$$\langle n_n \rangle_{\text{Av(sol)}} = 1/(1-\alpha' f/2). \qquad (25)$$

Since α' decreases as α increases, this equation predicts a continual decrease in the average size of the sol molecules as the reaction proceeds.

It may readily be demonstrated that the method of Flory predicts the occurrence of intramolecular reactions in the gel. Since the fraction of reacted groups in the sol is taken to be α', direct application of Eq. (23) leads to the expression

$$\alpha_{\text{gel}} = (\alpha + \alpha' - 2\alpha\alpha')/(1-\alpha\alpha'). \qquad (26)$$

At the critical point, we have $\alpha=\alpha'=\alpha_c$, so that

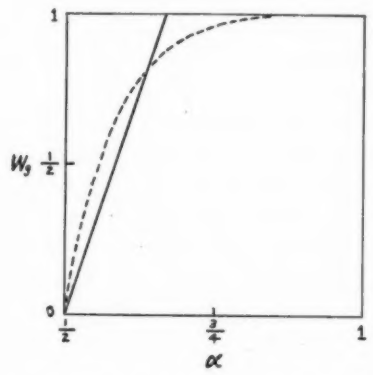

FIG. 2. Gel fraction as a function of the extent of reaction in a system of trifunctional units. Full line, Eq. (22) (no intramolecular reactions permitted); dotted curve, Eq. (24) (Flory) (intramolecular reactions in gel).

$\alpha_{\text{gel}}=2/f$, but as α proceeds beyond α_c, Eq. (26) predicts that α_{gel} exceeds $2/f$ (a limit which could not be surpassed if intramolecular reactions were forbidden). Quite aside from the fundamental logic involved in Flory's procedure, Eq. (26) demonstrates that it cannot be rigorous, for it predicts a very definite number of cyclic linkages in the system for any chosen total extent of reaction α, although the initial assumptions do not specifically treat such structures in any way. A

rigorous treatment of the problem would require the inclusion of at least one additional parameter defining the relative probability of occurrence of inter- and intramolecular reactions.

Nevertheless, Eqs. (23) to (26) represent an empirical scheme which may often give a better approximation to experimental conditions than the rigorously derived Eqs. (21) and (22), which exclude intramolecular reactions altogether. While such reactions undoubtedly occur in both sol and gel, they are certainly more prevalent in the gel, since their likelihood of occurrence must increase with molecular size. Under such conditions, it is qualitatively to be expected[14] that the average molecular size of the sol will decrease as the amount of intramolecular reaction in the gel increases. An analogy may again be found in vapor-liquid equilibrium.[5] As the temperature is lowered, the liquid becomes more tightly connected, the van der Waals forces exerting a greater binding, and this circumstance corresponds to greater connectivity in the gel, due to an increased number of intramolecular linkages. Simultaneously, the average cluster size of the saturated vapor (measured by the quantity RT/PV) decreases, corresponding to a decreased average molecular size in the sol.

In view of these considerations, it may be concluded that the qualitative features of Flory's discussion are probably correct, although his quantitative expressions are questionable. Further experimental and theoretical study of the problem is desirable, for its understanding would afford a possible method for the experimental characterization of gelled three-dimensional polymers.

III

A case of somewhat greater practical interest is that of a system containing both bifunctional and polyfunctional units. An example of such a system which possibly meets the requirements of assumption (b) is a mixture of vinyl acetate ($f=2$) with divinyl succinate ($f=4$). Staudinger and Heuer[15] have investigated the system styrene-*p*-divinylbenzene, but assumption (b) is invalid in this case, since the vinyl groups on the latter molecule are much more reactive than those on the former. Apparently experiments have yet to be performed on systems which meet the assumption.

Let the system consist of N units bearing $f(>2)$ functional groups each and L bifunctional units, all the groups being identical and of the same reactivity. The polymeric molecules will consist of branch units joined by linear chains of various lengths. If m_{nl} is the number of molecules composed of n polyfunctional units and l bifunctional units, the number of ways of obtaining a given distribution is

$$\Omega = N!L! \prod_{n,l} \left(\frac{w_{nl}}{n!l!}\right)^{m_{nl}} \frac{1}{m_{nl}!}, \tag{27}$$

where w_{nl} is the number of ways of forming an n, l-mer from n given polyfunctional and l given bifunctional units. Since an n, l-mer contains $(n+l-1)$ bonds when intramolecular reaction is excluded, the conditions imposed on Ω may be written

$$\begin{aligned} \sum_{n\geq 0}\sum_{l\geq 0} nm_{nl} &= N, \\ \sum_{n\geq 0}\sum_{l\geq 0} lm_{nl} &= L, \\ \sum_{n\geq 0}\sum_{l\geq 0} m_{nl} &= M, \\ m_{00} &= 0. \end{aligned} \tag{28}$$

The distribution of greatest probability is

$$m_{nl} = A\frac{w_{nl}\xi^n\eta^l}{n!l!}, \tag{29}$$

in which A, ξ, and η are Lagrangian multipliers. In Appendix A, w_{nl} is found to be

$$w_{nl} = \frac{f^n 2^l (fn-n+l)!}{(fn-2n+2)!}. \tag{30}$$

To obtain the result in terms of measurable quantities, the sums of Eq. (28) are required. The form of w_{nl} readily permits this operation, which is illustrated for the first sum. This may be written

$$N = \sum nm_{nl} = A\sum_{n=1}^{\infty} \frac{(f\xi)^n (fn-n)!}{(n-1)!(fn-2n+2)!} \times \sum_{l=0}^{\infty} \frac{(2\eta)^l (fn-n+l)!}{l!(fn-n)!}. \tag{31}$$

[14] The writer was privileged to discuss the question with Dr. Flory, who quoted some preliminary experimental results which support this expectation.

[15] H. Staudinger and W. Heuer, Ber. **68**, 1618 (1935).

The sum over l is given by the binomial theorem as

$$\sum_{l=0}^{\infty} \frac{(2\eta)^l (fn-n+l)!}{l!(fn-n)!} = 1/(1-2\eta)^{fn-n+1}. \quad (32)$$

Equation (31) then becomes

$$N = \frac{A}{(1-2\eta)} \sum_{n=1}^{\infty} \frac{x^n (fn-n)!}{(n-1)!(fn-2n+2)!}, \quad (33)$$

where

$$x = f\xi/(1-2\eta)^{f-1}.$$

The result is therefore (see Appendix B)

$$N/A = \frac{\alpha}{f(1-2\eta)(1-\alpha)^2}, \quad (x \leq x_c) \quad (34)$$

where α is again the lowest positive real root of Eq. (9) and x_c is defined in Eq. (10). The other sums may be found in similar fashion, and the results are

$$L/A = \frac{\eta}{(1-2\eta)^2(1-\alpha)^2}, \quad (35)$$

$$M/A = \frac{\eta}{1-2\eta} + \frac{\alpha(1-\alpha f/2)}{f(1-2\eta)(1-\alpha)^2}. \quad (36)$$

Now let two observable quantities be defined as

$$p = \frac{\text{functional groups on branch units}}{\text{all functional groups}} = \frac{fN}{fN+2L},$$

p = fraction of groups reacted, (37)

$$= \frac{\sum(2n+2l-2)m_{nl}}{fN+2L} = \frac{2(N+L-M)}{fN+2L}.$$

The quantities ξ, η, α, and A may then be written in terms of p and ρ, the results being

$$\begin{aligned} f\xi &= p\rho(1-p)^{f-2}, \\ 2\eta &= p(1-\rho), \\ \alpha &= p\rho/[1-p(1-\rho)], \\ A &= fN(1-p)^2/p\rho, \end{aligned} \quad (38)$$

and the distribution law becomes

$$m_{nl} = fN\rho^{n-1}(1-\rho)^l p^{n+l-1}(1-p)^{fn-2n+2} \times \frac{(fn-n+l)!}{n!l!(fn-2n+2)!}, \quad (39)$$

which reduces to Eq. (13), as it should, when the substitutions $l=0$, $\rho=1$, $\alpha=p$ are made. It also reduces to the law for linear polymers as ρ is made to approach zero. Weight fractions and average molecular weights can readily be calculated from this equation when the weights of the units are known. The general expressions are lengthy and need not be recorded here.

The sums of Eq. (28) diverge when the parameter x exceeds its critical value x_c, given by Eq. (10), or when α, as defined in Eq. (38), exceeds $1/(f-1)$. In this system, α is no longer simply the fractional extent of reaction; it has, however, a simple physical meaning.[3,4] Quite generally, α is the probability that a chain proceeding from a branch unit shall end in another branch unit (unreacted groups attached to branch units also being considered as "chains"). It was, in fact, by primary consideration of this probability that Flory first defined the critical conditions for the appearance of very large molecules.

The critical extent of reaction at which the gel should appear is found from Eq. (38), by substitution of $\alpha_c = 1/(f-1)$, to be

$$p_c = 1/[1+(f-2)\rho]. \quad (40)$$

It is possible to calculate the amount and composition of the gel and sol fractions as the reaction proceeds, but the interference due to intramolecular reactions makes the results of doubtful utility, so that they are not written down. It is sufficient here to note that the composition of the initial portion of gel may be found readily from the fact that at the critical point m_{nl} (for large values of n and l) has a maximum value when $n/(n+l) = \rho$. Large molecules of this composition will therefore appear most readily, and the gel is thus richer in branch units than the sol from which it forms. As gelation proceeds, the mol fraction of branch units in the sol continues to decrease, approaching zero at completion of the reaction.

An interesting special case of the foregoing type of system is one containing a very small number of branch units, so that the chains are on the average very long. Then practically all the weight resides in the bifunctional units, and the weight fraction of n, l-mers can be approximated by lm_{nl}/L. Then the weight fraction of molecules

containing n branches, irrespective of the number of bifunctional units, is found to be

$$W_n=\sum_{l=0}^{\infty} lm_{nl}/L=2(1-\alpha)^2\frac{(fn-n+1)!x^n}{n!(fn-2n+2)!}. \quad (41)$$

The complexity z is defined as the number of chains in a molecule. With the exclusion of intramolecular reactions,

$$z=fn-n+1, \quad (42)$$

so that average values may easily be found. For the special case of very long chains ($\rho\to 0$) the averages are

$$\langle z_n\rangle_{Av}=\operatorname*{Lim}_{\rho\to 0}\frac{\sum(fn-n+1)m_{nl}}{M}=\frac{1}{1-2\alpha(f-1)/f}; \quad (43)$$

$$\langle z_w\rangle_{Av}=\sum_{n=0}^{\infty}(fn-n+1)W_n=\frac{1+(f-1)\alpha}{1-(f-1)\alpha}. \quad (44)$$

These results were found by Flory for the special case $f=3$.

IV

We consider finally the case corresponding to polyesterification. Let the system contain N f-functional and L bifunctional units bearing the functional group A, and S bifunctional units bearing the group B. A groups can react only with B groups, and vice versa, and all groups of a kind are assumed to be equally reactive. Systems approximating these conditions (tricarballylic acid—adipic acid—diethylene glycol, pentaerythritol—diethylene glycol—adipic acid, etc.) were employed in the experiments of Flory.[3]

In this system, the total number of ways of forming a given distribution is

$$\Omega=N!L!S!\prod_{n,l,s}\left(\frac{w_{nls}}{n!l!s!}\right)^{m_{nls}}\frac{1}{m_{nls}!}, \quad (45)$$

where m_{nls} is the number of n, l, s-mers. Since an n, l, s-mer contains $(n+l+s-1)$ bonds, the conditions imposed on the system may be written

$$\begin{aligned}&\textstyle\sum nm_{nls}=N, \quad \sum lm_{nls}=L,\\ &\textstyle\sum sm_{nls}=S, \quad \sum m_{nls}=M. \quad (m_{000}=0).\end{aligned} \quad (46)$$

The sums go over all values of n and l from zero to infinity, but since A groups can react only with B groups, the values of s are limited to the range

$$\begin{aligned}&s=n+l-1+q,\\ &0\le q\le fn-2n+2.\end{aligned} \quad (47)$$

Maximizing Ω yields the distribution law

$$m_{nls}=\frac{Aw_{nls}\xi^n\eta^l\zeta^s}{n!l!s!}, \quad (48)$$

where A, ξ, η, and ζ are Lagrangian multipliers. For this case, the factor w_{nls} is (Appendix A)

$$w_{nls}=\frac{f^n2^l2^s(fn-n+l)!s!}{(fn-2n+2-q)!q!}, \quad (49)$$

q being defined in Eq. (47). The summations of Eqs. (46) may be found in straightforward though tedious fashion with the aid of the binomial theorem. The results are

$$\begin{aligned}N/A&=\frac{(1+2\zeta)^2}{2\zeta(1-4\eta\zeta)}\frac{\alpha}{f(1-\alpha)^2},\\ L/A&=\frac{(1+2\zeta)^2}{(1-4\eta\zeta)^2}\frac{\eta}{(1-\alpha)^2},\\ S/A&=\zeta\left[\frac{(1+2\zeta)(\alpha+4\eta\zeta-4\alpha\eta\zeta)}{2\zeta(1-4\eta\zeta)(1-\alpha)}+1\right]^2,\\ M/A&=\zeta+\frac{(1+2\zeta)^2\eta}{1-4\eta\zeta}+\frac{(1+2\zeta)^2}{2\zeta(1-4\eta\zeta)}\frac{\alpha(1-\alpha f/2)}{f(1-\alpha)^2},\end{aligned} \quad (50)$$

in which α is the lowest root of the equation

$$x=\alpha(1-\alpha)^{f-2}=\frac{(f\xi)(2\zeta)(1+2\zeta)^{f-2}}{(1-4\eta\zeta)^{f-1}}. \quad (51)$$

As before, these results hold only for $\alpha\le 1/(f-1)$.

We now introduce the observable quantities

$$\begin{aligned}p&=\frac{A\text{ groups on polyfunctional units}}{\text{total }A\text{ groups}}=\frac{fN}{fN+2L},\\ r&=\frac{\text{total }A\text{ groups}}{\text{total }B\text{ groups}}=\frac{fN+2L}{2S},\\ p&=\frac{\text{reacted }A\text{ groups}}{\text{total }A\text{ groups}}=\frac{N+L+S-M}{fN+2L}.\end{aligned} \quad (52)$$

In terms of these quantities, we obtain

$$\xi=\frac{pr\rho(1-p)^{f-1}}{f(1-rp)},$$

$$\eta=\frac{pr(1-\rho)(1-p)}{2(1-rp)},$$

$$\zeta=\frac{p(1-rp)}{2(1-p)}, \tag{53}$$

$$\alpha=\frac{p^2r\rho}{1-p^2r(1-\rho)},$$

$$A=fN(1-p)(1-rp)/pr\rho.$$

Once more, α is the probability that a chain proceeding from a branch unit shall end in another branch unit, and the critical extent of reaction is given by

$$p_c^2r=1/[1+(f-2)\rho]. \tag{54}$$

By the use of Eqs. (48), (49), and (53), size distributions may be evaluated in terms of observable parameters. Average sizes are readily found, but the length of the general expressions forbids their being recorded here. Since the experimental results[3] indicate that up to the gel point the intramolecular reactions play only a small disturbing role, the above distribution laws might profitably be employed as aids in an experimental study of the important question of the effect of chain branching on viscosity-molecular weight relationships. Flory observed viscosities during his gelation experiments with polyesters, but there are not enough data to permit definite conclusions to be drawn. There is some indication,[16] however, that the viscosity rises less rapidly with the weight-average molecular weight than it does in linear polyesters.[17] A more complete study of the viscosities of branched polyesters is being undertaken in this laboratory.

In conclusion, it is believed that this general method of seeking the most probable distribution should find application to other types of polymeric system. The limiting factor in its success will be the ability to evaluate combinatory factors such as those of Appendix A and to perform the summations which they require. It is hoped to gain in this manner a more detailed understanding of the occurrence and effect of intramolecular reactions.

The writer records his thanks for the aid and encouragement rendered by Professor Joseph E. Mayer, Dr. Maria Goeppert-Mayer, and Dr. Paul J. Flory.

APPENDIX

A. Combinatory problems

1. We seek w_n, defined as the number of ways in which n distinguishable polyfunctional units, each bearing f distinguishable equivalent functional groups capable of reacting with each other, can be formed into a single polymeric molecule containing no cyclic structures.

To permit visualization, a unit can be represented as a mechanical frame containing f holes. We shall represent the polymeric molecule by introducing a number of indistinguishable bolts to connect the frames. Since an n-mer requires $(n-1)$ bonds, $(n-1)$ bolts are required to connect the frames, each bolt passing through a pair of holes belonging to different frames. In addition, we shall place bolts through each of the other holes, these not serving to connect different frames with each other. The total number of bolts required to accomplish this structure is, therefore,

$$fn-(n-1)=fn-n+1.$$

Now consider a particular bolted arrangement, corresponding to one of the w_n ways of forming an n-mer. We wish to dissociate it into n separate frames, each containing $(f-1)$ holes filled by bolts and one empty hole, with one free bolt left over. If the free bolt is chosen first, the empty hole in each of the n frames is thereby uniquely determined. Since any one of the $(fn-n+1)$ bolts may be chosen to be the free one, there are consequently $(fn-n+1)$ different dissociated arrangements of the required type corresponding to the same bolted arrangement. Therefore, if P is the number of different dissociated arrangements of this type which are possible, and if Q is the number of ways in which each such dissociated arrangement can be bolted together, the number of different bolted arrangements is

$$w_n=PQ/(fn-n+1). \tag{A1}$$

Now the number P is simply

$$P=f^n, \tag{A2}$$

since any one of the f holes on a frame may be chosen as the empty one, and since the bolts are indistinguishable. To find Q, we introduce the device of assigning a washer to each bolt which is ultimately to be used in forming a bond by passing through two holes. The washers are indistinguishable. The $(n-1)$ bolts which must receive washers may, therefore, be selected in

$$\frac{(fn-n+1)!}{(n-1)!(fn-2n+2)!} \text{ ways,}$$

[16] The writer is indebted to Dr. Flory for the use of these unpublished measurements.

[17] P. J. Flory, J. Am. Chem. Soc. 62, 1057 (1940).

since each of the $(fn-n+1)$ bolts is now distinguishable by virtue of its having been assigned to a definite hole in forming a dissociated arrangement. The dissociated arrangement must now be bolted together. Washered bolts are chosen and placed through empty holes not on frames with which they are already connected, the free bolt always being kept for the last. Thus the first washered bolt can choose any of $(n-1)$ empty holes, for it must not pass through the empty hole on its own frame. Then there are still $(n-2)$ single frames and one "double frame," or altogether $(n-1)$ structures each still carrying one empty hole. Thus the second washered bolt can choose any of $(n-2)$ empty holes, the third can choose $(n-3)$, and so on. Finally, only the free bolt remains. If the free bolt has no washer, there remains just one empty hole into which it must go. If the free bolt has a washer, there remain two structures, each containing one empty hole, so that the free bolt serves to form the last bond. Hence for a given assignment of the washers the bolting process can be accomplished in $(n-1)!$ ways. Combining this result with the number of ways of assigning the washers, we find the number of ways of bolting together a given dissociated arrangement to be

$$Q=\frac{(fn-n+1)!}{(fn-2n+2)!}. \tag{A3}$$

Substitution of Eqs. (A2) and (A3) into (A1) then yields the desired result

$$w_n=\frac{f^n(fn-n)!}{(fn-2n+2)!}. \tag{A4}$$

This proof resembles closely that of an analogous problem[18] in imperfect gas theory. The writer is particularly indebted to Dr. Maria Goeppert-Mayer for her help in establishing this result.

2. An entirely similar procedure serves to determine w_{nl}, the number of ways in which n f-functional units and l g-functional units, each carrying the same group, can be bound into an nl-mer devoid of cyclic structures. In this case the number of bolts required is

$$fn+gl-(n+l-1)=fn-n+gl-l+1.$$

The other required quantities are

$$P=f^ng^l, \tag{A5}$$

$$Q=\frac{(fn-n+gl-l+1)!}{(fn-2n+gl-2l+2)!}, \tag{A6}$$

$$w_{nl}=\frac{f^ng^l(fn-n+gl-l)!}{(fn-2n+gl-2l+2)!}. \tag{A7}$$

For the special case $g=2$, which is considered in Section III of this paper, the expression is,

$$w_{nl}=\frac{f^n2^l(fn-n+l)!}{(fn-2n+2)!}. \tag{A8}$$

3. The results obtained above may be applied to the problem of finding the number of ways, w_{nls}, in which n f-functional units and l bifunctional units all bearing the groups A (to be called α-units) and s bifunctional units (called β-units) bearing the groups B, can be formed into a single molecule, A-groups being permitted to react only with B-groups and vice versa. As has been mentioned in Section IV, s is restricted to a range of values

$$s=n+l-1+q, \tag{A9}$$

where

$$0\leq q\leq fn-2n+2,$$

since at least $(n+l-1)$ β-units are required to bind together the $(n+l)$ α-units, and since the $(fn-2n+2)$ free chain ends may be terminated by either kind of group. To find w_{nls}, we note that the insertion of β-units between the α-units does not change the number of ways in which the latter can be arranged. Hence

$$w_{nls}=\frac{f^n2^l(fn-n+l)!}{(fn-2n+2)!}R, \tag{A10}$$

where R is the number of ways in which the s β-units may be placed in a given arrangement of the α-units. Now R will contain a factor 2^s, since in any location the bifunctional β-unit can have either of two orientations. Next, $(n+l-1)$ β-units are to be chosen from the total number s of such units, and placed in the $(n+l-1)$ "bonding" positions between the α-units. This operation may be accomplished in

$$\frac{s!}{(s-n-l+1)!}=\frac{s!}{q!} \text{ ways.}$$

The remaining q β-units are to be distributed among the $(fn-2n+2)$ free chain ends, and this can be done in

$$\frac{(fn-2n+2)!}{(fn-2n+2-q)!} \text{ ways.}$$

The result is

$$R=\frac{2^s s!(fn-2n+2)!}{(fn-2n+2-q)!q!}, \tag{A11}$$

so that finally

$$w_{nls}=\frac{f^n2^l2^s(fn-n+l)!s!}{(fn-2n+2-q)!q!}. \tag{A12}$$

B. Summations

We consider the sums

$$S_i=\sum_{n=1}^{\infty} n^i x^n\frac{(fn-n)!}{n!(fn-2n+2)!}, \tag{B1}$$

where f is an integer greater than unity and $i=0$, 1, or 2. For $f=2$, the results are well known. For $f>2$, we investigate the convergence by noting that the coefficient of x^n approaches the value

$$\frac{1}{(2\pi)^{1/2}(f-2)^{5/2}n^{5/2-i}}\left[\frac{(f-1)^{f-1}}{(f-2)^{f-2}}\right]^n \tag{B2}$$

for very large values of n. Since a series of the form $\sum_{n=1}^{\infty} z^n n^{-k}$ converges for $z\leq 1$ if $k>1$ and converges for $z<1$ if $k\leq 1$, it is apparent that all the sums S_i have a radius of convergence

$$x_c=(f-2)^{f-2}/(f-1)^{f-1} \tag{B3}$$

and that at this point S_0 and S_1 converge, while S_2 diverges.

[18] J. E. Mayer and M. G. Mayer, reference 5, page 455.

To evaluate the sums, it is most convenient to work with S_1. Making the substitution

$$x=\alpha(1-\alpha)^{f-2} \tag{B4}$$

and changing the notation slightly by letting $n=m+1$ and $f=\lambda+1$, we obtain

$$S_1=\frac{\alpha}{(1-\alpha)^2}\sum_{m=0}^{\infty}\frac{(\lambda m+\lambda)!}{m!(\lambda m+\lambda-m+1)!}\alpha^m(1-\alpha)^{\lambda m+\lambda-m+1}. \tag{B5}$$

Binomial expansion of the power of $(1-\alpha)$ yields

$$\begin{aligned}S_1(1-\alpha)^2/\alpha&=\sum_{m=0}^{\infty}\sum_{k}\frac{(\lambda m+\lambda)!(-1)^k\alpha^{m+k}}{m!k!(\lambda m+\lambda-m-k+1)!}\\&=\sum_{q=0}^{\infty}\frac{(-\alpha)^q}{q!}\sum_{m}\binom{q}{m}(-1)^m\frac{(\lambda m+\lambda)!}{(\lambda m+\lambda-q+1)!}\\&=\frac{1}{\lambda+1}+\sum_{q=1}^{\infty}\frac{(-\alpha)^q}{q!}\sum_{m}\binom{q}{m}(-1)^m\\&\qquad\times\frac{(\lambda m+\lambda)!}{(\lambda m+\lambda-q+1)!}.\end{aligned} \tag{B6}$$

Now consider the function (for $q\geq 1$)

$$F(q,z)=z^{\lambda}(1-z^{\lambda})^q=\sum_{m}\binom{q}{m}(-1)^m z^{\lambda m+\lambda}. \tag{B7}$$

Repeated differentiation gives

$$\left[\left(\frac{d}{dz}\right)^{q-1}F(q,z)\right]_{z=1}=\sum_{m}\binom{q}{m}(-1)^m\frac{(\lambda m+\lambda)!}{(\lambda m+\lambda-q+1)!}, \tag{B8}$$

or just the sum required in Eq. (B6). Since $F(q,z)$ contains the factor $(1-z^{\lambda})^q$, its $(q-1)$st derivative contains the factor $(1-z^{\lambda})$. Hence the sum of Eq. (B8) vanishes, and Eq. (B6) gives simply

$$S_1=\alpha/(1-\alpha)^2(\lambda+1)=\alpha/(1-\alpha)^2 f. \tag{B9}$$

Evaluation of S_0 and S_2 is then simply a matter of integration or differentiation with respect to $dx=(1-\alpha)^{f-3}\times[1-(f-1)\alpha]d\alpha$. The results are

$$S_0=\alpha(1-\alpha f/2)/(1-\alpha)^2 f, \tag{B10}$$

and

$$S_2=\frac{\alpha(1+\alpha)}{f(1-\alpha)^2[1-(f-1)\alpha]}. \tag{B11}$$

Since the function $x=\alpha(1-\alpha)^{f-2}$ passes through a maximum value, equal to x_c of Eq. (B3), at

$$\alpha_c=1/(f-1), \tag{B12}$$

it is seen from Eqs. (B9), (B10) and (B11) that at $\alpha=\alpha_c$ the sums S_0 and S_1 converge, while S_2 diverges.

It will be noted that the sums S_i, defined in terms of the parameter x, have been evaluated as functions of α, which is a root of Eq. (B4). In the interval $0\leq x\leq x_c$, however, there exist *two* positive real roots ($0\leq\alpha\leq 1$) of this equation, the one greater than and the other less than α_c. Consideration of the case $x=0$ demonstrates that the *lower* root is to be used in Eqs. (B9), (B10), and (B11).

The results of this section are applied to the consideration of a finite system, so that the index n of the sums S_i does not run to infinity, but to a limit which changes with the value of x. However, in the range $0\leq x\leq x_c$ the error in S_i is of the order of $N^{i-5/2}$, where N is the total number of particles in the system. In this range, therefore, the finite sums may safely be replaced by the infinite sums considered here.

C. Kinetic derivation of distribution formula

The distribution law for a system composed of N f-functional units may be derived from the following set of differential equations describing the kinetic process:

$$\frac{1}{k}\frac{dm_n}{dt}=\frac{1}{2}\sum_{s=1}^{s=n-1}(fs-2s+2)(fn-fs+2n-2s+2)m_s m_{n-s}-(fn-2n+2)m_n\sum_{s=1}^{\infty}(fs-2s+2)m_s. \tag{C1}$$

In this equation, the first sum represents formation of n-mers by reactions between pairs of smaller molecules, and the second term represents their destruction through reaction with other molecules. All the possible steps have the same bimolecular rate constant k (normalized to unit volume per molecule), except for factors of the form $(fn-2n+2)$, which give the number of unreacted groups on an n-mer, any of which can react when a collision or "coordination" occurs. The solution of the above set of equations is

$$m_n=\frac{fN(1-\alpha)^2}{\alpha}\frac{(fn-n)!}{n!(fn-2n+2)!}[\alpha(1-\alpha)^{f-2}]^n, \tag{C2}$$

where

$$d\alpha/dt=fNk(1-\alpha)^2,$$

or

$$\alpha=fNkt/(1+fNkt).$$

Equation (C2) for m_n is exactly the same as Eq. (13) of the text, which was derived by seeking the most probable distribution.

A Direct Experimental Determination of the Electron Affinity of Chlorine*

KENNETH JAMES MCCALLUM† ‡ AND JOSEPH E. MAYER
Department of Chemistry, Columbia University, New York, New York

(Received November 17, 1942)

The electron affinity of chlorine has been determined to be 85.84±1.0 kcal./mole by measuring the ratio of ions to electrons leaving a hot tungsten surface in contact with a low pressure of gas containing chlorine atoms. Both Cl_2 and $SnCl_4$ were used as carrier gases.

INTRODUCTION

THE electron affinity of an atom, the negative of the energy change at absolute zero accompanying the reaction

$$X_{gas}+e^-_{gas}\rightarrow X^-_{gas}, \quad (1)$$

may be determined by measuring the relative numbers of electrons, atoms, and negative ions leaving a hot filament surface of known temperature.[1,2] The assumption must be made that the reflection coefficient of the molecules hitting the filament is always zero. If so, the number z_j of atoms of atomic specie j leaving the filament may be related to the partial pressure P_j of this specie in an equilibrium gas mixture of the same temperature T_s as the filament, by the equation

$$z_j=P_j(2\pi m_j kT_s)^{-\frac{1}{2}}, \quad (2)$$

where m_j is the mass of the atom.

A supply of atoms X for the filament may be maintained by surrounding the hot filament with a cold gas at temperature T_r having molecules of mass m_r containing α atoms of X per molecule. If the temperature of the filament is such that complete dissociation of these molecules takes place, and if a negligible fraction of the atoms are converted into negative ions, we may equate the number of atoms carried to the filament by the surrounding gas to the number emitted at the filament temperature T_s as atoms. One may thus relate the pressure P_x of atoms in the hypothetical equilibrium gas at T_s, to P_r and T_r by the equation

$$P_x=P_r(\alpha^2 m_x T_s/m_r T_r)^{\frac{1}{2}}. \quad (3)$$

The ratio of the numbers of negative ions to the numbers of electrons leaving the filament surface z_i/z_e is measured as the ratio of two currents i_i/i_e carried from the filament, and is related to the ratio of the pressures P_i/P_e by

$$P_i/P_e=(i_i/i_e)(m_x/m_e)^{\frac{1}{2}}. \quad (4)$$

Combining (3) and (4) the equilibrium constant and the standard free energy change of the reaction (1) may be written as

$$K=\exp(-\Delta F^0/RT_s)=P_i/(P_eP_x)$$
$$=(i_i/i_e)P_r^{-1}(m_r/\alpha^2 m_e)^{\frac{1}{2}}(T_r/T_s)^{\frac{1}{2}}. \quad (5)$$

Monatomic gases are alone involved in reaction (1). The standard free energy at unit pressure and at T_s is readily evaluated for each specie as $F^0(T_s)=RT\ln[(h^2/2\pi mkT_s)^{\frac{3}{2}}(kT_sQ)^{-1}]$, where m is the mass of the atom and Q its internal partition function. This standard free energy assumes zero free energy at 0°K for the atomic specie. The ΔF^0 appearing in (5) is

$$-\Delta F^0(T)=-\Delta E_0-F_i^0(T)+F_e^0(T)+F_x^0(T), \quad (6)$$

with $-\Delta E_0$ the electron affinity of X.

Combining (5) and (6), using the fact that $m_x=m_i$, and that the internal partition function Q for electrons is 2, one finds for the electron affinity

$$-\Delta E=RT_s\ln\left[\frac{2^{5/2}\pi^{3/2}k^{5/2}}{h^3}\cdot\frac{m_e m_r^{\frac{1}{2}}}{\alpha}\cdot\frac{i_i}{i_e}\frac{T_s^2T_r^{\frac{1}{2}}}{P_r}\frac{Q_x}{Q_i}\right]. \quad (7)$$

* Publication assisted by the Ernest Kempton Adams Fund for Physical Research of Columbia University.

† Submitted in partial fulfillment of the requirements for the degree of Doctor of Philosophy at Columbia University.

‡ Present address: University of Saskatchewan, Saskatoon, Saskatchewan, Canada.

[1] P. P. Sutton and J. E. Mayer, J. Chem. Phys. **3**, 20 (1935).

[2] J. J. Mitchell and J. E. Mayer, J. Chem. Phys. **8**, 282 (1940).

For chlorine ions, $Q_i=1$, since the lowest electronic level is a singlet S level, and presumably no excited levels exist. The chlorine atom has a lowest $^2P_{3/2}$ level of degeneracy 4, while the next member of the doublet, $^2P_{1/2}$ is 881 wave numbers higher. Higher excited terms may be neglected. This leads to

$$Q_{Cl}=4+2\exp(-881\times1.439/T), \quad (8)$$

which, around $T=2150°$, may be used in the approximate form

$$\log_{10} Q_{Cl}=\log_{10} 4+0.0507+T(2.596\times10^{-5}). \quad (8')$$

If the carrier gas is Cl_2, the appropriate mass, $m_r=70.91/N_0$, $\alpha=2$, and $T_r=300°K$ may be inserted in (7) and the numerical constants evaluated. One finds for $-\Delta E$ in kcal. per mole

$$-\Delta E=4.574T_s\,10^{-3}[\log_{10}(100\Delta_i/\Delta_e) - \log_{10} P_{Cl_2}+2\log_{10}(T_s\,10^{-3}) + T_s(2.596\times10^{-5})+7.848], \quad (9)$$

in which Δ_i and Δ_e are the galvanometer deflections due to ions and electrons, respectively, and P_{Cl_2} is the pressure of Cl_2 surrounding the filament measured in microns of Hg. The temperature T_s is that of the filament.

If the carrier gas is $SnCl_4$, the numerical constant in (9) is changed by having $m_r=260.53/N_0$ and $\alpha=4$ from the value 7.848 appearing in (9) to the value 8.122.

Thus, by observing the ion and electron emissions from a heated surface at known temperature in an atmosphere of Cl_2 or $SnCl_4$ molecules at known pressure, it is possible to determine the electron affinity of chlorine, provided that the assumption of a zero reflection coefficient at the heated surface for all atomic species is valid.

In regard to this assumption there is little that can be said of conclusive nature at the present time. There are, however, many indications which point to the fact that it is justified, and that the error which it may introduce into the electron affinity values is small. The experiments on chlorine reported here, and those made on iodine[1] and bromine[3] cover a wide range of temperatures and pressures, over which the calculated values of the electron affinity show no trend, indicating a constant reflection coefficient. This would be remarkable if the reflection coefficients were not essentially zero. It may be calculated that in the range of temperatures and pressures used here, the chlorine molecules are almost completely dissociated at the surface, as is known to be true in the case of iodine.[1] Furthermore, it has been shown[4] experimentally that caesium atoms lose electrons completely on contact with a surface of high work function, and that the reflection coefficient of caesium atoms incident on a tungsten surface is zero.[5] It is usually assumed that the reflection coefficient for all alkali atoms and ions is equal to zero, and it seems safe to assume that this is also the case for the halogens.

In the case of electrons there is the possibility of the existence of a surface and temperature independent reflection coefficient of exactly one-half, as indicated by the fact that in some cases (tungsten, tantalum, molybdenum) there is a twofold discrepancy between the thermionic emission constants A_0 and A obtained from the theoretical and experimental equations, respectively. The discrepancy can be accounted for if the work function varies linearly with the temperature and has a temperature coefficient of the proper magnitude and sign. Theoretical calculations[6] show that such a variation of the correct order of magnitude should be expected, and measurements on tungsten filaments give values of the temperature coefficient which are able to account for the twofold discrepancy between A and A_0.[7] Quantum mechanical calculations show that the reflection coefficient should be less than 0.07 for the type of potential which exists at the surface of a metal. Becker and Brattain[8] have considered the available information on reflection coefficients and have concluded that the evidence indicates values which are less than 0.1.

[3] Harold B. Weissblatt, Dissertation, Johns Hopkins University, 1938.

[4] I. Langmuir and K. H. Kingdon, Proc. Roy. Soc. **A107**, 61 (1925).

[5] J. B. Taylor and I. Langmuir, Phys. Rev. **44**, 423 (1933).

[6] S. Seely, Phys. Rev. **59**, 75 (1941).

[7] J. G. Potter, Phys. Rev. **58**, 623 (1940).

[8] J. A. Becker and W. H. Brattain, Phys. Rev. **45**, 694 (1934).

DESCRIPTION OF APPARATUS

The apparatus used for the measurements of ion and electron currents under the required conditions is shown in simplified form in Fig. 1. The filament F is suspended vertically and may be heated electrically. This is closely surrounded by the radial grid G and the latter by a cylindrical plate P in such a fashion that the axes of P and G coincide as nearly as possible with the filament. These are fixed in a Pyrex tube, and the whole surrounded on the outside by the solenoid S, likewise coaxial with F. By means of a suitable electrical system, G and P may be maintained at the

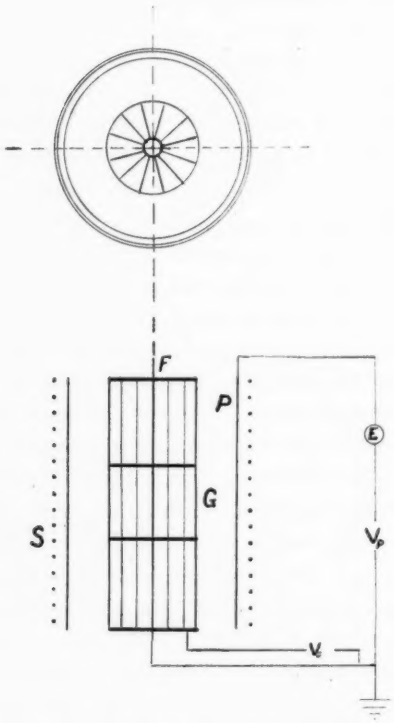

FIG. 1. Diagrammatic outline of electron tube.

potentials V_g and V_p, respectively, with $V_p > V_g > V_f = 0$. The flow of current to the plate may be determined by means of the galvanometer E, connected in series with P.

If the tube is filled with the carrier gas at a definite pressure and the filament temperature raised to a known value, ions and electrons will travel radially to the plate, where they are collected and recorded as a galvanometer deflection. If a current is now passed through the solenoid, the electrons will be deflected into the grid, while there will be no appreciable effect on the current to the plate due to the heavy ions. Therefore, the galvanometer deflections due to ions, Δ_i, and to electrons, Δ_e, may be independently determined under fixed conditions of P_r and T_a, and K and $-\Delta E_0$ evaluated in the manner presented above.

Details of the construction of the electron tube used in the measurements on chlorine are shown in Fig. 2.

The tube, made of Pyrex glass, consists of two parts: (1) the body D, which also serves as plate support, and (2) the grid-filament support, an inner tube A, fitted with a cap at its upper end, and having at its lower end a Nonex block B, in which are sealed the grid and filament leads. The inner tube fits into D, and the cap is united with D by sealing together the outer wall of the double-walled tube so formed. In addition, D, as shown, is fitted with an exhaust tube through which evacuation is accomplished, and with two smaller tubes sealed onto the shoulder. One was used for admission of the carrier gas, and the second was connected to two quartz fiber manometers, which allowed duplicate, independent measurements of the pressure of gas in the electron tube.

The exhaust tube is connected to a high vacuum line activated by a two-stage mercury diffusion pump with the required backing, and containing a carefully calibrated McLeod gauge. Liquid-nitrogen traps are placed at several points in the line to protect the tube from back diffusion of mercury vapor and the stopcock grease, Apiezon L. The last liquid-nitrogen trap is separated from the tube by an unlubricated stopcock, of the type operated by moving, with a magnet, a well-ground plunger to which a small glass-encased iron bar is attached. Between the tube and the chlorine, or $SnCl_4$, reservoir, there is placed a Pyrex capillary into which a fine tungsten wire can be inserted by means of a magnetic device. The plunger and the capillary allowed independent variation of the pressure of condensable gas in the tube with respect to the trap temperatures.

The construction of the quartz fiber manometer, used to measure the pressure in the tube itself, is shown in detail

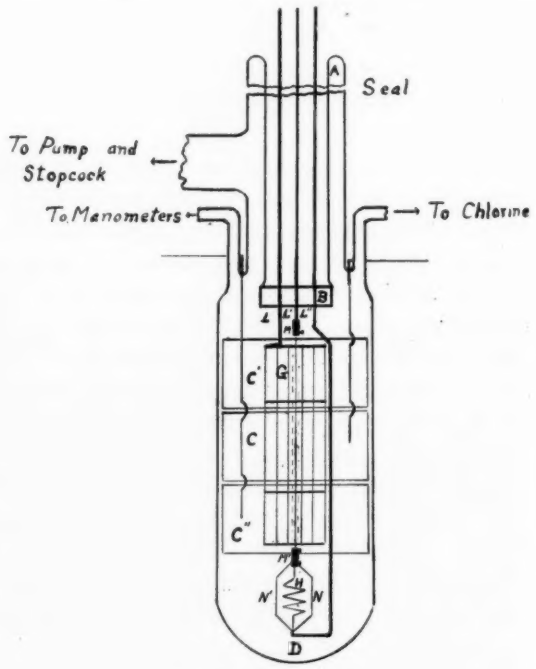

FIG. 2. Electron tube.

in Fig. 3. The fibers, of elliptical cross section so that they were constrained to vibrate in one plane, were fixed in position by sticking the heavy end into the molten tip of a short Pyrex rod which was later sealed to the wall of the tube. Near the lower end of the fiber, there was sealed to the wall a U-shaped rod carrying three short tungsten wires. The fibers are started vibrating by means of a hammer consisting of a glass-encased iron bar set into the tube on an axle of Pyrex rod, and operated magnetically. The time of decrement of the vibrations of the tip between the two tungsten wires W in front of the fiber, is measured, while W', behind the fiber, aids in eliminating errors due to parallax. This measurement is easily made by focusing an indirect source of illumination on the tip of the fiber, which then appears as a bright line decreasing in length as the amplitude of the vibration dies down. The manometers were surrounded by a bath of heavy mineral oil and were connected to the apparatus through an S-shaped glass tube, in order to damp undesirable modes of vibration which might be in resonance with natural frequencies in the clamping system. The fiber manometers were carefully calibrated against the McLeod gauge in various pressures of air, the calibration curves being accurately linear. As a check on the calibration, a pressure of mercury vapor was allowed to build up in the system by the warming of the liquid-nitrogen traps. The pressures as calculated from the temperature, and as read on the gauges, agreed to better than 0.1 micron. In practice, it was found that, in the range of the quartz fiber gauge, measurements of the same pressure carried out on the two manometers never differed by more than 5 percent, with an average discrepancy much less than this.

In the electron tube itself, as many of the metal parts as possible were constructed of silver coated with a thin layer of silver chloride, to reduce reaction with the chlorine atoms to a minimum. The collecting plate C, and the guard plates C' and C'' (4.9 cm in diameter and 2.5 cm long), of silver foil, were supported by tungsten leads sealed through small Nonex blocks in the shoulder of the tube. The grid-filament holder is formed of silver rod (2 mm in diameter), L, L', and L'', silver-soldered to nickel, which in turn was welded to the heavy tungsten leads. The tungsten portions are sealed in the Nonex block, which serves as a firm support from which the grid and filament are hung.

The grid G is formed of twelve rectangular, equally spaced silver vanes (8.0 cm long, 1.0 cm wide), arranged radially to form a cylinder 2.5 cm in diameter, with a cylindrical hole, 0.5 cm in diameter, through which the filament passes along the axis of the grid. The vanes fit snugly into four silver disks (1.5 cm in diameter, 0.125 cm thick). The grid is silver-soldered to L and supported by being attached to L'', from which it is electrically insulated.

The filament, of General Electric pure tungsten wire (9.80 cm long, 0.02 cm diam.), is tightly clamped by the silver connectors M and M'. M is silver-soldered to L', while M' is clamped to the upper end of a tungsten helix H,[9] which serves to keep the filament taut and in position when hot. The lower end of the helix is spot welded to L''. Silver wires N and N' are placed in parallel with the tungsten helix in order to decrease the electrical resistance of the lead.

The solenoid S surrounding the tube, consists of three windings of insulated copper wire (B.S. gauge No. 20) making thirty-one turns per centimeter on an insulated brass tube. Cooling water was continually passed through the space between the tube and the solenoid.

In order to determine precisely the temperature of the filament, it was necessary to measure accurately the potential drop across the filament, and the current flowing through it. The first of these was carried out directly using a potentiometric set-up, correction being made for the effect of the leads; the second, indirectly, as the potential drop across a standard 0.1 ohm resistance.

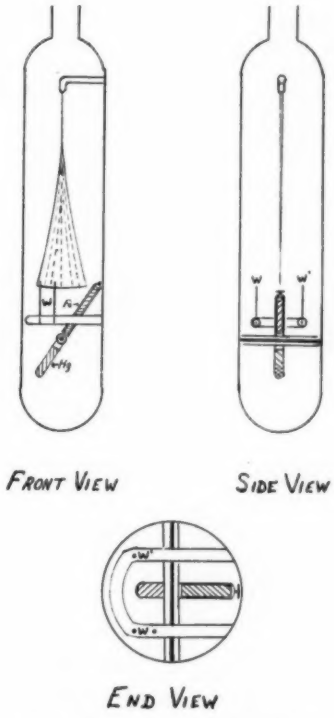

FIG. 3. Quartz fiber manometer.

The galvanometer used for the measurement of plate current was a Leeds and Northrup type HS with a sensitivity of 1.7×10^{-10} amp./mm. Equipped with an Ayrton shunt, currents as high as 10^{-3} amp. could be measured.

MATERIALS

The chlorine used was from the Ohio Chemical Company, and was purified with a view to removing foreign

[9] K. B. Blodgett and I. Langmuir, Rev. Sci. Inst. **5**, 321 (1934).

gases, especially fluorine. Any other impurities present would have a negligible effect on the measurements, except insofar as the pressure as read on the manometers would then no longer correspond to that of the chlorine in the system. The sample was fractionally distilled, with constant pumping, in a glass bead packed fractionating column (length 20 cm, diam. 2 cm) maintained at $-70°C$. The middle third fraction was stored in three-liter bulbs, from which portions could be condensed in small flasks and then sealed off from the remainder of the chlorine. These were connected to the electron tube through the capillary device mentioned above, by thin glass tubes which could be broken by moving a glass-encased iron bar with a magnet.

The stannic chloride was prepared by passing commercial chlorine over C.P. granulated tin cooled in a dry

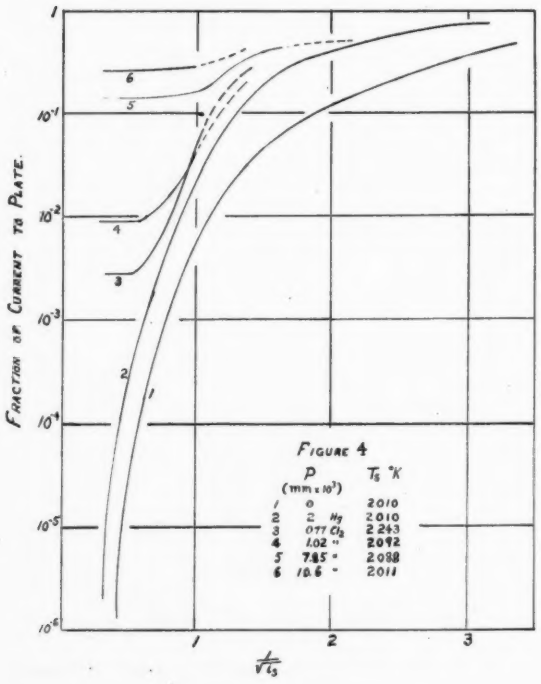

FIG. 4. Typical examples of the ratio of plate current to plate current at zero solenoid current for various conditions. The plate current fraction is plotted against the reciprocal square root of the solenoid current.

ice methyl alcohol mixture. The sample was fractionally distilled with constant pumping in a fractionating column (length 20 cm, diam. 2 cm), packed with glass beads and metallic tin maintained at a temperature of 0°C. The middle third fraction was stored in a glass bulb over metallic tin with a view to removing any last traces of chlorine which might have remained dissolved in the stannic chloride. It was connected to the electron tube through the capillary device by magnetic break-seals.

MEASUREMENTS

After the apparatus was assembled and tested for leaks, the electron tube was baked with an electric furnace at 450°C for twenty-four hours and the vacuum line baked with a hand torch, with constant pumping. After this process the pressure in the apparatus would not rise from $<10^{-6}$ to more than 10^{-4} mm after twenty-four hours. Before the measurements were made, the filament was aged by heating for several hours at 2600°K with continued pumping.

The measurements consisted of the observation of the plate current as a function of the solenoid current under various conditions of filament temperature and chlorine pressure.

The first set of observations was carried out in vacuum to determine the efficiency of the solenoid and grid in removing the electron current. The pressure of mercury in the apparatus was then allowed to build up to 2 microns of mercury and the measurements repeated (see Fig. 4). Thus it was assured that even in pressures of this magnitude, the electron current could be completely eliminated (to less than 10^{-5} of its original value), and that any ion current which persists unchanged with increasing solenoid current is due to heavy ions and not to collision-deflected electrons.

The same determinations were then carried out in known pressures of chlorine and $SnCl_4$ at various filament temperatures. The system was freed from mercury vapor by cooling the line traps with liquid nitrogen. The chlorine source was maintained at temperatures in the range $-70°C$ to $-100°C$ by a cooling bath, and the chlorine allowed to distill through the electron tube to a liquid-nitrogen trap. When stannic chloride was used the source was maintained at room temperature. In each case the pressure was varied by means of the capillary device, by changing the bath temperature, and by the size of the valve opening. Observations were made when the carrier gas pressure, as measured on the manometers, had reached a constant value with the filament at running temperature and the tube walls water-cooled. This procedure was repeated for various pressures and filament temperatures. Some of the measurements of plate current as a function of solenoid current are shown in graphical

form in Fig. 4, in terms of the fraction of that existing in the absence of the magnetic field.

It is seen from Eq. (9) that the most important experimental quantity, the accuracy of the measurement of which most affects the result, is the filament temperature T_s.

Essentially two independent functions of the voltage drop V across the filament and current A passing through it, may be used to determine the temperature of a filament of known length l and diameter d.[10] These are a quantity proportional to specific resistance, $R' = Vd^2/lA$, and one proportional to the energy loss per unit area, $W' = VA/dl$. The former is sensitive to the presence of impurities in the filament, whereas the latter is sensitive to the condition of the surface, the presence of gases in the surrounding space, and the presence of reflecting walls returning radiation to the filament.

Actually from measurements made in vacuum in the apparatus the discrepancy in the temperatures calculated from W' and R' amounted to as much as sixty degrees. This was due to reflection from the grid and plates. In another tube, without grid or plates, measurements showed agreement to better than twelve degrees or 0.6 percent in the temperatures calculated from the two functions. This was taken as evidence that the resistance function R' for the filament used was essentially that given in the tables.[10] In the actual measurements R' was used to determine the temperature of the filament. The total uncertainty in the temperature is considered to be less than one percent.

CALCULATIONS AND RESULTS

The results of the measurements in an atmosphere of chlorine gas are contained in Table I, and from them the value of the electron affinity was calculated for each set of measurements using Eq. (9). To each value there was assigned a weight which depended upon the constancy with which the temperature and pressure were maintained during the measurement. The values listed in Table I represent averages of several readings under the same conditions of T_s and P_{Cl_2}, but with differing plate and grid voltages.

The measurements recorded cover a temperature range from 1800°–2300°K, and a range of chlorine pressures from 5×10^{-4} to 1×10^{-2} mm Hg. Over these regions the electron current varied from 10^{-8} to 10^{-4} amp., and the ion current from 4×10^{-9} to 2×10^{-6} amp. The grid potential was maintained between +3 volts and +7 volts with respect to the filament, while the plate was usually kept 2 volts positive with respect to the grid. Over these ranges the calculated values of the electron affinity show no trend.

TABLE I. Electron affinity from measurements with Cl_2.

No.	T_s (°K)	P_{Cl_2} (mm $\times10^3$)	$100\frac{\Delta_{Cl^-}}{\Delta_{e^-}}$	$-\Delta E_0$	Wt.	No. of rdgs.
2	2330	2.11	0.438	85.19	3	3
5	2080	3.44	13.5	86.79	3	3
6	2070	10.6	48.0	86.92	2	4
7	2218	7.15	5.72	86.16	3	7
8	2149	7.85	17.9	87.57	2	3
9	1965	7.67	86.1	85.70	3	3
10	2028	7.35	51.2	86.75	3	4
11	2236	3.35	2.20	86.10	2	2
12	2232	3.52	2.06	85.44	2	2
13	2141	4.82	6.80	85.36	2	5
15	2089	2.92	2.85	81.50	1	3
16	2126	9.37	19.0	86.42	1	5
20	2196	6.27	4.20	85.20	3	3
21	2116	7.46	13.6	85.64	3	5
22	2030	7.34	35.0	85.67	3	3
25	1950	1.58	17.2	85.16	1	3
26	1859	1.37	52.3	85.36	1	4
27	2025	0.540	3.63	86.51	2	2
28	2022	0.824	6.05	86.70	3	3
29	2152	1.02	1.00	84.41	1	4
30	2229	0.773	0.389	84.84	1	4
31	2309	0.773	0.162	84.63	1	2
32	2381	1.18	0.170	84.92	1	3

Weighted Average 85.84 kcal.

The results of several measurements at higher temperatures are not listed in Table I. The method used here for separating the ion and electron currents and measuring them independently is based on the assumption that the plate current is not space-charge controlled. It was found experimentally that whenever the electron current exceeded 10^{-3} amp., a value of the negative ion current which remained unchanged with increasing solenoid current, could not be obtained. The extrapolation of the ratio $\Delta_{Cl^-}/\Delta_{e^-}$ to infinite solenoid current was uncertain by two to three hundred percent. That the difficulty was not to be attributed to incomplete removal of the electron current was indicated by the fact that a calculation of the electron affinity using the ratio $\Delta_{Cl^-}/\Delta_{e^-}$ obtained at the highest practical solenoid current gave values

[10] H. A. Jones and I. Langmuir, Gen. Elec. Rev. **419**, 310 (1927).

lower than those listed in Table I by as much as 10 percent. Under such conditions it appears that the ion current to the plate is less than would ordinarily be expected. It is probable that, at such high values of the electron current, the grid is not completely effective in removing the space charge, and that the chlorine ion current is, to a certain extent, space-charge controlled.

Disregarding the results of these measurements at high temperatures, the weighted average value for the electron affinity of chlorine from these measurements is 85.84 kcal./mole with an apparent average deviation of 0.10 kcal. (A.D.).

In Table II are given the results of 21 measurements using stannic chloride as carrier gas. The range of temperatures and pressures covered is not as great as with Cl_2. The averaged result 85.83 kcal./mole is in disturbingly good agreement with that obtained from the measurements using Cl_2.

TABLE II. Electron affinity from measurements with $SnCl_4$.

Run No.	T °K	P_{SnCl_4} (mm $\times 10^3$)	$100\frac{\Delta Cl^-}{\Delta_e^-}$	$-\Delta E_0$
1	2128	0.571	1.46	86.98
2	2027	0.732	5.37	86.69
3	2168	0.449	0.758	87.02
4	2077	0.577	2.71	87.21
5	1988	0.709	7.47	86.30
6	1912	0.792	2.06	86.12
7	1821	0.980	66.0	85.12
8	2102	0.676	2.00	86.44
9	2104	1.45	3.80	86.07
10	2013	1.85	12.9	85.91
11	1931	2.65	47.9	85.67
12	1850	3.10	148.0	85.34
13	2164	1.19	1.70	86.11
14	1963	2.54	26.0	85.00
15	2025	2.28	10.6	84.80
16	2082	2.64	6.63	84.84
17	2082	0.726	2.26	85.74
18	2079	0.501	1.55	85.56
19	1998	0.577	3.97	85.09
20	1922	0.749	14.7	85.52
21	1845	0.808	37.0	84.90
			Mean	85.83

In examining the probable accuracy of this value it can be seen from Eq. (9) that of the three observed quantities, T_s, P_r, and the ratio Δ_i/Δ_e, the experimental error in the determination of the currents and pressures contribute less to the error in the electron affinity than that introduced by the uncertainty in temperatures.

As discussed previously the error in temperatures is presumed not to exceed twenty degrees, or one percent, which contributes 0.8 kcal./mole error in the electron affinity.

The values of the ratio Δ_i/Δ_e, determined at a definite T_s and P_r, but at different plate and grid voltages, always agreed within 10 percent, with the exception of the experiments at very high temperatures mentioned above. An error of this magnitude leads to an uncertainty in the electron affinity of 0.4 kcal. The pressure of carrier gas as measured on the two quartz fiber gauges never differed by more than 5 percent, and it is believed certain that the pressure measurements are accurate to better than 10 percent, the uncertainty in the electron affinity from this source is 0.4 kcal. Thus the combined effect of the errors occurring in the measurements themselves yields an uncertainty in the value of the electron affinity given above of 1.0 kcal. Since it can be seen from Table I that, with the exceptions of runs 6, 8, 15, 28, and 29, the deviations of the individual runs from the mean value do not exceed this uncertainty, it is considered to be a satisfactory estimate.

Finally it may be pointed out that, in regard to the assumption of zero reflection coefficient, an error of 0.4 kcal. is introduced in the value for the electron affinity for a reflection coefficient of 0.1.

The value of the electron affinity reported here may be compared with the estimate of 92.7 kcal. given by Mitchell and Mayer[2] on the basis of experiments performed with an apparatus in which the metal parts were constructed of tantalum. Chemical reaction with the chlorine atoms led to the formation of some volatile chloride which later decomposed on the surface of the filament. This, of course, made the determination of filament temperatures very uncertain, and the calculated values of the electron affinity were dependent upon the time for which the filament had been exposed to chlorine. In previous experiments, using tantalum, for the determination of the electron affinity of iodine[1] (72.4 kcal.) and bromine[3] (80.04 kcal.), this difficulty was not encountered. In the present research, in which the metal parts were constructed of silver coated with silver chloride, reaction occurred to only a slight extent. The volatility of silver chloride is very much less than that of tantalum chloride, and there was no indication of deposition on the filament.

The determined value of the electron affinity, 85.84 kcal., may further be compared with those obtained from measurements on the dissociation of alkali halides; 86.6,[11,12] and 88.3[13] kcal., and further with those calculated using theoretical lattice energies and the Born cycle; 92.2,[14] 86.5,[15] 83.0,[16] and 85.1[17] kcal.

[11] N. K. Saha and A. H. Tandon, Proc. Nat. Inst. Sci. Ind. **3**, 287 (1937).
[12] A. H. Tandon, Indian J. Phys. **11**, 99 (1937).
[13] L. Helmholz and J. E. Mayer, J. Chem. Phys. **2**, 245 (1934).
[14] A. E. Van Arkel and J. H. de Boer, Physica **7**, 12 (1927).
[15] J. E. Mayer and L. Helmholz, Zeits. f. Physik **75**, 19 (1932).
[16] E. J. W. Verwey and J. H. de Boer, Rec. trav. chim. **55**, 431 (1936).
[17] M. L. Huggins, J. Chem. Phys. **5**, 143 (1937).

FEBRUARY, 1943 JOURNAL OF CHEMICAL PHYSICS VOLUME 11

The Relation between ζ-Potential and the Electrical Capacity of the Double Layer

W. G. Eversole and Charles R. Estee
Division of Physical Chemistry, State University of Iowa, Iowa City, Iowa

(Received November 5, 1942)

The usual calculation of the electrical capacity of the double layer from ζ-potentials is in error because (1) the electrogravitational plane of the outer charge is not at a distance $1/\kappa$ and (2) the inner charge is not in the ζ-potential plane. An equation is derived which makes allowance for the distribution of charge on both sides of the ζ-potential plane. Calculations from ζ-potentials of glass in dilute aqueous solutions of simple salts give values which increase from about 1μf/cm² at 10^{-5} molar to about 25μf/cm² at high salt concentrations (1 molar). The equations are related qualitatively to electrocapillary phenomena.

In recent articles in this journal[1] some of the electrical properties of the double layer have been discussed on the basis of certain simplifying assumptions, most of which are classical. These assumptions are essentially as follows:

(1) The curvature of the surface is negligible in comparison with the thickness of the double layer.

(2) The surface of the solid generally carries a charge which results either from exchange of potential determining ions, or from adsorption of other ions from the solution, or both.

(3) That beyond some point near the solid surface only electrical and kinetic energy need be considered in determining the distribution of charge and the potential in the solution. At this point the distance X is taken as zero and the potential ψ is called ψ^0. The plane $X=0$ has been considered as lying at the outer edge of a monomolecular layer of adsorbed ions and water molecules at the solid surface.

(4) ψ^0 is independent of the concentration of the salt solution (except at the very lowest concentrations) unless the salt contains strongly adsorbed ions or potential determining ions.

(5) The electrokinetic potential ζ is the potential at the distance $X=t$. t is the thickness of the immobilized liquid layer. This is considered to be a layer between the ψ^0 and ζ-potential planes which does not move in ordinary viscous flow but which does permit free diffusion and ion migration. This is analogous to the condition of water in a gel where viscous flow has disappeared but diffusion and ion migration are practically unretarded. Indeed, a gel may perhaps be considered as a capillary system in which t is approximately equal to the capillary radius.

The equations which have been derived previously[2] for binary salts and which are required for further calculations are as follows:*

$$\Pi = -2nZ\epsilon \sinh 2\bar{\psi}, \qquad (1)$$

[1] W. G. Eversole *et al.*, J. Chem. Phys. **9**, 530, 798 (1941); **10**, 78, 460 (1942).

[2] W. G. Eversole and P. H. Lahr, J. Chem. Phys. **9**, 530 (1941).

* All relations involving hyperbolic functions used in this and previous papers, as well as tables for numerical computations, can be found in B. O. Peirce, *A Short Table of Integrals* (Ginn and Company, Boston, 1929).

$$\ln \tanh \bar{\psi}/2 = \ln \tanh \bar{\psi}^0/2 - \kappa X, \quad (2)$$

$$\ln \tanh \bar{\zeta}/2 = \ln \tanh \bar{\psi}^0/2 - \kappa t. \quad (3)$$

Equation (1) expresses the density of the space charge in the solution Π as a function of the concentration of the solution n, the charge on the ions $Z\epsilon$, and the dimensionless ratio $\bar{\psi}$ $(=Z\epsilon\psi/2kT)$. Equation (2) expresses $\bar{\psi}$ as a function of $\bar{\psi}^0$ $(=Z\epsilon\psi^0/2kT)$, $\kappa=(8\pi nZ^2\epsilon^2/DkT)^{\frac{1}{2}}$, and X. Similarly Eq. (3) expresses $\bar{\zeta}$ $(=Z\epsilon\zeta/2kT)$ as a function of $\bar{\psi}^0$, κ, and t. As previously, only magnitudes of charges and potentials are considered.

Equation (2) may be solved for X to give

$$X=(1/\kappa)(\ln \tanh \bar{\psi}^0/2 - \ln \tanh \bar{\psi}/2). \quad (4)$$

Differentiating (ψ^0 and κ const.)

$$dX = -(1/\kappa)\ \mathrm{csch}\ \bar{\psi} d\bar{\psi}. \quad (5)$$

The total charge in the ion atmosphere beyond the ζ-potential plane is

$$\sigma_t = \int_{\bar{\psi}=\bar{\zeta}}^{\bar{\psi}=0} \Pi dX. \quad (6)$$

Substituting for Π and dX from Eqs. (1) and (5) and integrating

$$\sigma_t = -(4nZ\epsilon/\kappa)\sinh \bar{\zeta}. \quad (7)$$

Similarly the total charge in the ion atmosphere from $X=0$ to $X=\infty$ is

$$\sigma_0 = -(4nZ\epsilon/\kappa)\sinh \bar{\psi}^0. \quad (8)$$

The negative sign merely indicates that the sign of the charge is opposite to that of the charge in the solid wall.

The location of the electrogravitational plane of the charge σ_t is given by

$$\delta' = (1/\sigma_t)\int_{\bar{\psi}=\bar{\zeta}}^{\bar{\psi}=0} X\Pi dX. \quad (9)$$

This is the average distance of the charge σ_t from the ψ^0 plane. Substituting for X, Π, and dX from Eqs. (1), (4), and (5)

$$\delta' = \frac{4nZ\epsilon}{\sigma_t\kappa^2}\int_{\bar{\zeta}}^{0} (\ln \tanh \bar{\psi}^0/2 - \ln \tanh \bar{\psi}/2) \cosh \bar{\psi}\, d\bar{\psi}. \quad (10)$$

Integrating by parts

$$\delta' = \frac{4nZ\epsilon}{\sigma_t\kappa^2}[(\ln \tanh \bar{\psi}^0/2 - \ln \tanh \bar{\psi}/2) \times \sinh \bar{\psi} + \bar{\psi}]_{\bar{\zeta}}^{0}. \quad (11)$$

Introducing the limits and substituting from Eqs. (3) and (7)

$$\delta' = t + (1/\kappa)\frac{\bar{\zeta}}{\sinh \bar{\zeta}}. \quad (12)$$

Thus the average distance of the charge σ_t from the ζ-potential plane is less than $1/\kappa$ except for very small values of $\bar{\zeta}$.

In addition to the charge σ_t in the solution beyond the ζ-potential plane, there is an equal net charge of the opposite sign inside the ζ-potential plane. This consists of a charge σ_0 of opposite sign on the surface of the solid or in the adsorption layer, and a charge $\sigma_0-\sigma_t$ of the same sign as σ_t in the immobilized layer between the ψ^0 and ζ-potential planes.

The location of the electrogravitational plane of the charge $\sigma_0-\sigma_t$ is given by

$$\delta = \frac{1}{\sigma_0-\sigma_t}\int_{\bar{\psi}=\bar{\psi}^0}^{\bar{\psi}=\bar{\zeta}} X\Pi dX. \quad (13)$$

This is evaluated from Eq. (11) by replacing σ_t by $\sigma_0-\sigma_t$ and changing the limits of integration to $\bar{\psi}^0$ and $\bar{\zeta}$.

$$\delta = -\frac{4nZ\epsilon}{(\sigma_0-\sigma_t)\kappa^2}[\bar{\psi}^0 - (\ln \tanh \bar{\psi}^0/2 - \ln \tanh \bar{\zeta}/2)\sinh \bar{\zeta} - \bar{\zeta}]. \quad (14)$$

Substituting from Eqs. (3), (7), and (8)

$$\delta = (1/\kappa)\left(\frac{\bar{\psi}^0 - \bar{\zeta} - \kappa t \sinh \bar{\zeta}}{\sinh \bar{\psi}^0 - \sinh \bar{\zeta}}\right). \quad (15)$$

The electrogravitational plane of the charge σ_0 on the surface of the solid is behind the ψ^0 plane. However, at least for a non-conducting solid, it is probably in the monomolecular adsorption layer between the solid surface and the ψ^0 plane. Therefore since the electrical effects are being measured in terms of ζ-potentials, it is probable that no serious error will be introduced by

assuming that the charge σ_0 is in the ψ^0 plane. If t is large, the error in this assumption will be correspondingly less. The assumption is more questionable in the case of a conducting solid where there may be a distribution of charge in the solid, either induced by the adsorption of non-potential determining ions, or present in the solid as a result of the transfer of potential determining ions.

The electrogravitational plane (δ'') of the composite charge σ_0 at $X=0$ and $\sigma_0-\sigma_t$ at $X=\delta$, is given by

$$\sigma_0\delta''=(\sigma_0-\sigma_t)(\delta-\delta'') \tag{16}$$

or

$$\delta''=\frac{\sigma_0-\sigma_t}{2\sigma_0-\sigma_t}\delta. \tag{17}$$

Substituting from Eqs. (7), (8), and (15)

$$\delta''=\frac{1}{\kappa}\left(\frac{\bar{\psi}^0-\bar{\zeta}-\kappa t\sinh\bar{\zeta}}{2\sinh\bar{\psi}^0-\sinh\bar{\zeta}}\right). \tag{18}$$

From the standpoint of ζ-potential, therefore, the double layer may be considered to be a condenser with the excess charge σ_t on either side of the ζ-potential plane collected on the plates at

TABLE I. Characteristic distances in angstrom units for solutions of KCl in contact with glass. ($\psi^0=77$ mv : $t=30$).

Conc. μ moles/l.	ζ mv	δ'	δ''	$\delta'-\delta''$	$1/\kappa$
10	73	732	6.2	726	964.
25	72	477	0.8	476	610.
50	70	352	1.4	351	431.
100	67	263	2.8	260	305.
250	62	183	3.3	180	193.
500	58	141	2.7	138	136.
1000	52	112	3.2	109	96.
10^6	0	33	1.0	32	3.

δ' and δ''. It should be kept in mind that such a condenser will duplicate the actual potential of the double layer at $X=t$ but not at any other distance. In fact the straight line representing the field in the condenser is tangent to the actual potential curve in the double layer at the point $X=t$.

Substituting from Eqs. (12) and (18) into the condenser formula, the capacity of this hypothetical condenser is

$$C=D\div\left\{4\pi\left[t+\frac{1}{\kappa}\left(\frac{\bar{\zeta}}{\sinh\bar{\zeta}}-\frac{\bar{\psi}^0-\bar{\zeta}-\kappa t\sinh\bar{\zeta}}{2\sinh\bar{\psi}^0-\sinh\bar{\zeta}}\right)\right]\right\}. \tag{19}$$

Equations (12), (18), and (19) may be extrapolated to high salt concentrations by assuming

TABLE II. The electrical capacity of the glass surface in contact with aqueous salt solutions.

Conc. μ moles/l.	Capacity μf/cm² LiCl	KCl	CsCl	$\frac{D\kappa}{4\pi}$
10	1.0	0.9	—	0.7
25	1.5	1.4	1.3	1.1
50	2.1	2.0	1.8	1.6
100	2.8	2.7	2.5	2.3
250	4.1	3.8	3.6	3.6
500	5.4	5.0	4.6	5.1
1000	6.9	6.4	5.8	7.2
10^6	29.	23.	19.	227.

that $\bar{\psi}^0$ and t remain unchanged while $\bar{\zeta}$ becomes negligibly small giving

$$\delta'=t+\frac{1}{\kappa}, \tag{20}$$

$$\delta''=-\frac{1}{\kappa}\frac{\bar{\psi}^0}{2\sinh\bar{\psi}^0}, \tag{21}$$

and

$$C=D\div\left\{4\pi\left[t+\frac{1}{\kappa}\left(1-\frac{\bar{\psi}^0}{2\sinh\bar{\psi}^0}\right)\right]\right\}. \tag{22}$$

Results calculated from experimental data by means of these equations are given in Tables I and II. All calculations were made from the data of Kruyt and van der Willigen[3] for a glass surface in contact with dilute ($10^{-5}-10^{-3}$ molar) solutions of simple salts. The ψ^0 and t values used were those calculated previously[4] from the same data. While no allowance for surface conductivity was made in these data it is probable that the error is small except at the lowest concentrations. The value used for the dielectric constant was 78.8 and Eqs. (20), (21), and (22) were used for the 1-molar solutions only.

[3] H. R. Kruyt and P. C. van der Willigen, Kolloid Zeits. **45**, 307 (1929).

[4] W. G. Eversole and W. W. Boardman, J. Chem. Phys. **9**, 798 (1941).

The results given in Table I illustrate the magnitudes of the distances involved in the double layer. It will be noted that δ'' is almost negligible in comparison with δ' except at the 1-molar concentration. However, this is not true for smaller values of ψ^0 and t. While $1/\kappa$ is not equal to $\delta'-\delta''$ except at one concentration, it is similar in magnitude except at relatively high concentrations.

Table II gives values of the capacity of the double layer for the glass surface in contact with solutions of simple salts. The values of the capacity $D\kappa/4\pi$ are given in the same units for comparison. The greatest quantitative discrepancy is obviously at the 1-molar concentration where the value in the last column is approximately ten times the others.

Such unreasonably high values of the capacity in concentrated solutions have led to doubt as to the validity of the entire theory of the diffuse double layer. These high values of C result very largely from the assumption that the inner charge σ_i is located in the ζ-potential plane rather than at δ''. At low concentrations this difference $t-\delta''$ is relatively unimportant but at high concentrations it represents most of the thickness of the double layer.

While it might be expected that Eqs. (19) and (22) would give a good approximation of the capacity of the "outer" double layer at a nonconducting surface, it does not necessarily follow that they would give the "total" capacity as determined, for example, by direct measurement using a conducting solid. Accordingly, it is perhaps a surprising coincidence that the values calculated for the 1-molar solutions are very similar in magnitude to the measured capacities of a mercury surface in contact with similar solutions.

Probably of much greater significance is the dependence of the capacity on $\bar{\psi}^0$ as expressed by Eq. (22). This equation predicts a maximum capacity at $\bar{\psi}^0=0$. The height of this maximum will depend on the values of D, t, and $1/\kappa$, but the width is a function of $\bar{\psi}^0$ only and is determined by the narrow range of values of ψ^0 in which $\bar{\psi}^0/2\sinh\bar{\psi}^0$ differs appreciably from zero. Physically this maximum results mainly from a shift of the inner plate of the condenser [Eq. (21)] to larger values of X for small values of $\bar{\psi}^0$.

This is exactly the type of maximum, aptly described by Grahame[5] as a "hump," which occurs in the measured capacity of the mercury surface at or near the electrocapillary maximum. This "hump" may provide a means of locating, at least approximately, the "electrocapillary maximum" of solid metals.

The width of this maximum in the experimental curves[5] suggests that the change in ψ^0 may be nearly equal to the change in the applied potential. The displacement of the capacity maximum with respect to the surface tension maximum suggests as clearly that the ψ^0-plane does not coincide with the analogous plane which relates the electrical charge to the surface tension of the metal. Therefore, when the two maxima do coincide, as they very nearly do for mercury in contact with 1-molar $NaNO_3$, the condition may reasonably be assumed to be one of electrical neutrality in both phases as well as in the boundary layer.

The maximum capacity of the surface at $\psi^0=0$ is further evidence of the fundamental significance of t. If t were equal to zero, the ψ^0 and ζ-potential planes would coincide and therefore ψ^0 and ζ would be identical. If this were the case, the distance between the plates of the condenser representing the double layer would be $(1/\kappa)(\bar{\psi}^0/\sinh\bar{\psi}^0)$ [Eq. (12)]. This would require a minimum rather than a maximum capacity at $\psi^0=0$, and, further, the capacity would rapidly approach infinity for increasing values of ψ^0.

The qualitative implications of Eq. (22) are rather far reaching. However, large quantitative discrepancies should be expected to result from complications which were not taken into account in the present highly simplified derivation. Some of the complicating reactions at the mercury surface have been discussed by Grahame.[5]

[5] D. C. Grahame, J. Am. Chem. Soc. **63**, 1207 (1941).

Statistical Lengths of Rubber-Like Hydrocarbon Molecules

FREDERICK T. WALL
Noyes Chemical Laboratory, University of Illinois, Urbana, Illinois
(Received November 16, 1942)

The root mean square lengths of *trans*-, *cis*-, and random rubber-like hydrocarbon molecules are calculated. These results are compared with the maximum possible lengths of the *trans*- and *cis*-varieties and interpreted from the point of view of recent theories of rubber elasticity. It is found that the *cis*-structure should be more elastic than the *trans*-structure but the calculated difference is not large. The theory is probably sufficient to account for the properties of polychloroprene as compared to natural rubber, but stearic forces are necessary to explain the lack of elasticity in balata or gutta-percha.

INTRODUCTION

IT has been known for some time that the pure hydrocarbons of balata (or gutta-percha) and natural rubber have the same chemical composition and chemical properties.[1] Both balata and rubber appear to be polymers of isoprene, $(C_5H_8)_n$, with the same degree of unsaturation. Their physical properties are sufficiently different, however, to make it clear that their structures must differ in some important respect. Since the molecules contain numerous double bonds, it has been suggested that rubber and balata are geometric isomers.

Every fourth bond in a rubber or balata molecule is a double bond, so it follows that the possibilities for geometric isomerism are considerable. It was proposed by Meyer and Mark[2] that the natural rubber hydrocarbon has a structure for which the molecular chain is *cis* with respect to all of the double bonds. Balata (or gutta-percha) is then supposed to have a *trans*-structure throughout, this view having been verified by Fuller[3] and Bunn.[4] It is the purpose of the present paper to consider, from the point of view of recent theories of rubber elasticity,[5] to what extent these structures explain the differences in physical properties. The method to be employed will involve the calculation of the root mean square lengths of the *cis*- and *trans*-structures, which when compared to their maximum lengths should give an indication of their extensibilities.

In 1932 Eyring[6] treated the problem of the average square length of a hydrocarbon chain. In the present paper a different derivation of Eyring's equation will be given (for illustrative purposes), after which this derivation will be extended to the rubber-like molecules with double bonds.

SATURATED HYDROCARBON CHAIN

Consider an unbranched hydrocarbon chain containing n carbon-carbon bonds each of length σ and each making an angle α with the extension of an adjacent bond (Fig. 1). Let us represent the bonds by vectors, $\boldsymbol{\sigma}_1, \boldsymbol{\sigma}_2, \boldsymbol{\sigma}_3, \cdots, \boldsymbol{\sigma}_n$, and let

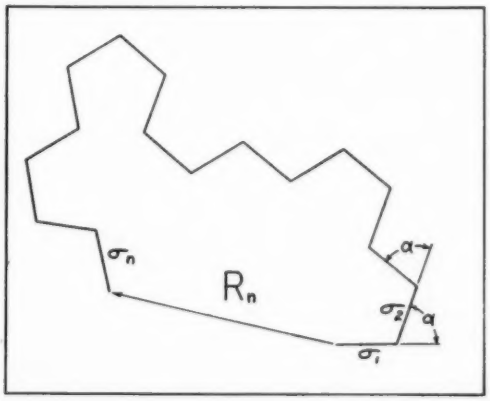

FIG. 1. Saturated hydrocarbon chain.

[1] For a general discussion see H. L. Fisher and R. H. Gerke, *Chemistry and Technology of Rubber*, edited by C. C. Davis and J. T. Blake (Reinhold Publishing Company, New York, 1937), chapter 3.
[2] Meyer and Mark, *Der Aufban der Hochpolymeren Organischen Naturstoffe* (Leipzig, 1930).
[3] C. S. Fuller, Ind. Eng. Chem. **28**, 907 (1936).
[4] C. W. Bunn, Proc. Roy. Soc. **A180**, 40 (1942).
[5] E. Guth and H. M. James, Ind. Eng. Chem. **33**, 624 (1941); F. T. Wall, J. Chem. Phys. **10**, 132, 485 (1942).
[6] H. Eyring, Phys. Rev. **39**, 746 (1932). See also Bresler and Frenkel, Acta Physicochemica U. S. S. R. **11**, 485 (1939).

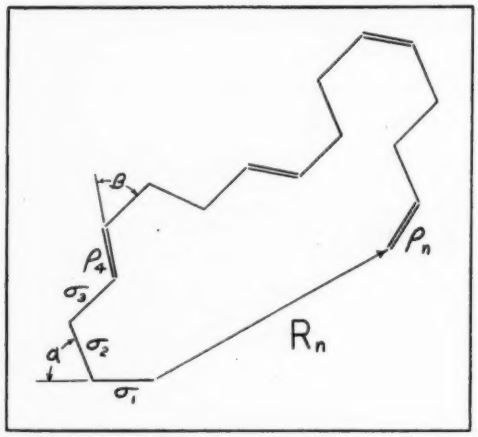

FIG. 2. Random rubber-like molecular chain.

$\mathbf{R}_n$ be the vector joining the first and last carbon atoms. Then

$$\mathbf{R}_n=\boldsymbol{\sigma}_1+\boldsymbol{\sigma}_2+\boldsymbol{\sigma}_3+\cdots\boldsymbol{\sigma}_n. \tag{1}$$

From (1) it follows that

$$\begin{aligned}\mathbf{R}_n^2=&\boldsymbol{\sigma}_1^2+\boldsymbol{\sigma}_2^2+\boldsymbol{\sigma}_3^2+\cdots\boldsymbol{\sigma}_n^2\\&+2(\boldsymbol{\sigma}_1\cdot\boldsymbol{\sigma}_2+\boldsymbol{\sigma}_2\cdot\boldsymbol{\sigma}_3+\cdots\boldsymbol{\sigma}_{n-1}\cdot\boldsymbol{\sigma}_n)\\&+2(\boldsymbol{\sigma}_1\cdot\boldsymbol{\sigma}_3+\boldsymbol{\sigma}_2\cdot\boldsymbol{\sigma}_4+\cdots\boldsymbol{\sigma}_{n-2}\cdot\boldsymbol{\sigma}_n)+\cdots\\&+2(\boldsymbol{\sigma}_1\cdot\boldsymbol{\sigma}_{n-1}+\boldsymbol{\sigma}_2\cdot\boldsymbol{\sigma}_n)+2(\boldsymbol{\sigma}_1\cdot\boldsymbol{\sigma}_n).\end{aligned} \tag{2}$$

But

$$\boldsymbol{\sigma}_1^2=\boldsymbol{\sigma}_2^2=\boldsymbol{\sigma}_3^2=\cdots\boldsymbol{\sigma}_n^2=\sigma^2 \tag{3}$$

and

$$\boldsymbol{\sigma}_1\cdot\boldsymbol{\sigma}_2=\boldsymbol{\sigma}_2\cdot\boldsymbol{\sigma}_3=\cdots=\boldsymbol{\sigma}_{n-1}\cdot\boldsymbol{\sigma}_n=\sigma^2\cos\alpha. \tag{4}$$

Moreover, if there is perfectly free rotation about the various bonds, then

$$\langle\boldsymbol{\sigma}_1\cdot\boldsymbol{\sigma}_{1+j}\rangle_{Av}=\langle\boldsymbol{\sigma}_2\cdot\boldsymbol{\sigma}_{2+j}\rangle_{Av}=\cdots\langle\boldsymbol{\sigma}_{n-j}\cdot\boldsymbol{\sigma}_n\rangle_{Av}. \tag{5}$$

Letting R_n equal the root mean square length, we have

$$\begin{aligned}R_n^2=\langle\mathbf{R}_n^2\rangle_{Av}=&n\sigma^2+2(n-1)\sigma^2\cos\alpha\\&+2(n-2)\langle\boldsymbol{\sigma}_1\cdot\boldsymbol{\sigma}_3\rangle_{Av}\\&+2(n-3)\langle\boldsymbol{\sigma}_1\cdot\boldsymbol{\sigma}_4\rangle_{Av}+\cdots2\langle\boldsymbol{\sigma}_1\cdot\boldsymbol{\sigma}_n\rangle_{Av}.\end{aligned} \tag{6}$$

To evaluate $\langle\boldsymbol{\sigma}_1\cdot\boldsymbol{\sigma}_{1+j}\rangle_{Av}$ note that the component of $\boldsymbol{\sigma}_{1+j}$ on $\boldsymbol{\sigma}_j$ is $\sigma\cos\alpha$. Similarly the *average* component of $\boldsymbol{\sigma}_{1+j}$ on $\boldsymbol{\sigma}_{j-1}$ will be $\sigma\cos^2\alpha$, etc. Hence

$$\langle\boldsymbol{\sigma}_1\cdot\boldsymbol{\sigma}_{1+j}\rangle_{Av}=\sigma^2\cos^j\alpha \tag{7}$$

and

$$\begin{aligned}R_n^2=&n\sigma^2+2(n-1)\sigma^2\cos\alpha\\&+2(n-2)\sigma^2\cos^2\alpha+\cdots2\sigma^2\cos^{n-1}\alpha.\end{aligned} \tag{8}$$

Upon rearranging (8) there is obtained

$$\frac{1}{n\sigma^2}R_n^2=\frac{1+\cos\alpha}{1-\cos\alpha}-\frac{2\cos\alpha}{n}\left\{\frac{1-\cos^n\alpha}{(1-\cos\alpha)^2}\right\}. \tag{9}$$

If n is large, Eq. (9) can be replaced by the approximate equation

$$(1/n\sigma^2)R_n^2\doteq(1+\cos\alpha)/(1-\cos\alpha), \tag{10}$$

which result was used by Guth and James[5] and others in connection with the statistical theory of rubber elasticity.

RUBBER-LIKE MOLECULES

The above derivation will now be generalized and applied to molecules of the rubber type. Three cases will be considered: first, it will be assumed that the chain is *trans* throughout, next, it will be supposed that the chain is *cis*, and finally, it will be imagined that it is sometimes *trans* and sometimes *cis* in a perfectly random way.

Let the molecular chain under consideration be made up of n vectors $\boldsymbol{\sigma}_1$, $\boldsymbol{\sigma}_2$, $\boldsymbol{\sigma}_3$, $\boldsymbol{\rho}_4$, $\cdots$, where the $\boldsymbol{\sigma}$'s refer to single bonds and the $\boldsymbol{\rho}$'s to double bonds (Fig. 2). Once more let α be the angle between a single bond and the extension of an adjacent single bond, and let β be the angle between a double bond and the extension of an adjacent (single) bond. Let $\mathbf{R}_n$ be the vector joining the first and last carbon atoms of the chain. Then

$$\mathbf{R}_n=\boldsymbol{\sigma}_1+\boldsymbol{\sigma}_2+\boldsymbol{\sigma}_3+\boldsymbol{\rho}_4+\boldsymbol{\sigma}_5+\cdots \tag{11}$$

and

$$\begin{aligned}\mathbf{R}_n^2=&\boldsymbol{\sigma}_1^2+\boldsymbol{\sigma}_2^2+\boldsymbol{\sigma}_3^2+\boldsymbol{\rho}_4^2+\boldsymbol{\sigma}_5^2+\cdots\\&+2(\boldsymbol{\sigma}_1\cdot\boldsymbol{\sigma}_2+\boldsymbol{\sigma}_2\cdot\boldsymbol{\sigma}_3+\boldsymbol{\sigma}_3\cdot\boldsymbol{\rho}_4+\boldsymbol{\rho}_4\cdot\boldsymbol{\sigma}_5+\cdots)\\&+2(\boldsymbol{\sigma}_1\cdot\boldsymbol{\sigma}_3+\boldsymbol{\sigma}_2\cdot\rho_4+\boldsymbol{\sigma}_3\cdot\boldsymbol{\sigma}_5+\boldsymbol{\rho}_4\cdot\boldsymbol{\sigma}_6+\cdots)\\&+2(\boldsymbol{\sigma}_1\cdot\boldsymbol{\rho}_4+\boldsymbol{\sigma}_2\cdot\boldsymbol{\sigma}_5+\boldsymbol{\sigma}_3\cdot\boldsymbol{\sigma}_6+\boldsymbol{\rho}_4\cdot\boldsymbol{\sigma}_7+\cdots)\\&+2(\boldsymbol{\sigma}_1\cdot\boldsymbol{\sigma}_5+\boldsymbol{\sigma}_2\cdot\boldsymbol{\sigma}_6+\boldsymbol{\sigma}_3\cdot\boldsymbol{\sigma}_7+\boldsymbol{\rho}_4\cdot\boldsymbol{\rho}_8+\cdots)\\&+\cdots.\end{aligned} \tag{12}$$

It is readily seen from the model that many of

the products which appear in (12) are equivalent, for example,

$$\boldsymbol{\sigma}_1\cdot\boldsymbol{\sigma}_2=\boldsymbol{\sigma}_2\cdot\boldsymbol{\sigma}_3=\boldsymbol{\sigma}_5\cdot\boldsymbol{\sigma}_6=\cdots$$

$$\langle\boldsymbol{\sigma}_1\cdot\boldsymbol{\sigma}_3\rangle_{Av}=\langle\boldsymbol{\sigma}_5\cdot\boldsymbol{\sigma}_7\rangle_{Av}=\cdots,$$

$$\boldsymbol{\sigma}_3\cdot\boldsymbol{\varrho}_4=\boldsymbol{\varrho}_4\cdot\boldsymbol{\sigma}_5=\boldsymbol{\sigma}_7\cdot\boldsymbol{\varrho}_8=\cdots, \quad \text{etc.} \tag{13}$$

Introducing relationships (13) into (12), and making an approximation equivalent to going from Eq. (9) to Eq. (10), there is obtained the following approximate equation valid for large values of n.

$$\begin{aligned}\frac{1}{n}R_n^2=&\tfrac{3}{4}\sigma^2+\tfrac{1}{4}\rho^2+(\boldsymbol{\sigma}_1\cdot\boldsymbol{\sigma}_2+\boldsymbol{\sigma}_3\cdot\boldsymbol{\varrho}_4)\\&+\tfrac{1}{2}(\langle\boldsymbol{\sigma}_1\cdot\boldsymbol{\sigma}_3\rangle_{Av}+2\langle\boldsymbol{\sigma}_2\cdot\boldsymbol{\varrho}_4\rangle_{Av}+\langle\boldsymbol{\sigma}_3\cdot\boldsymbol{\sigma}_5\rangle_{Av})\\&+(\langle\boldsymbol{\sigma}_1\cdot\boldsymbol{\varrho}_4\rangle_{Av}+\langle\boldsymbol{\sigma}_2\cdot\boldsymbol{\sigma}_5\rangle_{Av})\\&+\tfrac{1}{2}(3\langle\boldsymbol{\sigma}_1\cdot\boldsymbol{\sigma}_5\rangle_{Av}+\langle\boldsymbol{\varrho}_4\cdot\boldsymbol{\varrho}_8\rangle_{Av})\\&+(\langle\boldsymbol{\sigma}_1\cdot\boldsymbol{\sigma}_6\rangle_{Av}+\langle\boldsymbol{\sigma}_3\cdot\boldsymbol{\varrho}_8\rangle_{Av})+\cdots.\end{aligned} \tag{14}$$

But by a generalization of the method used for the hydrocarbon chain, it is seen that

$$\begin{aligned}\boldsymbol{\sigma}_1\cdot\boldsymbol{\sigma}_2&=\sigma^2\cos\alpha,\\ \boldsymbol{\sigma}_3\cdot\boldsymbol{\varrho}_4&=\sigma\rho\cos\beta,\\ \langle\boldsymbol{\sigma}_1\cdot\boldsymbol{\sigma}_3\rangle_{Av}&=\sigma^2\cos^2\alpha,\\ \langle\boldsymbol{\sigma}_2\cdot\boldsymbol{\varrho}_4\rangle_{Av}&=\sigma\rho\cos\alpha\cos\beta,\\ \langle\boldsymbol{\sigma}_1\cdot\boldsymbol{\varrho}_4\rangle_{Av}&=\sigma\rho\cos^2\alpha\cos\beta,\end{aligned} \tag{15}$$

and

$$\langle\boldsymbol{\varrho}_4\cdot\boldsymbol{\varrho}_8\rangle_{Av}=\rho^2\cos^2\alpha\cos^2\beta.$$

Equations (15) are true whether the chain is *cis*, *trans*, or random. The other averages which appear in (14) depend upon the nature of the chain and will be given by expressions of the following type.

$$\begin{aligned}\langle\boldsymbol{\sigma}_3\cdot\boldsymbol{\sigma}_5\rangle_{Av}&=\sigma^2 && (\textit{trans})\\ &=\sigma^2\cos 2\beta && (\textit{cis})\\ &=\sigma^2\cos^2\beta, && (\text{random})\\ \langle\boldsymbol{\sigma}_2\cdot\boldsymbol{\sigma}_5\rangle_{Av}&=\sigma^2\cos\alpha && (\textit{trans})\\ &=\sigma^2\cos\alpha\cos 2\beta && (\textit{cis})\\ &=\sigma^2\cos\alpha\cos^2\beta, && (\text{random})\\ \langle\boldsymbol{\sigma}_1\cdot\boldsymbol{\sigma}_5\rangle_{Av}&=\sigma^2\cos^2\alpha && (\textit{trans})\\ &=\sigma^2\cos^2\alpha\cos 2\beta && (\textit{cis})\\ &=\sigma^2\cos^2\alpha\cos^2\beta. && (\text{random})\end{aligned} \tag{16}$$

Moreover, for terms like $\langle\boldsymbol{\sigma}_1\cdot\boldsymbol{\sigma}_6\rangle_{Av}$ and higher terms, it is seen that

$$\begin{aligned}\langle\boldsymbol{\sigma}_i\cdot\boldsymbol{\sigma}_{j+4}\rangle_{Av}&=\langle\boldsymbol{\sigma}_i\cdot\boldsymbol{\sigma}_j\rangle_{Av}\cos^2\alpha && (\textit{trans})\\ (j\gtrless i)\quad&=\langle\boldsymbol{\sigma}_i\cdot\boldsymbol{\sigma}_j\rangle_{Av}\cos^2\alpha\cos 2\beta && (\textit{cis})\\ &=\langle\boldsymbol{\sigma}_i\cdot\boldsymbol{\sigma}_j\rangle_{Av}\cos^2\alpha\cos^2\beta, && (\text{random})\\ \langle\boldsymbol{\sigma}_i\cdot\boldsymbol{\varrho}_{j+4}\rangle_{Av}&=\langle\boldsymbol{\sigma}_i\cdot\boldsymbol{\varrho}_j\rangle_{Av}\cos^2\alpha && (\textit{trans})\\ (j>i)\quad&=\langle\boldsymbol{\sigma}_i\cdot\boldsymbol{\varrho}_j\rangle_{Av}\cos^2\alpha\cos 2\beta && (\textit{cis})\\ &=\langle\boldsymbol{\sigma}_i\cdot\boldsymbol{\varrho}_j\rangle_{Av}\cos^2\alpha\cos^2\beta, && (\text{random})\\ \langle\boldsymbol{\varrho}_i\cdot\boldsymbol{\varrho}_{j+4}\rangle_{Av}&=\langle\boldsymbol{\varrho}_i\cdot\boldsymbol{\varrho}_j\rangle_{Av}\cos^2\alpha && (\textit{trans})\\ (j>i)\quad&=\langle\boldsymbol{\varrho}_i\cdot\boldsymbol{\varrho}_j\rangle_{Av}\cos^2\alpha\cos 2\beta && (\textit{cis})\\ &=\langle\boldsymbol{\varrho}_i\cdot\boldsymbol{\varrho}_j\rangle_{Av}\cos^2\alpha\cos^2\beta. && (\text{random})\end{aligned} \tag{17}$$

Introducing (15), (16), and (17) into (13), it is possible to evaluate $(1/n)R_n^2$ for the different kinds of chains. Upon simplification and rearrangement, the following expressions are obtained. For the *trans*-structure

$$\frac{1}{n}R_n^2=\rho^2\left\{\frac{1+\cos^2\alpha\cos 2\beta}{4(1-\cos^2\alpha)}\right\}+\rho\sigma\left\{\frac{\cos\beta(1+\cos\alpha+\cos^2\alpha)}{1-\cos^2\alpha}\right\}+\sigma^2\left\{\frac{5+8\cos\alpha+5\cos^2\alpha}{4(1-\cos^2\alpha)}\right\}. \tag{18}$$

For the *cis*-structure

$$\begin{aligned}\frac{1}{n}R_n^2=&\rho^2\left\{\frac{1+\cos^2\alpha}{4(1-\cos^2\alpha\cos 2\beta)}\right\}+\rho\sigma\left\{\frac{\cos\beta(1+\cos\alpha+\cos^2\alpha)}{1-\cos^2\alpha\cos 2\beta}\right\}\\&+\sigma^2\left\{\frac{(3+2\cos 2\beta)+4\cos\alpha(1+\cos 2\beta)+\cos^2\alpha(2+3\cos 2\beta)}{4(1-\cos^2\alpha\cos 2\beta)}\right\}.\end{aligned} \tag{19}$$

For the random structure

$$\frac{1}{n}R_n^2=\rho^2\left\{\frac{1+\cos^2\alpha\cos^2\beta}{4(1-\cos^2\alpha\cos^2\beta)}\right\}+\rho\sigma\left\{\frac{\cos\beta(1+\cos\alpha+\cos^2\alpha)}{1-\cos^2\alpha\cos^2\beta}\right\}$$
$$+\sigma^2\left\{\frac{(3+2\cos^2\beta)+4\cos\alpha(1+\cos^2\beta)+\cos^2\alpha(2+3\cos^2\beta)}{4(1-\cos^2\alpha\cos^2\beta)}\right\}. \quad (20)$$

NUMERICAL CALCULATIONS

To obtain numerical values for the average square lengths of the different rubber-like molecules, it is necessary to assume definite values for α, β, ρ, and σ. Using the values of Brockway and co-workers,[7] the angles will be taken to be $\alpha=68°\ 30'$ and $\beta=55°\ 40'$. These values were obtained by electron diffraction methods applied to small molecules and it is assumed that they are valid for polymers as well. These figures differ slightly from the experimental values obtained for crystalline rubber-like materials,[4] but it is supposed here that the non-crystalline rubber-like molecules will have angles close to those for small gaseous molecules. For σ and ρ, Pauling's values[8] for the single and double carbon-carbon bond distances will be used. These are $\sigma=1.54$A and $\rho=1.34$A.

For the root mean square lengths of the molecules, numerical calculations using Eqs. (18), (19), and (20) yield the following results:

$$R_n=2.90\sqrt{n}\text{ A}, \qquad (\textit{trans})$$
$$R_n=2.01\sqrt{n}\text{ A}, \qquad (\textit{cis})$$
$$R_n=2.45\sqrt{n}\text{ A}. \qquad \text{(random)}$$

It follows from the above figures that a *trans*-molecule is, on the average, 44 percent longer than a *cis*-molecule, providing both have the same number of members in their respective chains. The average length of a random molecule is just about half-way between those of the *cis*- and *trans*-varieties.

Since a *cis*-molecule tends to be more curled up than a *trans*-molecule, it might be expected that a mass of *cis*-molecules would be capable of greater stretching than a mass of *trans*-molecules. This is in qualitative agreement with the fact that natural rubber can be stretched more than balata. Since some varieties of synthetic rubbers may be random, they would be expected to possess intermediate elastic properties.

MAXIMUM LENGTHS OF MOLECULES

For a quantitative measure of the elastic possibilities, it is necessary to consider still another factor. The average lengths of the molecules (which are nearly the same as the root mean square lengths) must be compared with the maximum possible lengths. Since the maximum length of a *trans*-molecule is greater than the maximum length of a *cis*-molecule, it is conceivable that an average *trans*-molecule might undergo as great a relative stretch as one of the *cis*-variety. To check this possibility, we shall calculate the maximum possible lengths for the two forms.

In Fig. 3 are pictured the two regular varieties of rubber-like polymers arranged in such a way as to make the maximum lengths. By purely geometric considerations, it is seen that for the *trans*-variety,

$$R_{n(\max)}=\frac{n}{4}\{\rho^2+2\rho\sigma[2\cos\beta+\cos(\beta-\alpha)]$$
$$+5\sigma^2+4\sigma^2\cos\alpha\}^{\frac{1}{2}} \quad (21)$$

and for the *cis*-form

$$R_{n(\max)}=\frac{n}{4}\{\rho+2\sigma\cos\beta+\sigma\cos(\beta-\alpha)\}. \quad (22)$$

In deriving (21) and (22) it is assumed that the molecules are long and made up of recurring units each containing one double and three single bonds.

Performing the necessary numerical calculations, using the same values for α, β, ρ, and σ as

[7] See L. Pauling, *The Nature of the Chemical Bond* (Cornell University Press, Ithaca, 1940), second edition, p. 84, for a convenient summary of data.
[8] See reference 7, p. 164.

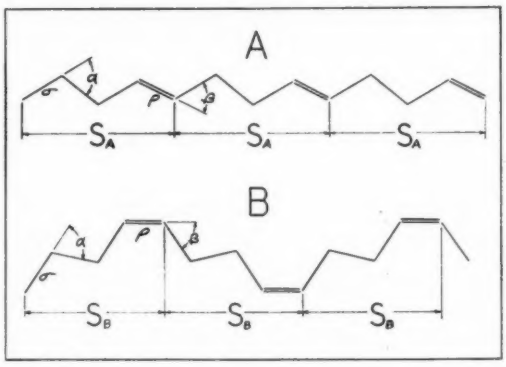

FIG. 3. Rubber-like molecules arranged for maximum length. A. *Trans*-variety. B. *Cis*-variety. In each case $R_{n(\max)} = (n/4)S$.

before, it is found that

$$R_{n(\max)} = 1.27n \text{ A} \quad (trans)$$

and

$$R_{n(\max)} = 1.14n \text{ A}. \quad (cis)$$

The quantity of significance for our purpose is the ratio of $R_{n(\max)}$ to R_n, which will provide a measure of the elastic possibilities. These ratios are for the *trans*- and *cis*-varieties equal, respectively, to $0.438\sqrt{n}$ and $0.567\sqrt{n}$. Moreover, the ratio for the *cis*-variety is 1.30 times as great as that for the *trans*.

DISCUSSION

On the basis of the molecular picture of rubber elasticity,[5] the figure 1.30 might be interpreted in the following way. Take two pieces of *cis*- and *trans*-material of the same size and shape made up of molecules of the same chain length. Let each be stretched until it reaches some characteristic place in the stress-strain curve or reaches some particular state of crystallization. Then the *cis*-material should be 30 percent longer than the *trans*-material. In other words, if 100 percent elongation should cause crystallization for the *trans*-substance, then 160 percent elongation should be necessary for the corresponding effect in the *cis*-substance. (Incidentally, small changes in α, β, ρ, or σ will not alter the above ratios appreciably.)

Qualitatively the argument advanced above is in the right direction as far as rubber and balata are concerned. Unfortunately, the difference predicted is not nearly great enough, especially at room temperature, under which condition balata is scarcely elastic at all. A better comparison is obtained between polychloroprene and natural rubber. Polychloroprene has a *trans*-structure,[4, 9] yet possesses considerable elasticity. No accurate experimental data are available comparing samples of polychloroprene and natural rubber of the same molecular weight and in the same state of vulcanization, but there appears to be qualitative evidence supporting the above arguments.

To account fully for the different elastic properties of the various rubber-like polymers, it is necessary to take into account other effects such as those suggested by Bunn.[10] Bunn recognized that stearic influences of different substituents (CH_3 or Cl) in the polymer chains have an important effect on the curling up of molecules. Such stearic effects become of major importance in balata, thus accounting for its non-elastic properties at room temperature. For natural rubber, the structure is such that the effect of the methyl group is not important and for polychloroprene the dimensions are such that the stearic effect is rendered small. The present calculation, though inadequate as a complete explanation, does indicate to what extent the chain structure without substituents affects the elastic properties of polymers.

[9] C. J. B. Clews, Proc. Roy. Soc. **A180**, 100 (1942).
[10] C. W. Bunn, Proc. Roy. Soc. **A180**, 82 (1942).

The Variation in the Structure of Water in Ionic Solutions. II

G. W. STEWART
University of Iowa, Iowa City, Iowa

(Received November 6, 1942)

Earlier experiments with 15 strong electrolytes have been extended to 38 and there continues to be a striking correspondence between the rate of variation of the partial molal ionic volume with concentration and the rate of variation of water structure as crudely indicated by the x-ray diffraction pattern. The concentration in mole fraction of the solutions varied from 0.001 to 0.096 having a mean of 0.028. The influences of concentration on adiabatic compressibility and of solubility on the variation of water structure are mentioned. Qualitative explanation of the effect of the ions in solution may be obtained by assuming a direct effect on the breaking of H bonds and the indirect effect of altering the pure temperature expansion of the water.

THE x-ray diffraction intensity-angular distribution data for water has shown[1] that with increasing temperature the minor diffraction peak is strikingly reduced. Careful measurements have further shown that[2] the radial density distribution of molecules about any one of them is altered by increasing temperature so that the number of nearest neighbors is increased. This involves breaking hydrogen bonds and producing a more compact water structure, but of course there is also the simultaneous pure temperature expansion. These opposing effects account qualitatively for the existence of a maximum density of water at 4°C. It is well known that in aqueous solutions the variation of the partial molal ionic volume with concentration follows a course that is similar in many strong electrolytes. Again this can be interpreted[3] as the formation of new liquid structures occasioned by the breaking of hydrogen bonds and resulting in a greater density of the solvent water. Also it is found[3] that with increasing concentration in an ionic solution, the minor x-ray diffraction peak, mentioned above, decreases in a manner similar to the effect with increasing temperature in pure water. The question is, does this similarity of the effect on the diffraction curves in pure water and ionic solutions have any significance? The experimental results gave credence to the view that this similarity is significant. For it was shown[3] that with sixteen strong electrolytes at the concentration of 0.55 mole per liter, the rate of change of the partial molal ionic volume φ, with the concentration c, varied from one electrolyte to another much as did the change in the relative minor peak x-ray intensity. More definitely, an n was found for each electrolyte which would make $(\partial\varphi/\partial c^n)$ constant in the region of 0.55 mole per liter. Then the values of $\partial h/\partial m$, where h is the height of the minor diffraction peak and m is the concentration in mole fraction, were experimentally obtained. When these two variables for the sixteen samples were plotted as coordinates, there was a crudely approximate linear relation. Lines drawn from the origin through each point did not vary from a median straight line by more than 9°. A previous discussion[3] indicates that in a dilute solution the relative variation in the experimental intensity distribution curve at the diffraction angles herein considered, may be regarded as approximately a relative variation in the scattering curve for the solvent water. This approximation grows increasingly poorer with concentration. Out of this semi-quantitative, approximate procedure comes the conclusion that the chief cause of $(\partial\varphi/\partial c^n)$ and of $\partial h/\partial m$ is the same, and that ions also break the hydrogen bonds and cause a denser water structure. This is in harmony with the suggestion of Bernal and Fowler.[4] To this early list of fifteen strong electrolytes are now added twenty-three more. The data for all are now presented in Table I. They are also plotted as before in Fig. 1.

[1] G. W. Stewart, Phys. Rev. **37**, 9 (1931).
[2] J. Morgan and B. E. Warren, J. Chem. Phys. **6**, 666 (1938).
[3] G. W. Stewart, J. Chem. Phys. **7**, 869 (1939).
[4] J. D. Bernal and R. H. Fowler, J. Chem. Phys. **1**, 515 (1933).

TABLE I. Correspondence of the variation of the apparent molal ionic volume with the indicated change in the liquid structure of the solvent, water.

Electrolyte	Temperature	Concentration (mole fraction)	$(\partial\varphi/\partial c^n)$ (Exp.)	(n)	$0.01\ \partial h/\partial m$ at 25°C
$NH_4C_2H_3O_2$	17°	0.0908	0.58	(1)	1.00
$LiNO_3$	17°	.0557	0.78	(0.8)	1.6
KCN	15°	.0647	1.03	(1)	0.73
KCNO	15°	.0527	1.15	(1)	1.12
NH_4F	15°	.07359	1.27	(1)	0.49
NH_4Cl	25°	.0325 .0619 .0960	1.33	(0.5)	1.18
LiCl	25°	.0357 .0853	1.67	(0.5)	1.38
NaCl	25°	.0231 .0331 .0799	2.06	(0.5)	1.48
LiOH	15°	.0543	2.2	(0.8)	1.7
$KClO_3$	15°	.0086	2.46	(0.5)	5.0
KCl	25°	.0152 .0378	2.73	(0.5)	2.25
$NaClO_4$	15°	.033	3.6	(0.4)	1.86
NaOH	15°	.0375	2.59	(1.0)	2.0
H_2SO_4	15°	.018	3.63	(0.5)	3.0
$MgCl_2$	25°	.0182 .0431	3.8	(1)	3.8
	15°	.018	3.8	(1)	3.6
$Mg(NO_3)_2$	15°	.00848	4.0	(1)	4.6
$Ca(NO_3)_2$	15°	.02605	4.8	(1)	2.2
$(NH_4)_2SO_4$	15°	.01016	6.0	(1)	5.3
H_3PO_4	15°	.025	6.3	(<0.2)	3.3
$Al(NO_3)_3$	15°	.00935	8.54	(0.5)	6.2
$MnSO_4$	15°	.014	6.85	(0.5)	5.5
K_2CO_3	15°	.01424	8.6	(1)	4.6
$CdCl_2$	15°	.019	7.6	(0.5)	2.5
$KHCO_3$	15°	.02203	8.8	(0.1)	4.3
$KNaC_4H_4O_6$	15°	.0149	9.57	(0.5)	5.55
$MgSO_4$	15°	.00945	9.6	(0.5)	7.5
K_2SO_4	15°	.00613	10.7	(1)	9.5
$ZnSO_4$	15°	.0104	10.8	(1)	4.5
$CuSO_4$	15°	.00878	12.4	(0.5)	9.4
$AlCl_3$	15°	.0090	14.0	(0.3)	7.9
$CoCl_2$	15°	.0065	16.0	(0.5)	8.1
$K_2Cr_2O_7$	17°	.00491	16.0	(1)	16.0
$NiCl_2$	17°	.0048	17.3	(0.5)	14.0
Na_2AsO_4	15°	.00378	22.2	(0.8)	23.5
$CoSO_4$	15°	.00806	22.8	(0.25)	7.3
$Ce_2(SO_4)_3$	15°	.003	79.0	(0.2)	23.7
$Co(NO_3)_2$	15°	.00175	38.8	(0.5)	36.0
$Co(C_2H_3O_2)_2$	15°	.0010	100	(1)	60.0

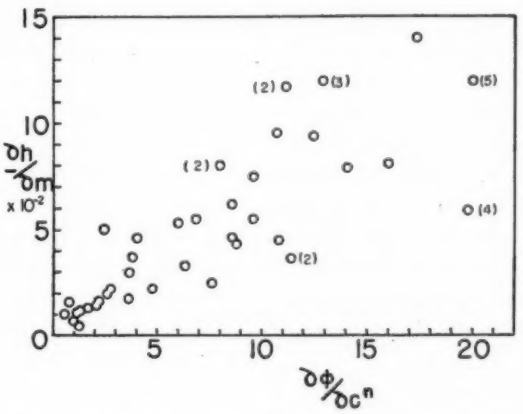

FIG. 1. The values of rate of change of minor peak height (major peak 100) with mole fraction, divided by 100, compared with values of $(\partial\varphi/\partial c^n)$. Coordinates should be multiplied by the number in parenthesis.

DISCUSSION OF DATA AND INTERPRETATION

The data for φ were taken from the *International Critical Tables*, volumes 4 and 6, and Landolt and Börnstein, fifth edition. The x-ray diffraction curves for the samples were obtained with the same equipment as previously described.[3] There are several unsatisfactory features of the data and their use, though the interpretation here made is not vitiated thereby. The values of φ are, in general, probably not reliable. For example, with $KClO_3$, φ is recorded in the above sources as decreasing with concentration, whereas Redlich and Bigeleisen have recently shown[5] that it increases.[6] Most of the φ data were taken at 20°C, and some of them from 15°C to 18°C. No temperature correction was applied. The experimental determination of h was determined usually at 15°C, and in each case the temperature correction found for water was applied to give the value at 25°C. The values of $(\partial\varphi/\partial c^n)$ and values of n were obtained from the plotted data for φ in the neighborhood of 0.55 mole per liter. The values given in the fourth and sixth column of Table I for H_3PO_4, H_2SO_4, and $CdCl_2$ are questionable. Nevertheless, with all inaccuracies considered, Table I and Fig. 1 do give striking results. In general large values of $(\partial\varphi/\partial c^n)$ correspond to large values of $\partial h/\partial m$. The change in φ, the

[5] O. Redlich and J. Bigeleisen, J. Am. Chem. Soc. **64**, 758 (1942).

[6] The data on $KClO_3$, using these new values, have been placed in the table and on Fig. 1.

partial molal ionic volume, is interpreted as most importantly caused by the change in specific volume of the water. Hence the larger the $(\partial\varphi/\partial c^n)$[7] the greater the rate of change of the specific volume of the water with the concentration. Thus there should be a general correspondence between the two indicators of the rate of change of the water structure with concentration. A quantitative correspondence, in the very nature of the case, cannot possibly be expected. This general correspondence is strikingly shown by Fig. 1. The experimental results thus give impressive evidence of the correctness of the interpretation, namely, that the changes in φ are caused importantly (not exclusively) by the changes in the structure of the solvent water. Thus the conclusion from the earlier paper is extended and verified.

There are several other comparisons that can be made with $\partial h/\partial m$. One is with the change of *adiabatic compressibility* β of these same electrolytes. In an article shortly to be published, Dr. Victor B. Corey has shown that there is also a definite trend for $-\partial h/\partial m$ to increase with $-\partial\beta/\partial m$. The interpretation is that the change in the structure of the solvent, water, is responsible for both, at least to an important degree.

Solubility has been a property of great interest and complexity as well. If the solubility of these strong electrolytes as found in the *International Critical Tables* be plotted with $-\partial h/\partial m$, the points, though widely scattered, show a marked general trend, the solubility decreasing as the values of $-\partial h/\partial m$ increase. Empirical methods of allowing for the temperature below melting point, do not decrease the scattering materially. Evidently the more soluble the electrolyte the less disturbance per ion is caused in the water structure. This is in harmony with the simple view that solubility is determined by the ease of participation in the water structure.

In approximately 200 strong electrolytes there are five in which the slope $\partial\varphi/\partial c$ is negative and in none of them is there a linear relation between φ and c^n. In two of them, $Ba(OH)_2$ and $(NH_4)_2\,Cr_2O_7$, the values for $-(\partial h/\partial m)/100$ were measured and are 16.0 and 10.0, respectively, indicating nothing unusual in the change of structure. They are thus exceptional cases and do not fit in with the simple interpretation given above. More exact data for the computation of φ in these cases might alter this situation as in the case of the data for $KClO_3$ already mentioned.

The effect of the ions on the water structure, on adiabatic compressibility, and on the temperature of minimum compressibility and also the possibility of a decreasing φ with increasing c and yet show no uniqueness in x-ray diffraction, can receive qualitative explanation on the following simple and apparently reasonable hypotheses. In water an increase in temperature (1) breaks hydrogen bonds and alters the water structure, decreasing its molal volume and (2) causes a pure temperature expansion increasing the molal volume. Ions in aqueous solution (1) break hydrogen bonds and alter the water structure, decreasing its molal volume, and as a consequence (2) increase the pure temperature expansion of the solvent. The discussion of this suggestion is reserved for further report.

I wish to express my indebtedness to Dr. James Jacobs and Mr. Harold Froslie, the former for much of the x-ray diffraction data.

[7] The reasoning is better if but one value of n is used, say $n=\frac{1}{2}$, but the correspondence in Fig. 1 is a little better if n is chosen as here indicated.

Stability and Structure of Burner Flames[1, *]

BERNARD LEWIS[2] AND GUENTHER VON ELBE[3]
Bureau of Mines and Carnegie Institute of Technology, Pittsburgh, Pennsylvania
(Received September 1, 1942)

It has been shown that the condition of equality of gas and burning velocities, required for stabilization of a flame above a burner, is established near the rim of the orifice or an obstruction within the stream by the effects of friction and inhibition of the explosive reaction. This condition is maintained between two critical gradients of the gas velocity at the solid surface, the lower gradient bordering on the flash-back and the upper gradient on the blow-off range. Values of the gradients in the range of laminar flow were determined by hydrodynamic equations from gas flow and tube dimensions; and their independence of tube diameter, except for extreme sizes, has been demonstrated both for upright and inverted flames. In the latter the critical velocity gradient for blow-off was also found to be independent of the diameter of the centrally mounted wire within a considerable range. The effect of the surrounding atmosphere on the critical blow-off gradient has been shown. The gas-flow pattern was studied experimentally by photographing stroboscopically illuminated magnesium oxide dust particles. No appreciable redistribution of velocities over the cross section of the stream was observed below the combustion zone. The burning velocity was found constant over the surface of the inner cone, except at the tip, where it increases to the axial gas velocity, and at the base, where it decreases to zero. The experimental flame cone outline and flow pattern agree with the theoretical within the limitations imposed by simplifying assumptions. The temperature distribution in the flame was determined by the sodium line-reversal method, only the center of the flame being colored, and observations of the width and emission spectrum of the luminous combustion zone were made. In natural gas-air flames C−C and C−H bands are observed in the zone, and the temperature rises gradually behind the zone to a maximum that corresponds to the theoretical flame temperature. In natural gas-oxygen flames no C−C or C−H bands are observed; and the temperature attains a maximum, exceeding the theoretical, immediately behind the combustion zone. Temperature distribution and flow pattern have been correlated. The flow pattern of inverted flames was also studied with particular attention to the region of flame attachment just above the central wire where the formation of an annular vortex is demonstrated. An interpretation of the formation of polyhedral flame cones, described by Smith and Pickering, has been given.

WHEN an explosive gas mixture is ignited, combustion takes place in a narrow zone, separating burned and unburned gas, which propagates as a Huygens wave in a direction normal to itself into the unburned gas at the rate at which combustion reactions are induced in successive gas layers by the processes of heat transfer (essentially conduction) and diffusion of active species. The rate of progress of the combustion zone is called the burning velocity. A burner flame remains stationary above the orifice because there are regions, either near the rim or near an obstruction in the stream like the grid of a Méker burner, where the gas velocity equals the burning velocity. These regions serve as continuous sources of ignition for the neighboring gas elements whose velocity exceeds the burning velocity. As the combustion zone propagates from these regions of equality it assumes an angle to the direction of gas flow so that everywhere the normal component of the gas velocity equals the burning velocity. For example, in the ordinary Bunsen burner flame the region of equality is established in a concentric circle above the orifice, and the combustion zone must take the form of an upright, circular cone.

The theory of burner flames has been comprehensively discussed by Mache.[4] His conclusions, however, do not explain satisfactorily how the regions of equality of gas velocity and burning velocity are established[5] and consequently do not yield the exact conditions for flash-back and blow-off. This omission is reme-

[1] Published by permission of the Director, Bureau of Mines, U. S. Department of the Interior, and the Director, Coal Research Laboratory, Carnegie Institute of Technology.
[2] Senior Physical Chemist, Physical Chemistry Section, Central Experiment Station, Bureau of Mines, Pittsburgh, Pennsylvania.
[3] Coal Research Laboratory, Carnegie Institute of Technology, Pittsburgh, Pennsylvania.
[*] Presented at the Buffalo meeting of the American Chemical Society.

[4] H. Mache, *Die Physik der Verbrennungserscheinungen* (Leipzig, 1918).
[5] Cf. W. Jost, *Explosions-und Verbrennungsvorgänge in Gasen* (Berlin, 1939), pp. 72 *et. seq.*

FIG. 1. Tracks of stroboscopically illuminated magnesium oxide particles in a flame burning on a rectangular tube of 0.755 cm $\times$2.19 cm cross section. The short side of the burner tube faces the camera. The light beam, about 1 mm wide and several cm high, bisects the long side. Time between interruptions, 1.44×10^{-3} sec. Mixture composition 7.50 percent natural gas in air; gas flow, 204 cc/sec.

died in the present paper. Furthermore, the fundamental concepts of the theory of flame structure have been verified and extended in detail by experimental studies of the direction and velocity of the gas flow (flow pattern) throughout the flame, of the burning velocity in various parts of the combustion zone, and of the distribution of temperature, so that a comprehensive description of burner flames can now be given that should be applicable to various problems in gas technology.

1. APPARATUS AND PROCEDURE

Mixtures of natural gas and air were used in most of the experiments. Air was taken from a constant-pressure reservoir, and all other gases were drawn from tanks, using two-stage regulators to insure constant flow. The Orsat analysis of the natural gas corresponded to 81.8 percent methane, 17.7 percent ethane, and 0.5 percent nitrogen, and hence the stoichiometric percentage in air was 8.49. The actual composition was somewhat different because of the presence of traces of higher hydrocarbons. The gas and air were passed separately through calibrated flowmeters to a mixing chamber. The mixture composition as determined from the flowmeter readings was confirmed by analysis. In determinations of blow-off and flash-back the mixture passed directly to Pyrex burner tubes of about 1-meter length to insure laminar flow at the orifice, of inside diameters from 0.315 to 1.550 cm and a wall thickness of about 1 mm. For blow-off experiments in atmospheres of gases other than air, the burner tube was surrounded by a wide glass tube through which a stream of the gas was passed upward around the flame. For the study of blow-off of inverted flames, a straight wire of steel or brass with a flat end was mounted in the axis of the tube and the end of the wire extended about 1 cm above the rim. The other end of the wire was looped into a spiral that fitted the tube snugly and served as a support at a distance of over 40 times the tube diameter below the rim. Gas mixtures were ignited by applying a small flame to the region of low gas velocity near the rim of the tube or, in experiments with inverted flames, just above the central wire. Between trials the burner was cooled to room temperature.

The gas-flow pattern was determined by photographing stroboscopically illuminated dust

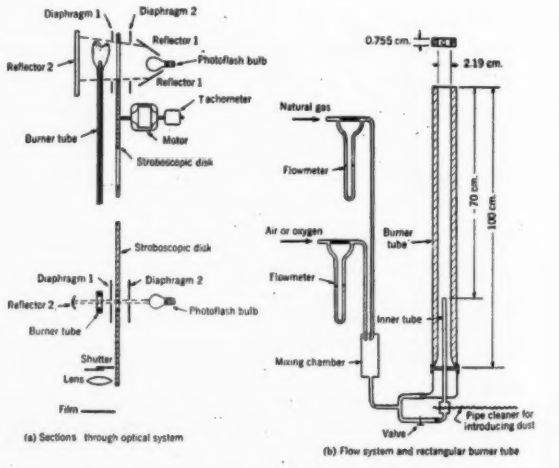

FIG. 2. Apparatus for determining the flow pattern of ignited and unignited gas streams.

particles carried by the stream.[6] The photographs show the flame outline and interrupted particle tracks (Fig. 1), the velocity of the particles being determined from the distance between two interruptions and the speed of the stroboscopic disk. The experimental arrangement is shown in Fig. 2. Diaphragms 1 and 2 define a 1 to 2-mm wide sheet-like beam of light from the photoflash bulb and reflectors 1, which is interrupted by the rotating disk. The beam passes across the center of the orifice of the burner and is reflected in itself by cylindrical reflector 2; thus the dust particles are illuminated from two sides. The camera is arranged at right angles to the direction of illumination. The stroboscopic disk was enclosed in a housing to protect the flame from drafts and was divided into 24 sectors open over four-fifths of their width. Except as otherwise indicated experiments were made with the disk rotating at 1740 r.p.m., as measured by a tachometer. The photographic shutter consisted of four blades which opened and closed completely in 0.05 second with maximum opening about 40 percent of the time, and carried electric contacts to synchronize photoflash and photographic exposure. The photoflash bulbs were Mazda No. 21 with a peak of 4½ million lumens and more than 2½ million lumens for 0.01 second. A 3¾-inch diameter, *f*:2.5, Taylor-Hobson lens and triple-S pan film were used. For experiments with upright flames, a brass burner tube 1 meter long and of rectangular cross section (0.755 cm ×5 cm) was used, the longer dimension being reduced to 2.19 cm by inserting two metal strips, as shown in Fig. 2.

MgO dust (metallographic polish) was used. The particles produce sharp interrupted tracks, as their incandescence in the burned gas is insufficient to register on the film. Talcum powder is also suitable but not aluminum dust, which burns brightly. The dust was added to the stream at the bottom of the tube by inserting a pipe cleaner, covered with the dust, through opposite holes in the tube and moving it back and forth. No appreciable leakage of gas occurred through the holes past the pipe cleaner. The particles were distributed over the entire cross section, but only those in the path of the light beam registered on the film. It was possible to concentrate the particles by introducing them into a smaller tube mounted in the center of the burner tube, as shown in Fig. 2. The gas stream was divided before entering the tubes and the velocity regulated so that the stream was laminar in the inner and outer tubes. The particles remained centrally located during their travel up the burner tube (about 70 cm). This distance sufficed to restore the normal velocity distribution over the cross section of the burner tube before reaching the orifice. The rectangular burner is advantageous compared to a cylindrical burner because in the flame no flow lines in the zone of illumination are refracted away from or toward the camera. The films were measured by mounting them on an accurately ruled grid and reading between the grid lines by means of a fine scale on a transparent film, specially drawn and photographed, mounted under a lens. The readings were transferred to coordinate paper, of which Fig. 24 is an example.

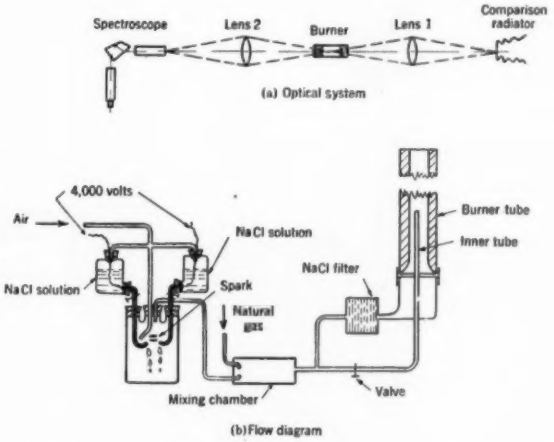

FIG. 3. Apparatus for determining temperatures in center of burner flame by the sodium line-reversal method.

Some photographs were made with smoke substituted for particles; such smoke was produced by passing moist air over stannic chloride impregnated pumice, forming solid hydrates, probably mostly the trihydrate.

Flame temperatures were measured by the sodium line reversal method, which has been

[6] F. A. Smith, Chem. Rev. **21**, 389 (1937) used the method to determine velocity distribution in an unignited stream.

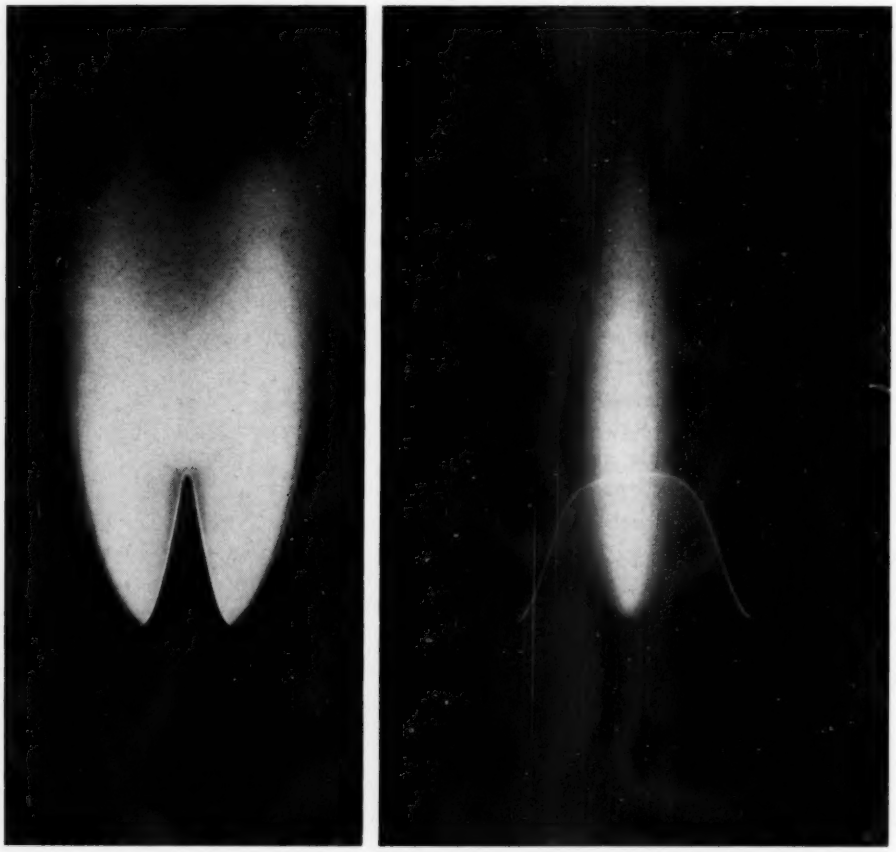

FIG. 4. Front and side views of flame on rectangular burner, colored centrally with sodium chloride.

described elsewhere.[7] The apparatus was mounted on an optical bench and is shown diagrammatically in Fig. 3a. The image of the tungsten band comparison radiator is focused onto the center of the flame and both the former and the image of the flame are in turn focused on the slit of the spectroscope. To obtain correct temperature readings the light-gathering power of lens 1 must not be smaller than that of lens 2. The tungsten band lamp was calibrated at the Nela Park Laboratory of the General Electric Company for brightness temperature in the red as a function of current. Corrections were made for reflection from lens 1 and for yellow brightness as described elsewhere.[8] Temperature readings could be reproduced within 4°C. The images of flame and band on the slit were approximately of natural size; therefore, the temperature reading corresponded to the colored portion of the flame within a beam of the cross section of the slit, which was 0.02 mm wide and 0.1 mm long. To insure that measured temperatures corresponded to the center of the flame where the flow pattern was determined, only the central portion of the flame was colored by passing sodium chloride mist through the inner tube. The mist was formed in the air stream before entering the mixing chamber by continuously sparking between the open ends of two small glass tubes from which NaCl solution dripped (Fig. 3b). Continuous flow of fresh solution prevented sodium chloride from caking on the electrodes. Metal wires were introduced into the tubes to prevent the formation of bubbles by electrostriction. The bulk of the mixture was passed

[7] B. Lewis and G. von Elbe, *Combustion, Flames, and Explosions of Gases* (Cambridge Press, 1938), pp. 333–337.
[8] Jones, Lewis, Friauf, and Perrott, J. Am. Chem. Soc. **53**, 869 (1931).

through a cotton filter to remove the mist before it entered the main burner tube, while a small part of the mist-laden mixture passed directly into the inner tube. Figure 4 shows front and side views of the centrally colored flame. Some spreading of the sodium vapor takes place by diffusion. Although the flame was brightly colored, the concentration of NaCl was insufficient to lower the temperature appreciably. The entire flame could be explored by moving the burner tube vertically and horizontally while the rest of the system remained fixed; the point of measurement relative to the axis of the burner and the orifice was read on scales with Vernier attachments to 0.1 mm. 250 to 300 readings were made for the temperature contours in each of Figs. 31 to 34.

2. CONDITIONS FOR STABILITY OF FLAME ABOVE THE ORIFICE

(a) Upright Flames

Figure 5 is a photograph of a dust-laden laminar air stream (Reynolds number = 1500) from a cylindrical tube 1.298 cm in diameter. The measured gas velocities near the orifice at various distances from the axis, corrected for free fall of the particles (average 5 cm per second) are plotted in Fig. 6. They follow closely the Poiseuille parabola which is shown as a full line in the figure and is calculated from the equation:

$$U = n(R^2 - r^2). \tag{1}$$

U is the velocity at distance r from the axis, R is the radius of the tube, and $n = -a/4\eta$, where η is the viscosity and a the hydrodynamic pressure gradient along the length of the tube. The value of n is determined from flow V (volume per unit time) and radius R by the equation:

$$V = \int_0^R 2\pi U r dr = \frac{\pi}{2} n R^4. \tag{2}$$

The velocity distribution gradually changes downstream from the orifice owing to transfer of momentum from the inner to the outer flow lines and the surrounding atmosphere; it is noteworthy that, except for very small flow, the velocity in any flow line remains virtually con-

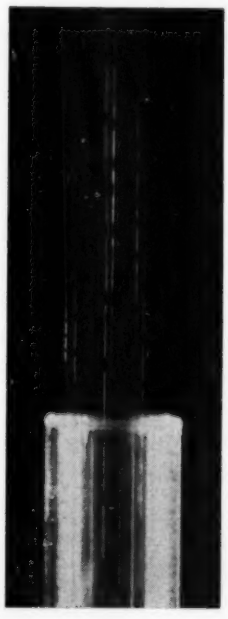

FIG. 5. Particle tracks in an air stream from a cylindrical tube of 1.298-cm diameter; gas flow, 241 cc/sec.; time between interruptions, 2.08×10^{-3} sec.

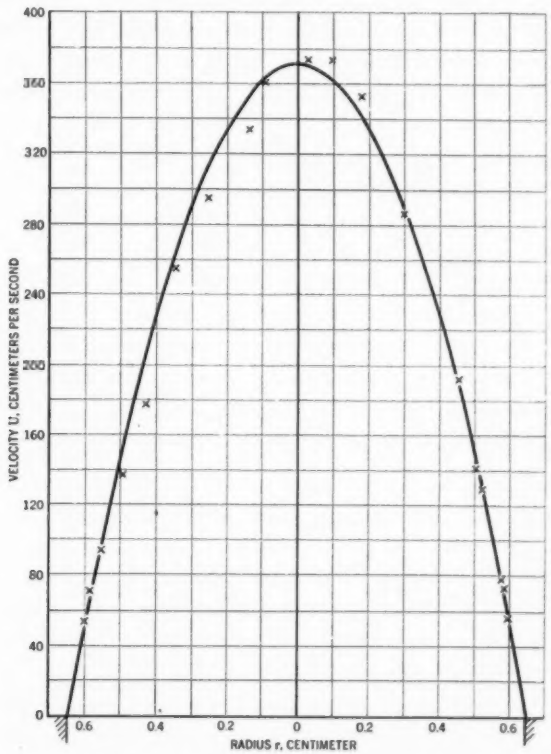

FIG. 6. Velocity distribution in a laminar stream of air (241 cc per second) at the orifice of a cylindrical tube of 1.298-cm diameter; temperature, 25°C; pressure, 740 mm Hg. ×, experimental velocity. ——, calculated velocity.

stant over a length of the order of the distance between orifice and combustion zone. That there is no noticeable slipping at the wall of the tube, as postulated by Poiseuille's equation, is confirmed by the experimental points near the boundary, since the line through these points would extrapolate to zero at the boundary. This result was confirmed in other determinations in different size tubes and for different flows.

The wall not only reduces the gas velocity by friction but also the burning velocity by its quenching effect on the explosive reaction. This effect is observed even in the usual kinetic experiments where the gas and wall are at the same temperature and only the destruction of chain carriers is involved. With a cold burner tube there is the additional effect of cooling, which is in itself very powerful because chain-carrier reactions generally require substantial activation energies. Hence, when, at flows in the flash-back range, a flame travels down the tube, it is observed that the luminous combustion zone does not make contact with the wall and that its fringe trails behind the more central portions; that is, the burning velocity is zero over a short distance from the wall and, farther in, gradually increases to its normal value for undisturbed explosive reaction as shown in Fig. 7a. Flash-back occurs if the burning velocity exceeds the gas velocity somewhere in the stream, as illustrated by curve 1 of Fig. 7a. As the flow is increased, a critical gradient of the gas velocity at the boundary is reached (curve 2) where flash-back is just possible. On further increase of the flow the gas velocity exceeds the burning velocity everywhere in the stream (curve 3), and the flame is swept out of the tube. The critical

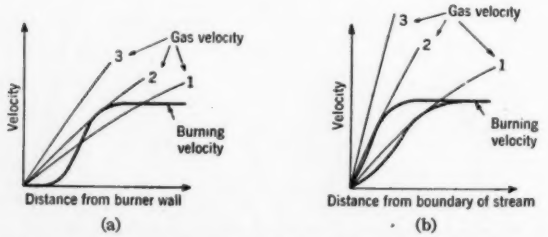

FIG. 7. Illustration of flash-back and blow-off conditions. (a) Velocity gradients at wall of burner tube. Curve 1, flash-back; curve 2, flash-back limit; curve 3, no flash-back. (b) Velocity gradients at boundary of stream above orifice. Curve 1, stable flame; curve 2, blow-off limit; curve 3, blow-off.

velocity gradient for flash-back is obviously determined solely by factors that affect the burning velocity near the wall, namely, the condition of the wall and the mixture composition. Outside of the tube the gas near the boundary regains its explosivity; the combustion zone establishes itself as close to the rim of the orifice as the quenching effect on the explosive reaction permits. At some point gas and burning velocities are equal, as illustrated by curve 1 of Fig. 7b, and the flame is thus attached to the orifice. When the flow is increased, the combustion zone moves away from the rim and thus gains in burning velocity until a new point of equality is established farther out and farther above the rim. This cannot be continued indefinitely because, independent of the quenching action of the rim, the burning velocity vanishes toward the boundary of the stream; eventually (as illustrated by curves 2 and 3) the gas velocity exceeds the burning velocity everywhere in the stream, and the flame blows off the tube. Thus, there is a critical velocity gradient at the boundary for blow-off. The reason why the burning velocity vanishes toward the boundary needs no explanation if the surrounding atmosphere is a diluent gas that reduces the explosivity by interdiffusion. However, if the surrounding atmosphere is a gas that enriches the mixture, the following reasons must be considered: (1) The mixture is over-enriched in the outermost flow lines; (2) the gas movement extends beyond the confines of the explosive mixture by transfer of momentum. It is clear that, with diluent surrounding atmospheres, the critical gradient is much smaller than with enriching surrounding atmospheres.

The relation between the velocity gradient at the boundary,

$$\lim_{r\to R}\left(-\frac{dU}{dr}\right),$$

and experimental quantities V and R, is found by differentiating Eq. (1).

$$\lim_{r\to R}\left(-\frac{dU}{dr}\right)=2nR. \tag{3}$$

Combining with Eq. (2) this becomes

$$\lim_{r\to R}\left(-\frac{dU}{dr}\right)=\frac{4}{\pi}\frac{V}{R^3}. \tag{4}$$

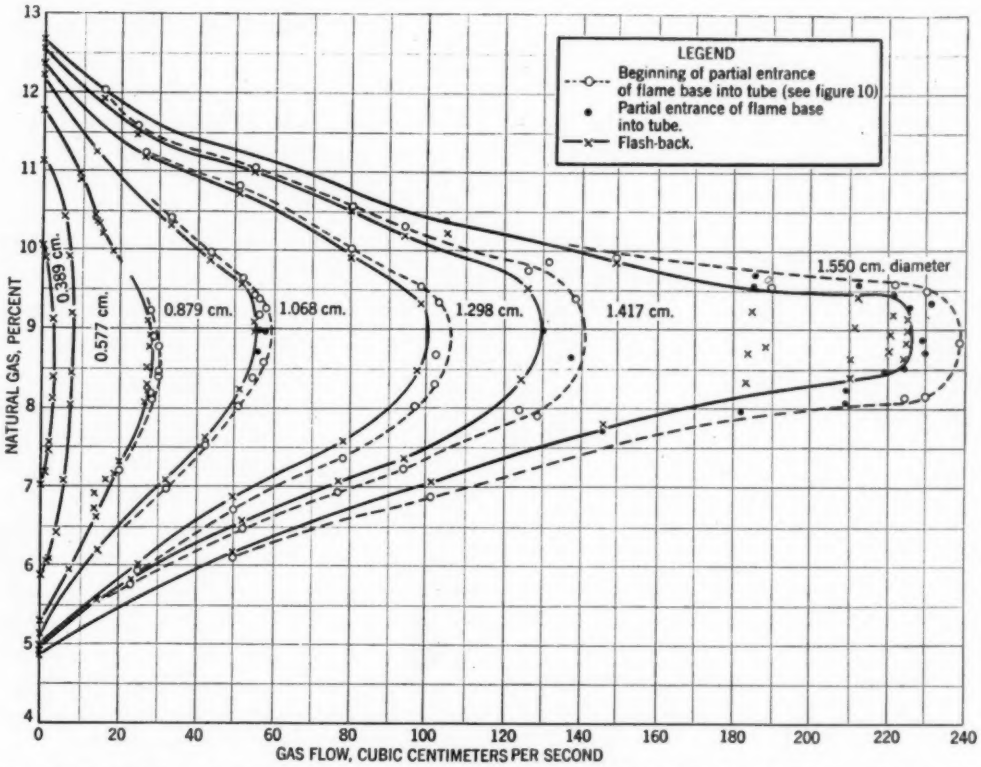

FIG. 8a. Critical flows for flash-back of natural gas-air flames in cylindrical tubes of different diameters at room temperature.

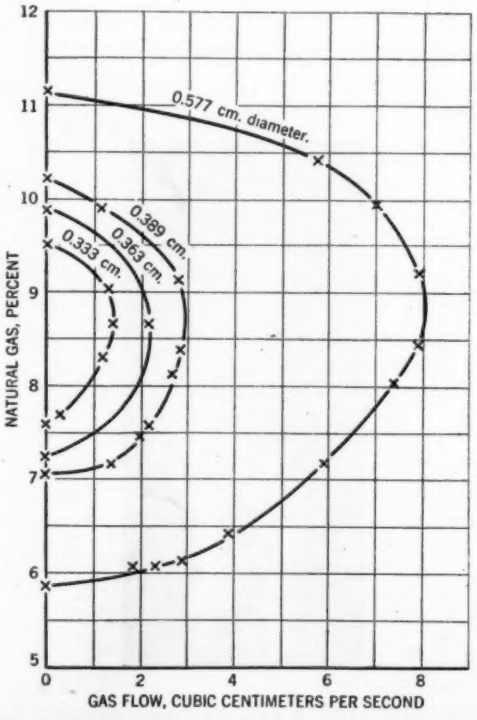

FIG. 8b. Critical flows for flash-back of natural gas-air flames in cylindrical tubes of different diameters at room temperature.

Figures 8a and 8b show critical flows, that is, maximum flows at which flash-back occurs, as a function of mixture composition in cylindrical glass tubes of different diameters at room temperature. The results are little affected by increase of tube temperature up to about 100°C. The points at zero flow, where the wall exerts its quenching effect on the explosive reaction over the whole cross section, are usually referred to as the limits of inflammability for downward propagation. These limits are plotted separately in Fig. 9. At flows just above the flash-back curves (solid curves, Fig. 8), flames of the type shown in Fig. 10, in which the base of the flame cone is partly drawn into the tube, are formed spontaneously. The formation of such flames may be explained as follows: If some point on the rim of the orifice becomes overheated, which may occur fortuitously by some small irregularity, the burning velocity at this point exceeds the gas velocity in the boundary layer and the flame penetrates into the tube at this point, the penetration gradually increasing unless arrested by cooling the tube. Because of confinement of the

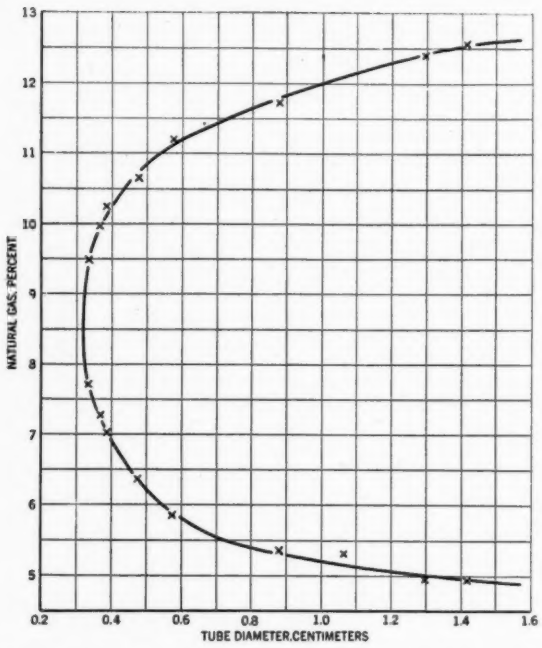

FIG. 9. Limits of inflammability in natural gas-air mixtures for downward propagation.

gas in the tube the expansion of the burned gas crowds the unburned gas to the side, increasing its velocity and keeping the flame there well above the orifice. The flow range for occurrence of flames of this type is confined to the region between dotted and solid curves in Fig. 8a. Above the flow indicated by the dotted curves normal flame cones are stable above the orifice, although over some additional range flames as in Fig. 10 may be forced by heating the tube locally.

Figure 11 is a plot of

$$\lim_{r \to R} \left(-\frac{dU}{dr} \right),$$

calculated from Eq. (4) for the flash-back curves in Figs. 8a and 8b, against mixture composition. Coincidence of the curves confirms that flash-back is essentially controlled by the velocity gradient at the wall. Exceptional deviations occur only in tubes close to the limiting diameter of 0.315 cm in which flame propagation in the most explosive mixture is arrested (see Fig. 9), although even with a tube diameter of 0.333 cm, close coincidence is found near the stoichiometric. The effect of tube diameter is further illustrated in Fig. 12. As the tube diameter is decreased the critical boundary velocity gradient first increases and then decreases sharply to zero. The increase is caused by the fact that the branch of the parabola lying between the wall and the point of equality of burning velocity and gas velocity (Fig. 7a, curve 2) extends over a larger fraction of the radius and is, therefore, more strongly curved. When the tube diameter is decreased to the range where the burning velocity in the center is depressed below its normal value, the critical velocity parabolas again become flatter; this diameter range, in the case illustrated by Fig. 12, lies between 0.39 cm and 0.35 cm, so that the critical velocity gradient rapidly drops to zero. The deviation around the stoichiometric mixture for the largest tube (1.550 cm) may be linked to the pronounced turbulence accompanying flash-back observed in this tube in this mixture range. Turbulence increases the burning velocity and hence the critical flow for flash-back. Although the Reynolds number for turbulence is not exceeded in the flow of unburned and burned gases, turbulence may be induced if the diffraction of the stream lines that takes place at the combustion zone exceeds some critical limit. The diffraction increases with increasing ratio of combustion surface to cross section of the tube, that is, with increasing tilt of the combustion zone in the tube. The cross

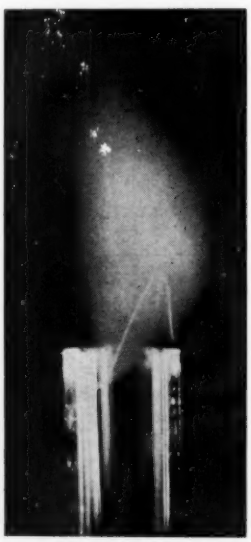

FIG. 10. Flame partly drawn into burner tube at gas flow just exceeding critical flow for flash-back.

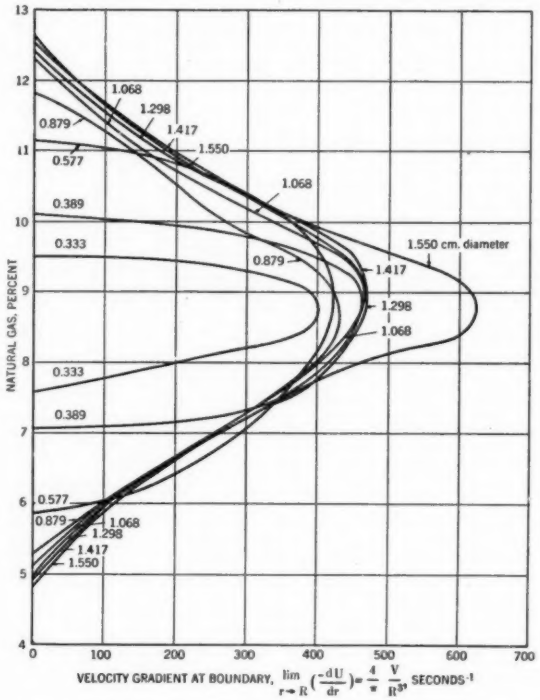

FIG. 11. Critical velocity gradients at boundary of gas stream for flash-back of natural gas-air flames in cylindrical tubes of different diameters at room temperature.

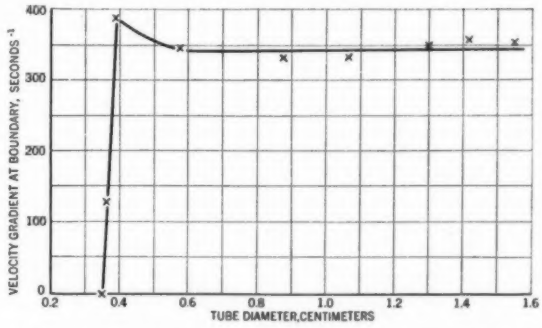

FIG. 12. Critical velocity gradients at boundary of gas stream for flash-back of flames of 7.5 percent natural gas-air mixtures in cylindrical tubes of different diameters at room temperature.

section increases with the square of the diameter; the combustion surface at the critical flow for flash-back, being approximately proportional to the flow, increases [according to Eq. (4)] with the cube of the diameter.

Figure 13 shows critical flows for various tube diameters above which flames burning in air are blown off. The slope of the curves changes markedly on approaching the condition of turbulent flow (Reynolds number > 2000). The junction of blow-off and flash-back curves is shown in detail in Fig. 14 for several tube diameters. For the larger tubes, the blow-off curve approaches the flash-back curve asymptotically. In smaller tubes a region of extinction appears at small flows. On approaching this region from the region of stable flame the effects of dilution and the rim increase, the point of equality of burning velocity and gas velocity shifts to the axis, and the flame assumes a water-meniscus-like shape. Finally, at the extinction limit the explosive reaction is quenched and the flame goes out. In a small tube where flash-back is possible, the latter can be forced at the appropriate flow, either by heating the rim of the tube or, where extinction and flash-back curves are close together, by first forming a stable flame and suddenly reducing the flow to the appropriate value. Where flash-back and extinction curves are very close to each other, for example, at 9.04 percent natural gas in the 0.333-cm tube, the flame is curiously unstable, tending unpredictably to extinction or flash-back.

A plot of

$$\lim_{r\to R}\left(-\frac{dU}{dr}\right)$$

against mixture composition, calculated from Eq. (4) for the blow-off curves in Figs. 13 and 14, is shown in Fig. 15. The points are not drawn in because the agreement is so close, even for the blow-off curves for small tubes almost down to the junction with the extinction curves, as to be indistinguishable on the plot. Thus, for otherwise equal conditions, the velocity gradient at the boundary for blow-off is the same for all tubes. To Fig. 15 is added the average flash-back curve derived from Fig. 11 for medium-size tubes, thus providing a graph of the region of stable flames of natural gas for the condition of laminar flow.

As shown in Fig. 16, the blow-off condition changes profoundly with the nature of the surrounding atmosphere. If the surrounding atmosphere is oxygen, the region of stable flame greatly increases (see also Fig. 13); if an inert gas, the region is sharply limited, the blow-off closing in to the flash-back curves both on the lean and rich sides. The effect increases in the order nitrogen, carbon dioxide, helium. It

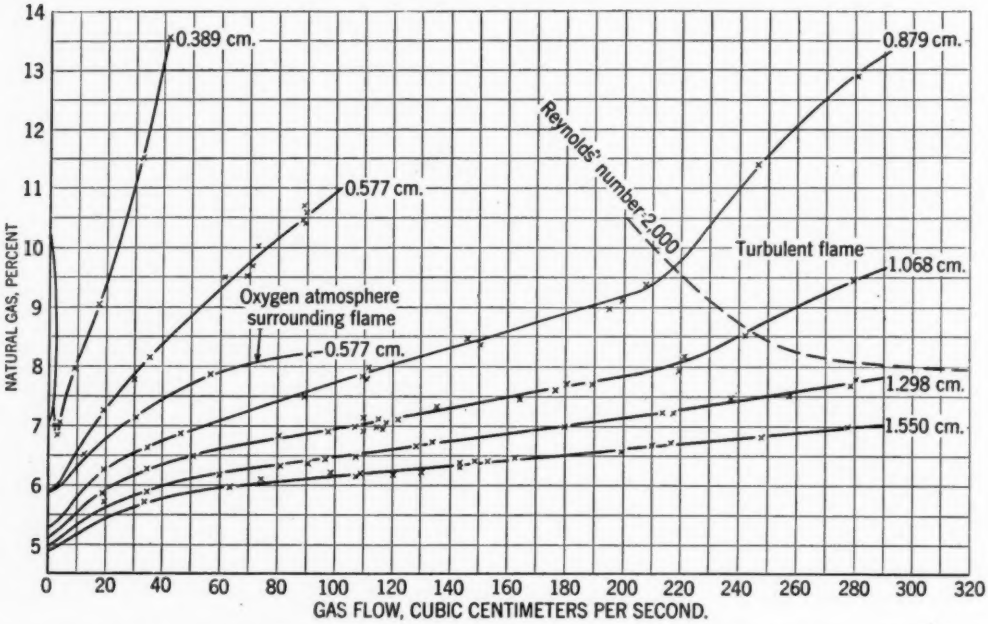

FIG. 13. Critical flows for blow-off of natural gas-air flames from cylindrical tubes of different diameters at room temperature. Flames surrounded by air except as indicated.

demonstrates the effect of interdiffusion on the burning velocity in the boundary layer of the stream. That the largest effect is obtained with a surrounding atmosphere of helium is understood from the larger diffusion coefficient of this gas. The greater effect of carbon dioxide as compared with nitrogen suggests the influence of the higher heat capacity of this gas on the temperature in the combustion zone at the boundary. It was found that the velocity of the surrounding gas parallel to the burner tube had no effect on the blow-off over a considerable range. This is understandable because the surrounding gas in contact with the flame gas at the burner rim is retarded by friction at the outer surface of the burner tube. Only if the gas is blown across the rim does its velocity affect the blow-off strongly.

Since quenching of the explosive reaction by the surface of the tube is attributed to cooling and destruction of chain carriers (atoms, free radicals), the question may be raised whether the nature of the surface of the burner tube influences the flash-back and limit of inflammability. Experiments with Pyrex tubes coated with salts such as sodium tungstate and potassium chloride and with silver showed the same limits and flash-backs as with clean Pyrex tubes. This contrasts sharply with the effect of these surface treatments on reaction rates and explosion limits of hydrogen-oxygen and hydrocarbon-oxygen mixtures enclosed in heated vessels. In the latter experiments cooling effects are negligible because the reacting gas is virtually at the same temperature as the wall of the reaction vessel, and the quenching effect of surface is confined to the destruction of chain

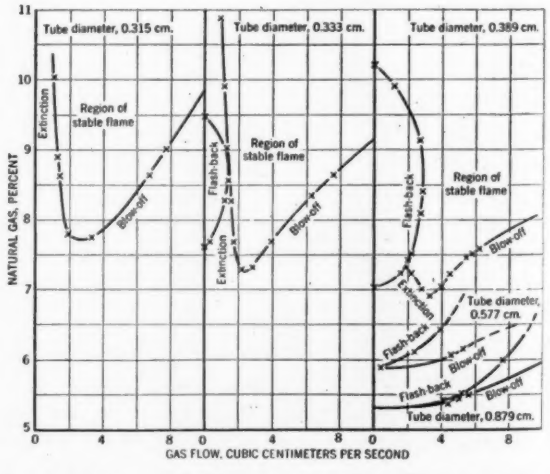

FIG. 14. Regions of stable natural gas-air flames in air for several cylindrical tubes at small flows.

carriers. In the present experiments, however, the cooling effect is very large. It is virtually independent of the nature of the tube material because the heat conductivity of a solid exceeds that of a gas by several orders of magnitude. The wall, therefore, constitutes an effective temperature-sink, and the rate of heat transfer is governed by the heat conductivity of the gas. Whether cooling overshadows destruction of chain carriers by the wall cannot be stated with certainty at present; the experiments do not allow a decision because destruction of chain carriers may also be independent of the nature of the surface for the following reason: In the combustion zone the concentrations of atoms and free radicals are very large, being comparable (within an order of magnitude) to the concentrations of the reactants themselves.[9] Therefore, any surface close to the combustion zone is well-covered with adsorbed atoms and radicals, and such species diffusing to the surface easily find reaction partners for recombination to neutral molecules, the wall serving as third body. The rate of chain-carrier destruction, therefore, becomes equal to the rate of diffusion independent of the nature of the surface. This contrasts with the slow reaction between hydrogen or hydrocarbons and oxygen, where the chain-carrier concentrations are very low; here the probability of recombination at the surface depends strongly on the adsorptivity of the surface. A clean Pyrex surface, for example, permits many chain carriers to return to the gas phase and therefore has a low chain-breaking efficiency. A salt-coated surface has a relatively large adsorptivity for chain carriers and therefore a high chain-breaking efficiency.[10]

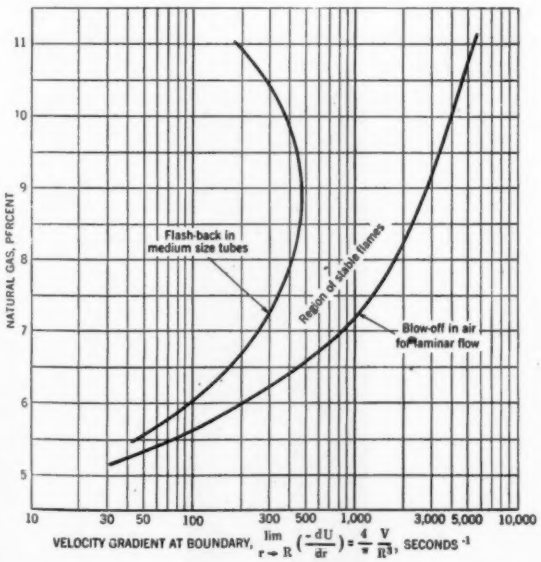
NATURAL GAS, PERCENT
Flash-back in medium size tubes
Region of stable flames
Blow-off in air for laminar flow
VELOCITY GRADIENT AT BOUNDARY, $\lim_{r \to R}(-\frac{dU}{dr}) = \frac{4}{\pi}\frac{V}{R^3}$, SECONDS^{-1}

FIG. 15. Region of stable natural gas-air flames for laminar streams in cylindrical burner tubes.

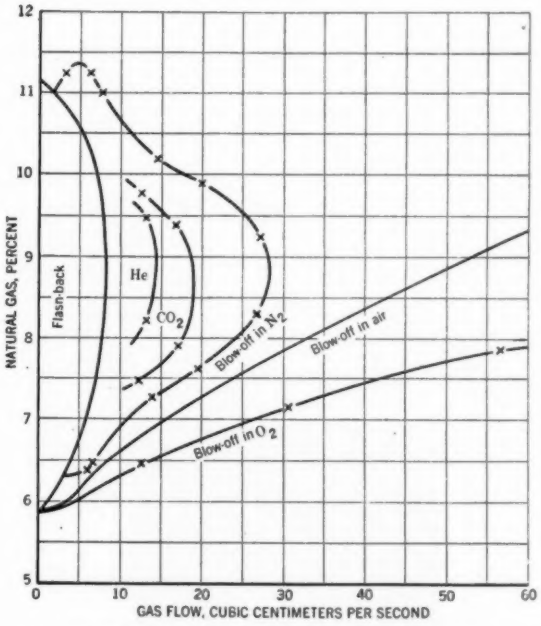

FIG. 16. Effect of nature of surrounding atmosphere on blow-off of natural gas-air flames from cylindrical burner tube. Tube diameter 0.577 cm.

(b) Inverted Flames

At flows exceeding the critical for blow-off, a zone of equality of burning and gas velocities may be formed above an obstruction in the stream by the effects of friction and quenching and may support a stable flame over some range of flows. If the obstruction consists of a wire mounted in the axis of a cylindrical burner tube, the outward propagation of the combustion zone from the point of equality above the wire and the upward flow of the gas results in an inverted cone, of which the photograph in Fig. 17 is an example. In taking this and similar photographs,

[9] B. Lewis and G. von Elbe, J. Chem. Phys. **2**, 537 (1934).

[10] G. von Elbe and B. Lewis, J. Chem. Phys. **10**, 366 (1942).

the light beam was narrower than the wire to avoid illuminating particles in front of and behind it. Particles in the shadow of the wire are invisible. The inverted cone blows off above some critical flow. When the flow is decreased the tip approaches the wire and as the latter is heated its quenching effect may decrease sufficiently to permit the combustion zone to travel down its length within the adjacent slow-moving gas layer. The inverted flame is then drawn through the burner tube as successively lower parts of the wire are heated by conduction.

Figure 18 is a photograph of a dust-laden air stream from a cylindrical tube of 1.068-cm diameter containing a centrally mounted wire of 0.107-cm diameter. The measured velocities at various distances r from the axis of the tube, corrected for free fall of the particles, are plotted in Fig. 19. Close agreement is found with the velocities calculated from the equation of flow through an annular space,[11]

$$U=n\left(R^2-r^2+\frac{R_w^2-R^2}{\ln R_w/R}\ln r/R\right), \tag{5}$$

FIG. 17. Inverted flame cone with particle tracks. Tube diameter, 1.717 cm, wire diameter, 0.211 cm; mixture composition, 6.20 percent natural gas in air; gas flow, 168 cc/sec. Particles invisible in shadow of wire on the left.

[11] Lamb, *Hydrodynamics* (Cambridge Press, 1924), fifth edition, p. 555.

and

$$V=\frac{\pi}{2}n\left(R^4-R_w^4+\frac{(R_w^2-R^2)^2}{\ln R_w/R}\right), \tag{6}$$

where R_w is the radius of the wire.

For a given wire the critical flows for blow-off of the inverted cone for various tubes are such that the velocity gradient at the surface of the wire remains constant (Figs. 20 and 21). The gradients are calculated from the following equations, which are obtained by differentiation of Eq. (5) and combining with Eq. (6),

$$\lim_{r\to R_w}\frac{dU}{dr}=n\left(-2R_w+\frac{R_w^2-R^2}{\ln R_w/R}\frac{1}{R_w}\right), \tag{7}$$

$$=-\frac{2}{\pi}\frac{V}{R^3}\frac{b\left(\dfrac{1-1/b^2}{\ln b}-2\right)}{1-b^4+\dfrac{(b^2-1)^2}{\ln b}}, \tag{7a}$$

where $b=R_w/R$.

If the diameter of the wire is varied for a given tube diameter (Fig. 22), the critical velocity gradient remains constant over a considerable range of wire diameters, as shown in Fig. 23. For the smallest wire (0.0643 cm) a slight decrease and for the largest wire (0.536 cm) a considerable increase are observed. The decrease toward smaller wires is explained by the decrease of the burning velocity at the tip of the inverted cone:

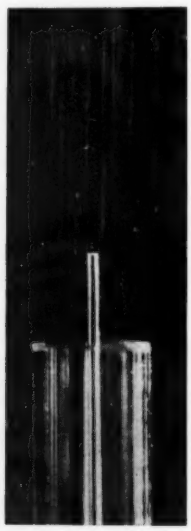

FIG. 18. Particle tracks in an air stream from a cylindrical tube of 1.068-cm diameter with central wire of 0.107-cm diameter. Gas flow, 155 cc/sec.

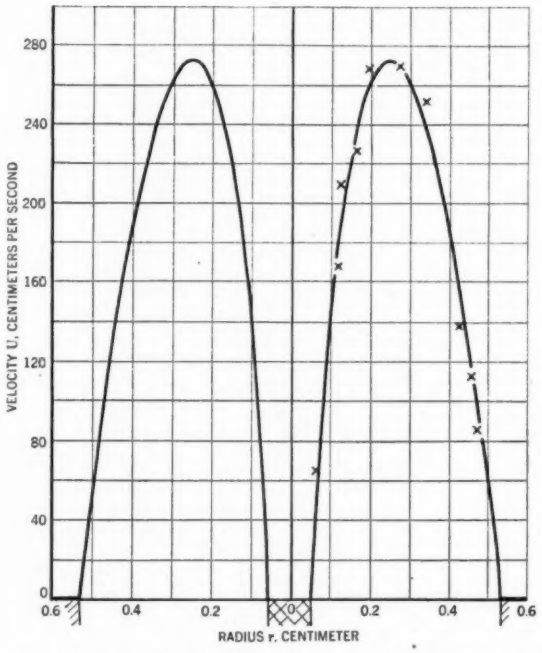

FIG. 19. Velocity distribution in a laminar stream of air (155 cc per second) at the orifice of a cylindrical tube of 1.068-cm diameter, in whose axis a wire of 0.107-cm diameter is mounted. Temperature 25°C; pressure 740 mm Hg. ×, experimental velocity. ——, calculated velocity.

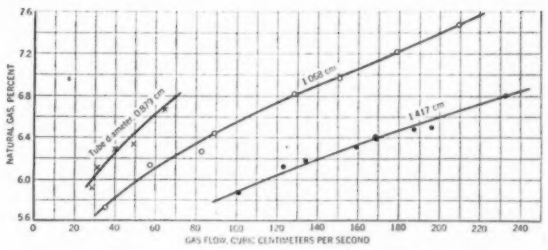

FIG. 20. Critical flows for blow-off of inverted natural gas-air flame cones from end of a wire mounted in axes of cylindrical tubes of various diameters. Diameter of wire 0.107 cm.

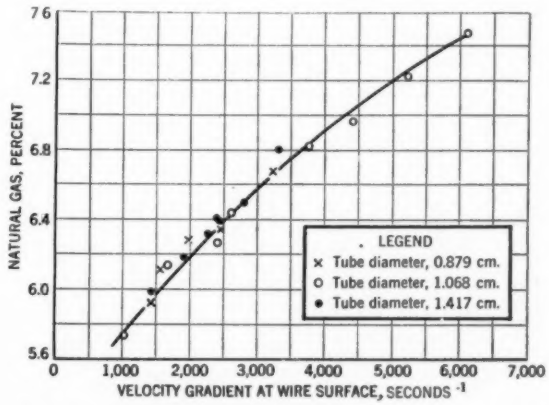

FIG. 21. Critical velocity gradients at wire surface for blow-off of inverted natural gas-air flame cones from end of a wire mounted in axes of cylindrical tubes of various diameters. Diameter of wire 0.107 cm.

the stream of slow-moving gas above a fine wire is confined to such a fine filament that the combustion zone at the tip of the inverted cone tends to become highly curved and therefore loses more heat and chain carriers to the unburned gas than the relatively flatter cone tip above a larger wire. For very large wires there is an appreciable decrease of gas velocity above the wire because, as the flow lines close in toward the axis (as may be observed in the example of Fig. 18), the cross section of the stream is increased. Large wires therefore retain the flame better.

Comparison of velocity gradients for blow-off from wires with those for blow-off of upright flames in air shows that the former are much larger, due to absence of the diluent effect of the surrounding atmosphere; this fact explains why a Méker burner may operate on leaner mixtures than the ordinary Bunsen burner.

3. FLOW PATTERN AND TEMPERATURE DISTRIBUTION IN THE FLAME

(a) Upright Flames

The diagram in Fig. 24, which was drawn from photographic records of flames obtained under the same conditions as Fig. 1, illustrates the flow pattern of the laminar gas stream in the flame. The combustion zone forms an angle with the flow lines so that the normal component of the gas velocity equals the burning velocity. Thermal expansion increases the gas velocity as well as the angle of the flow lines in such a way that the mass flow in any filament remains constant. It is observed that the refraction of a flow line begins well before it enters the luminous combustion zone, indicating penetration of heat into the unburned gas to a considerable depth. This effect gives rise to schlieren, or striations, in front of the combustion zone which are particularly well observed with inverted flames because there the burned gas is not in the line of sight. It is also strikingly demonstrated in Fig. 25 where stannic chloride hydrate smoke has been added to an inverted flame. The smoke disappears on approaching the combustion zone owing to dissociation of the hydrate, the zone of disappear-

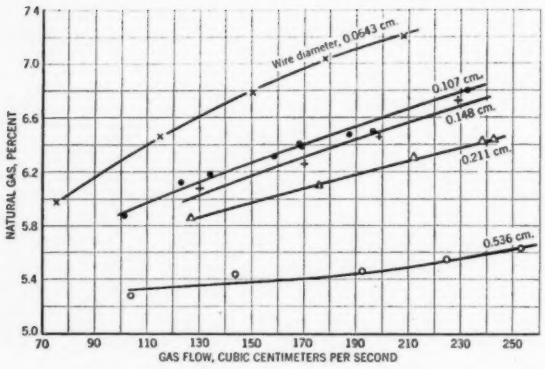

FIG. 22. Critical flows for blow-off of inverted natural gas-air flame cones from end of wires mounted in axis of a cylindrical tube of 1.417-cm diameter.

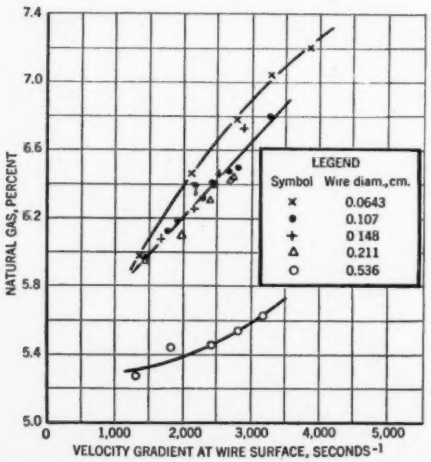

FIG. 23. Critical velocity gradients at surfaces of wires for blow-off of inverted natural gas-air flame cones from ends of wires mounted in axis of a cylindrical tube of 1.417-cm diameter.

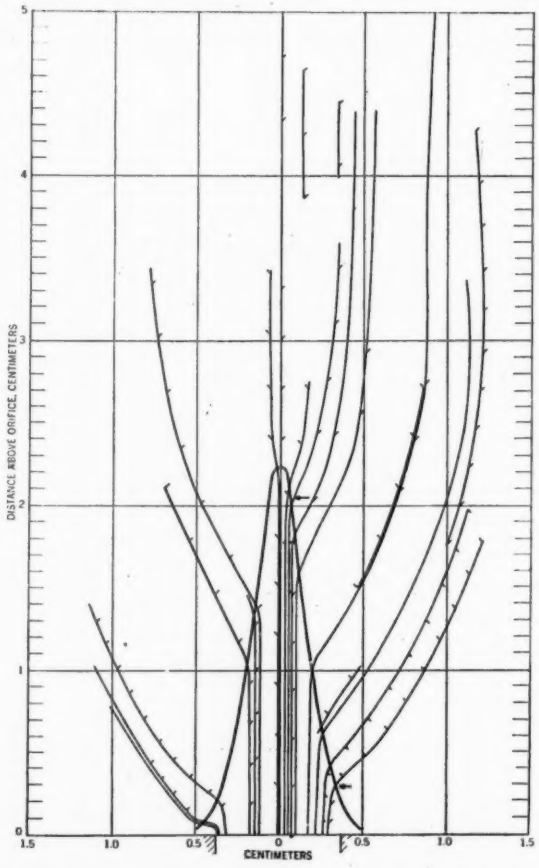

FIG. 24. Diagrammatic reproduction of the flame and particle tracks in Fig. 1 and additional photographs. Rectangular burner tube, 0.755×2.19 cm. 204 cc per second, 7.50 percent natural gas in air. Cone outline is the inner border of the luminous combustion zone of 0.2- to 0.3-mm thickness. Arrows indicate range of constant burning velocity. Particle tracks are interrupted in intervals of 1.436×10^{-3} second.

ance presumably beginning at a temperature close to 83°C at which the tri-hydrate is known to decompose. Furthermore, Fig. 24 shows that the outer flow lines deflect away from the axis considerably before they reach the zone of heat penetration; this is attributable to back pressure caused by acceleration of expanding gas in the combustion zone, forcing the stream to diverge as it emerges from the orifice. The divergence is particularly noticeable in flames of low gas velocity, of which Fig. 26 is an example. The outermost flow lines near the rim bend around sharply owing to heat as well as back pressure. In consequence, combustible gas is carried beyond the radius of the tube, causing the base of the cone to extend beyond the orifice and forming the overhang commonly observed. Following the combustion zone downward, one observes that the angle between flow lines and combustion zone increases until a flow line enters it at right angles; here the gas velocity, modified by thermal and dynamic effects, and burning velocity, modified by the rim effect and interdiffusion with the surrounding atmosphere, are equal. Below this point the gas velocity is again larger than the burning velocity, as may be seen from the fact that the angles between flow lines and combustion zone are not right angles. This corresponds to the illustration in Fig. 7b. The lowest visible flow lines are seen to skirt the luminous zone, and the gas carried up in the

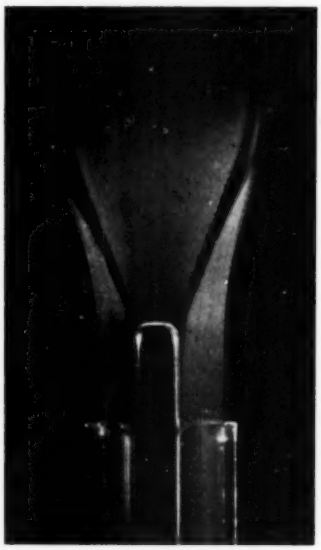

FIG. 25. Penetration of heat from combustion zone into unburned gas made visible by disappearance of stannic chloride hydrate smoke.

outermost layers reacts comparatively slowly downstream in the envelope.

The burning velocity S_u, that is, the rate of progress of the combustion zone in the normal direction, is defined by the equation of conservation of mass:

$$S_u dl = U_u dr, \tag{8}$$

where U_u is the velocity of the unburned gas in a filament of width dr, and dl is the width of the same filament as it enters the combustion zone. From a diagram of the type of Fig. 24, the length l of the cone outlined from the tip to the intersection of any of the registered flow lines originating at various radii r at the orifice may be determined, and from the plot of l *versus* r the differential quotient dl/dr for any value of r may be obtained. As U_u is also known as a function of r [Eq. (1)], S_u can be determined over the entire cross section of the stream from Eq. (8): Figure 27 shows burning velocities over the cross section

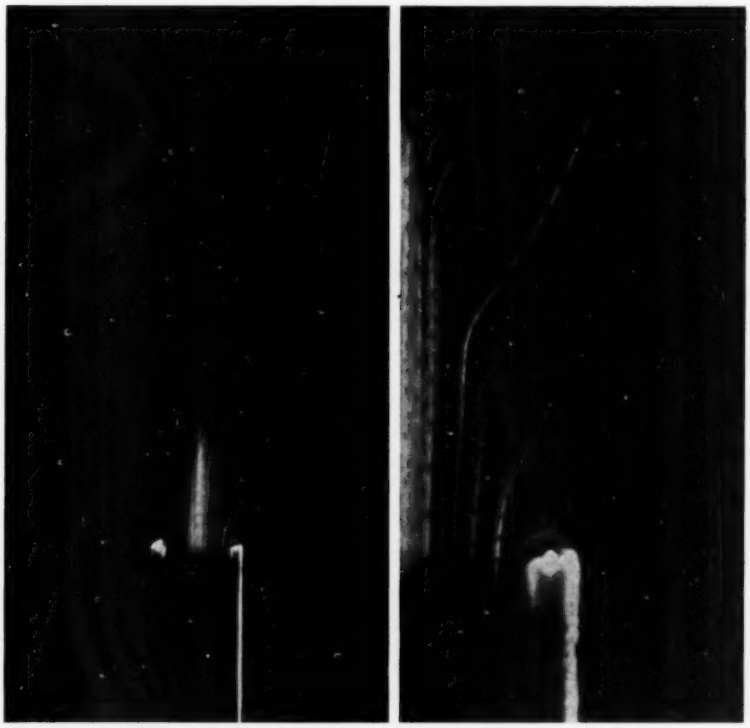

FIG. 26. Flame of low gas velocity, showing divergence of unburned stream caused by back pressure. Enlargement shows outermost flow lines skirting base of cone. Rectangular burner tube; gas flow, 88 cc/sec.; mixture composition, 6.32 percent natural gas in air.

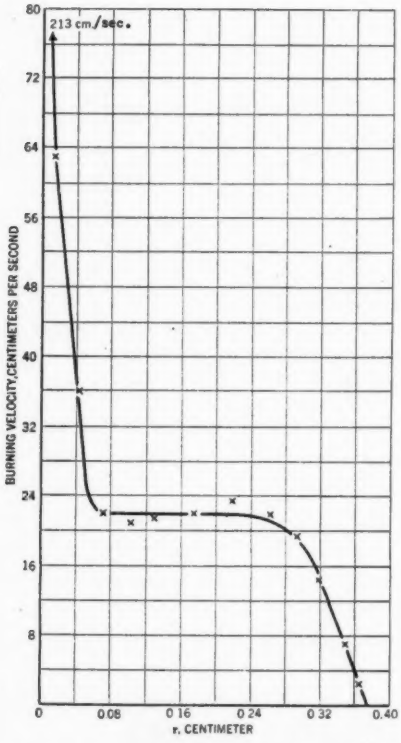

FIG. 27. Burning velocity of flame (Fig. 24) in the flow lines originating at distance r from axis of burner tube. Points correspond to readings of dl/dr from plot of l *versus* r (see text).

of the stream for the flame illustrated in Fig. 24. The burning velocity is highest at the rounded tip where the axial flow line enters the combustion zone in the normal direction, namely $S_u = U_u = 213$ cm per second. From the tip downward, the burning velocity decreases sharply to a constant value of 22.0 cm per second, which extends over the length of flame outline indicated by arrows in Fig. 24, and then drops to zero on approaching the base. The high value at the tip reflects the convergence of heat flow and chain-carrier diffusion into the narrow unburned stream from the adjacent burning gas.[12] At the base, besides the rim effect and interdiffusion with the surrounding atmosphere, the divergence of heat flow and chain-carrier diffusion contributes to the low burning velocity.

The usual procedure for determining burning velocity has been to divide the flow by the cone area, which provides an average value over the whole flame. The corresponding procedure—namely, dividing the flow in the plane shown in Fig. 24 by the total length of the cone outline—yields the average burning velocity of 23.4 cm per second in agreement with the above constant value, showing that the high and low burning velocities around the tip and the base, respectively, approximately cancel each other. It is clear that such agreement is conditioned by the choice of orifice dimension and gas flow and cannot be expected as a general rule. If, for example, the orifice were smaller, the cone height would, for the same average gas velocity, decrease approximately proportionately, while the height of the disturbed zone from the base upward would remain approximately constant and contribute proportionately more to depressing the average burning velocity. Corresponding considerations apply to circular burners, and indeed Smith[6] found that the average burning velocity obtained from cone area and flow decreases with decreasing tube diameter. Smith

[12] The increase in burning velocity from this cause also may explain the formation on cylindrical tubes of Bunsen flames of polyhedral structure described by F. A. Smith and S. F. Pickering [Bur. Stand. J. Research **3**, 65 (1929)]. These authors found that under certain conditions a circular Bunsen cone changed to a polyhedral cone having from 3 to 7 sides and the appearance of a "tent supported by ropes loosely draped from a center pole to pegs located at the corners of a regular polygon." The figure can be made to remain stationary or to rotate by changing very slightly the composition or velocity of the gas mixture. As the burning velocity is obviously larger along the ridges than along the planes of the polyhedron, the equality of gas and burning velocity is established at the end of the ridges at the base; the flame is, therefore, stabilized only at discrete points above the rim. A steady state requires that the angle between the faces of the polyhedron which is necessary to provide a burning velocity equal to the gas velocity be that of a regular polygon, because only in this way can dynamic symmetry be established. When the angle is not that of a regular polygon, this symmetry is destroyed and the figure rotates. Consequently, it is expected that for otherwise constant conditions a gradual change of mixture composition toward lower burning velocities should produce successive transitions from a circular cone to many-sided, down to three-sided polyhedrons and finally blow-off, the decreasing angle between the faces compensating for the loss of burning velocity on changing the mixture. Unfortunately, the experiments have not been performed in this way. Smith and Pickering varied the composition and gas flow simultaneously. The phenomena are readily observed with rich flames of the heavier hydrocarbons surrounded by a diluent gas, as is the case in a Smithells separator. The susceptibility of the heavier hydrocarbons to formation of polyhedral flames may be ascribed to the slowness of the explosive reaction with the consequent relatively large loss of heat and chain carriers to the preheated zone. If this loss is diminished by the approach of another combustion zone a large gain in reaction rate results. If the flame is surrounded by air then obviously the increased burning velocity at the base caused by interdiffusion of secondary air always preserves a circular cone.

himself determined the burning velocity from the angle of the cone surface at the distance 0.707 R, the supposition being that the cone surface at this point is intersected by a flow line in which the gas velocity is the average velocity over the cross section. It is true that within the tube the average gas velocity is at 0.707 R, but, as seen from Fig. 24, the flow lines bend outward above the orifice and at 0.707 R the cone surface is intersected by a more central flow line. This introduces a methodical error into Smith's method which, however, is not serious as long as the cone angle does not greatly change in the neighborhood of the point of measurement. Another criticism[13] of Smith's method, namely, that the velocity distribution over the cross section changes above the orifice, is invalidated by the present experiments, which show this effect to be negligible for usual cone heights.

The example of Figs. 24 and 27 is typical for flames of all mixture compositions outside of the very rich mixture range where the combustion zone becomes diffuse and is eventually obscured by the formation of free carbon (yellow tip) and combustion in secondary air. Several flames of different mixture compositions have been analyzed and the burning velocities in the constant range plotted in Fig. 28. The burning velocity is affected by the introduction of fine dust in considerable and uncontrolled quantity together with coarser particles. No effort was made to eliminate this source of error, since determination of burning velocity was not the primary purpose of this work, and the results, therefore, show considerable scattering.

In the course of these experiments it was noted that the introduction of stannic chloride hydrate smoke markedly lowered the burning velocity and, correspondingly, the critical flow for blow-off. That the inhibition of the explosive reaction was not caused by hydrochloric acid set free in the hydrolysis of stannic chloride was shown by the ineffectiveness of hydrochloric acid gas prepared from sulphuric acid and sodium chloride. The smoke gives rise to incandescence at the combustion zone, reminiscent of soot-forming flames, and the formation of particles of stannic oxide.

[13] Reference 5, page 86.

From knowledge of the burning velocity and the flow pattern it appears possible, in principle, to calculate the form of the inner cone from the condition that at the cone surface the normal component of the gas velocity equals the burning velocity, that is:

$$S_u = U_u \sin \alpha, \tag{9}$$

where α is the angle of the cone surface with the flow line on the unburned side. It is not possible, however, to treat this problem in closed mathematical form without simplifying assumptions because of disturbances at the tip and base of the cone, the finite thickness of the combustion zone, and the outward deflection of the flow lines caused by back pressure. Michelson's[14] treatment makes the following simplifying assumptions:

(a) The burning velocity is constant over the whole cone surface.
(b) The boundary between unburned and burned gases approximates a mathematical surface, the temperature changing abruptly from the initial to the final on passing through it.
(c) The flow lines retain their direction and velocity from the orifice right up to the cone surface.

Despite obvious limitations imposed by these assumptions, it is instructive to compare the cone surface calculated from Michelson's equation with the actual. In the following calculation Eq. (1) is used for the velocity distribution in

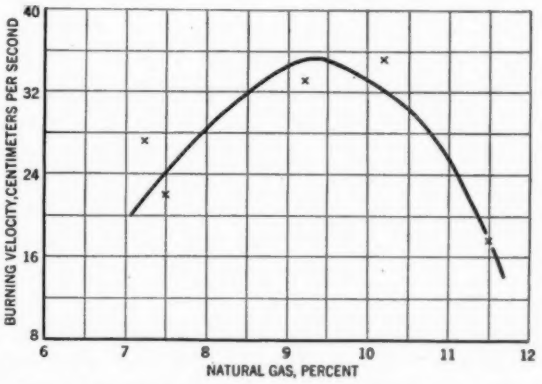

FIG. 28. Burning velocities in the constant range between tip and base of flame cones for various mixtures of natural gas and air.

[14] Cf. reference 4, page 48.

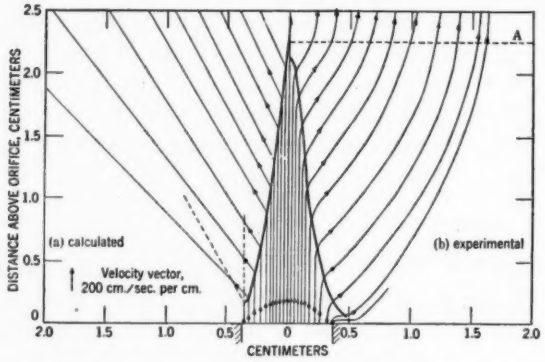

FIG. 29. Flame cone and flow pattern from analysis of the flame of Fig. 24.

the unburned gas; this differs from Michelson's treatment in which a finite gas velocity at the boundary exceeding the burning velocity was assumed, contrary to actual conditions. By retaining assumption (*a*) and using Eq. (1) it is evident that the cone surface can only be followed to a point near the boundary where the gas velocity equals the assumed constant burning velocity. The latter exceeds the gas velocity beyond this point, and no real solution to the equation of the cone surface exists. This is unimportant, however, because it concerns the disturbed boundary region where the theory is not applicable. The treatment yields only the shape of the cone and does not define its position with respect to the orifice. It may be mentioned that this is not remedied by Michelson's assumption of a finite gas velocity at the boundary exceeding the burning velocity. That is, Michelson's theoretical flame would blow off while the present theoretical flame would flash back.

The equation for coordinates r and z for any point on the cone surface, where r is the distance from the axis and z the height of the cone tip above the point, was obtained by Michelson by integrating the equation

$$dz/dr=\cot\alpha, \tag{10}$$

which, by means of Eq. (9), transforms to

$$\frac{dz}{dr}=\pm\frac{(U_u^2-S_u^2)^{\frac{1}{2}}}{S_u}, \tag{11}$$

where U_u as a function of r is given by Eq. (1), and S_u is constant. The result is:

$$z=\pm\frac{M}{3}\left[\sin\varphi\cos\varphi\Delta\varphi+\left(1-\frac{1}{k^2}\right)F(k,\varphi)+\left(1+\frac{1}{k^2}\right)E(k,\varphi)\right], \tag{12}$$

where

$$M=[nR^2/S_u-1][(nR^2+S_u)/n]^{\frac{1}{2}},$$
$$k^2=(nR^2-S_u)/(nR^2+S_u),$$
$$\sin^2\varphi=nr^2/(nR^2-S_u),$$
$$\Delta\varphi=(1-k^2\sin^2\varphi)^{\frac{1}{2}},$$

and $F(k,\varphi)$ and $E(k,\varphi)$ are elliptical integrals of the first and second kinds,

$$\int_0^\varphi\frac{d\varphi}{\Delta\varphi}\quad\text{and}\quad\int_0^\varphi\Delta\varphi d\varphi,$$

respectively. $n=-a/4\eta$ as above. Depending on the sign, the cone is upright or inverted. It can be shown theoretically that the upright cone is the stable form when the base is fixed in the stream and the inverted cone is the stable form when the tip is fixed in the stream.[15]

Figure 29a shows a cone calculated from Eq. (12) for the flow and burning velocity (22 cm per second) of the flame of Fig. 24. In Fig. 29b the experimental cone of Fig. 24 is reproduced with an interpolated set of flow lines. The calculated cone is placed in such a position above

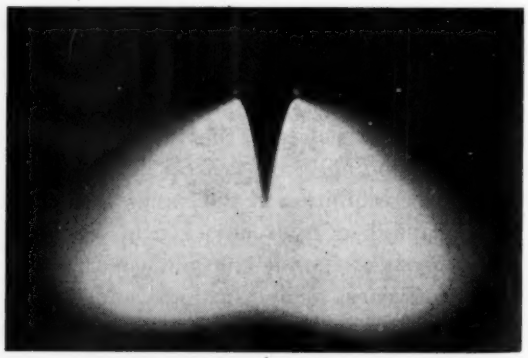

FIG. 30. Flame from rectangular burner tube, directed downward to accentuate separation of flame envelope. Sodium-colored for photographic contrast. Mixture composition, 8.46 percent natural gas in air; gas flow, 185 cc/sec.

[15] Reference 4, page 51.

the orifice that the flow line at $r=0.147$ cm intersects the cone outline at the same height above the orifice as the corresponding flow line of the experimental cone outline, namely, at 1.10 cm. It is seen that over the range of constant burning velocity the heights of the intersections of all other flow lines agree well in experiment and theory. Toward the base and the tip there occur the discrepancies expected from the decrease and increase of S_u, respectively; that is, toward the base the calculated cone outline is too short and toward the tip too long. The calculated outline ends at $r=0.357$ cm, where $U_u=S_u$, that is, 0.02 cm from the stream boundary. At this point the cone surface is highly curved, in itself suggesting a physical instability; that is, the burning velocity should decrease because of the extreme divergence of heat flow and diffusion in the direction of burning gas to unburned gas. Some curvature is preserved at the base of the actual cone, and this may contribute to the decrease of burning velocity toward the base. The sharp tip of the theoretical cone is evidently physically impossible; as mentioned before, preheating and preactivation of the unburned gas in this region from the adjacent combustion zone transform this to a rounded tip in the actual flame.

The theoretical flow lines are continued in the burned gas in Fig. 29a by means of the relation

$$\rho_b U_b \sin \beta = \rho_u U_u \sin \alpha, \qquad (13)$$

which equates the components of mass flow normal to the cone surface. ρ_u and ρ_b are the densities of unburned and burned gases, respectively, and β is the angle between flow line in the burned gas and cone surface. Assumption (*b*) above leads, furthermore, to the relation

$$U_b \cos \beta = U_u \cos \alpha, \qquad (14)$$

and hence

$$\rho_u/\rho_b = \tan \beta/\tan \alpha. \qquad (15)$$

ρ_u/ρ_b is taken as 5.90, corresponding to the flame temperature of 1750°C (see below), the initial temperature of 27°C and a change in molar volume of 1½ percent. The theory is inadequate for the description of convergent flow at the highly curved base, but this problem has no interest, inasmuch as the calculated base is unreal. It is seen that on passing through the

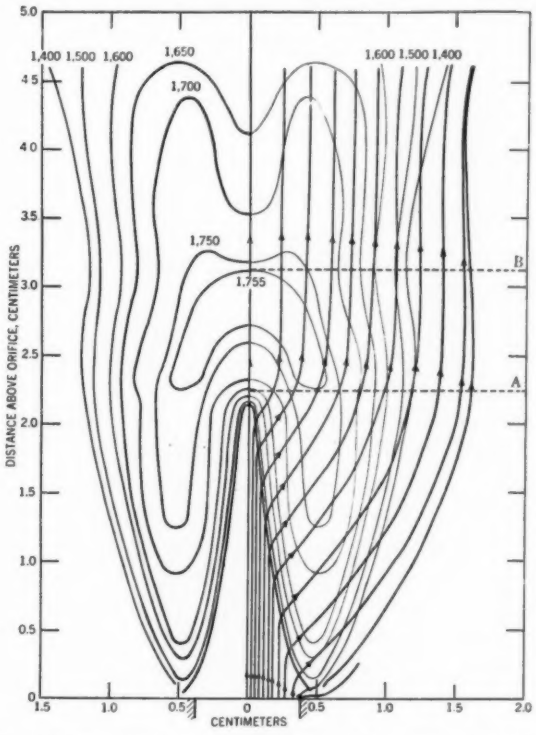

FIG. 31. Temperature distribution and flow pattern in the flame of Fig. 24. Temperatures in °C.

combustion zone the gas acquires a substantial velocity normal to the axis. The resulting divergence of the stream causes the maximum gas velocity to shift from the central flow line outward, as is shown by the actual flow pattern in Fig. 29b (compare velocity vectors at plane *A*). If the burner tube were circular, the horizontal velocity components along any flow line would decrease proportional to the distance from the axis because of the requirement of constancy of mass flow while the velocity components parallel to the axis remain constant (except for secondary effects of cooling, friction, and convective rise). The flow lines, therefore, would bend upward. In a burner tube of narrow rectangular cross section used in the present experiments the flow lines retain their direction, except as modified by convective rise of the hot gas, because the area through which the burned gas passes remains constant with distance from the axis. In this burner the flame envelope, therefore, splits into two parts. This is seen, for example, in Fig. 4. The separation would be greater were it not for convective rise. If the burner tube is turned

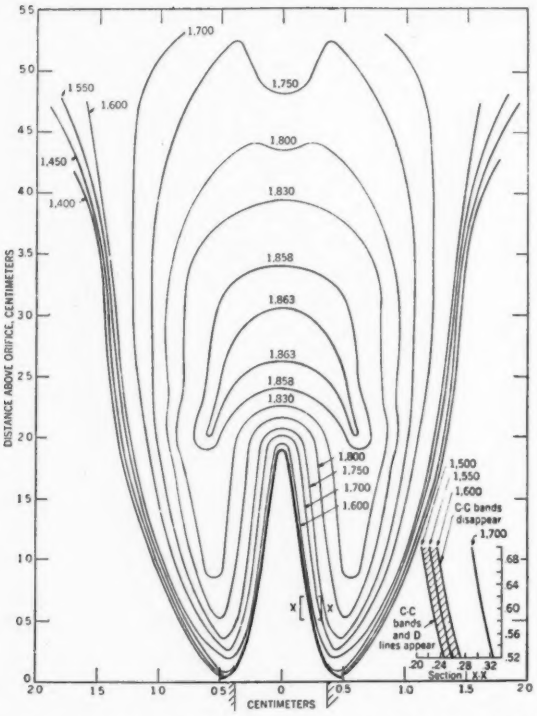

FIG. 32. Temperature distribution in flame of 8.70 percent natural gas in air; 224 cc per second; rectangular burner tube, 0.755×2.19 cm. Temperatures in °C.

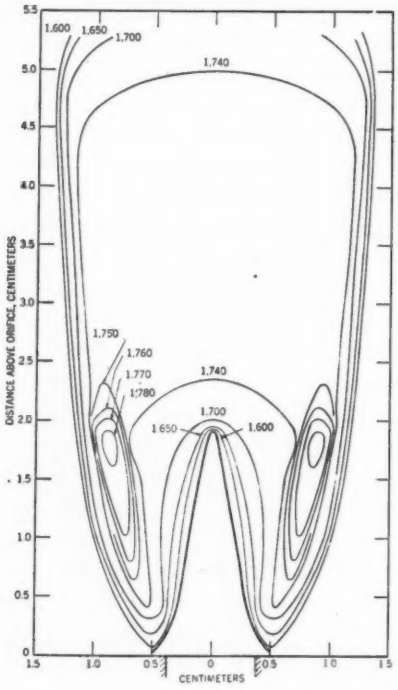

FIG. 33. Temperature distribution in flame of 10.96 percent natural gas in air; 161 cc per second; rectangular burner tube, 0.755×2.19 cm. Temperatures in °C.

upside down, convective rise accentuates the separation as shown in Fig. 30.

Because of assumption (*b*), the refraction of the flow lines in the theoretical flame is discontinuous. In the actual flame, where the temperature rise is spread out over some distance (see Fig. 31), the refraction is gradual. Nevertheless, the refraction angles agree rather well in experiment and theory, except in the neighborhood of the tip and base of the cone, until convective rise becomes effective. Similarly, the calculated velocities U_b [from Eqs. (14) and (15)] agree with the experimental U_b's except in the neighborhood of the tip, where the gas in the actual flame passes through a much smaller cone surface; hence U_b is much larger than calculated.

The flow lines in Fig. 29b were corrected for inertia of the particles, which tend to retain their original direction of motion and not to follow completely the change in direction of the gas. There is evidence of inertia from occasional photographic tracks that show unusually small refraction angles. Furthermore, for a number of tracks it was found that the condition of constancy of mass flow was not fulfilled. This condition requires that the area between the velocity vectors of two neighboring flow lines in the burned gas should be ρ_u/ρ_b times the corresponding area in the unburned gas. Particularly at the tip, particles in the burned gas are generally too close together. This region is marked by considerable divergence of the flow lines, and hence the inertia effect is most pronounced here. On the side of the cone, especially in the region of constant burning velocity where the flow lines are approximately parallel, tracks of two adjacent particles are about equally affected by inertia, and the error tends to cancel out. In this region the ratio of the areas between the velocity vectors agrees with the theoretical value of ρ_u/ρ_b, increasing from the combustion zone outward in correspondence with the temperature rise.

Correction of the flow lines in Fig. 29b for particle inertia was made in the following way. Except in the immediate neighborhood of the combustion zone, particles may be supposed to follow the gas flow closely; from Fig. 24 the

velocity and direction of the gas at any point in the plane A above the tip may be obtained. If r_b is the distance of a point in plane A from the axis and $U_{b(n)}$ is the velocity component normal to the plane, the condition of constancy of mass flow in burned and unburned gases is

$$\rho_b U_{b(n)} dr_b = \rho_u U_u dr. \qquad (16)$$

ρ_u/ρ_b at any r_b is obtained from the experimental temperature-distribution chart of Fig. 31. A curve of r_b *versus* r is constructed so that for any r_b differential quotient dr_b/dr equals $(U_u/U_{b(n)})(\rho_u/\rho_b)$. Thus, the intersection of any flow line originating at r in the plane of the orifice with plane A is known. To construct the flow lines, it suffices to determine the curve of r_b *versus* r in the plane A only, because for points not too close to the axis the intersections with plane A differ little from the photographed particle tracks, and near the axis (where the particle tracks are least reliable) the curved part of the flow line between r and r_b extends over only a short distance and cannot be appreciably in error.

Figure 31 shows the temperature distribution in the flame of Fig. 24. The corrected flow pattern of Fig. 29b is superimposed and extended with the aid of Fig. 24. The maximum temperature of 1755°C agrees with the temperature calculated for conditions of adiabatic combustion and thermodynamic equilibrium. It is attained in the protected central portion of the flame in about 0.0025 second after the gas has passed through the luminous combustion zone, although the main temperature rise, say to 1650°C, is completed in about 0.0005 second. Near the base, the cooling effect of the rim and dilution with the surrounding atmosphere is reflected in a sharp decrease of the temperature and, as is seen in Fig. 27, of the burning velocity. The temperature distribution in the envelope above the cone is conditioned by heat loss to the atmosphere, not only in the plane of the diagram but on all sides of the flame, because the envelope expands in the plane of the diagram and contracts in the plane normal to it, as may be seen in Fig. 4. The closed isotherms thus develop two maxima corresponding to the regions of highest flow (compare velocity vectors in plane B), since the slower-moving gas in the center, although protected by regions of higher temperature in the plane of the diagram, loses heat in the direction normal to the plane. The progress of cooling of the flame gas is further recorded in the pattern of the outer isotherms which move first inward, coincident with the upward-bending of the flow lines, and then outward again as the heat flow from the interior of the stream becomes noticeable.

Figure 32 shows the isotherms for a near-stoichiometric flame. The temperature distribution is similar to that of Fig. 31. A detail (see insert) of the region near the luminous combustion zone is also given. In natural gas-air mixtures the luminous zone is marked by the sharp appearance and disappearance of the C−C (Swan) bands and C−H bands. The sodium D lines appear simultaneously with these bands, so that temperature readings can be taken within the combustion zone itself. As seen from the inset, the luminous combustion zone is about 0.2 mm thick. At the inner boundary of the zone where the D lines first appear the temperature has already risen to 1500°C, and at the outer boundary of

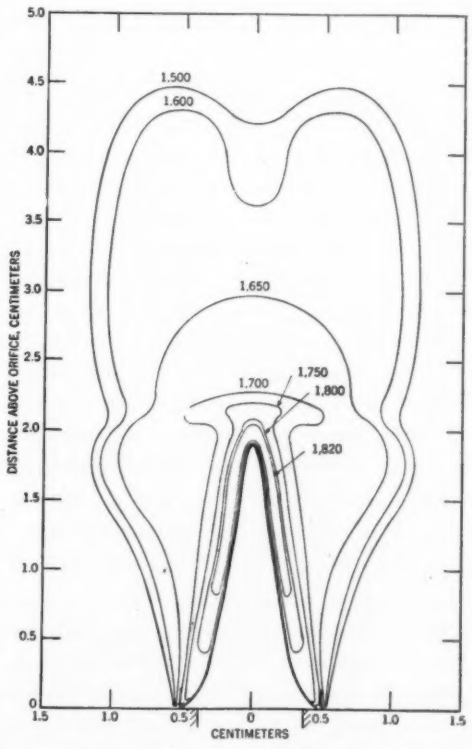

FIG. 34. Temperature distribution in flame of 7.06 percent natural gas in oxygen; 256 cc per second; rectangular burner tube, 0.755×2.19 cm. Temperature in °C.

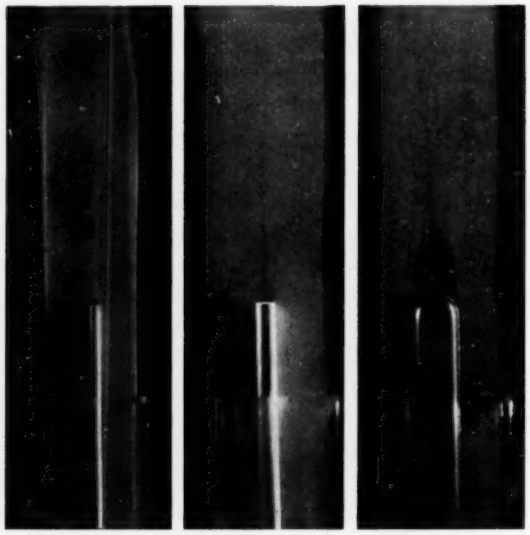

(a) (b) (c)

FIG. 35. Air streams with smoke from tubes with centrally mounted wires, showing annular vortex above wires.

	(a)	(b)	(c)
Tube diameter, cm	1.068	1.417	1.417
Wire diameter, cm	0.107	0.211	0.536
Gas flow, cc/sec.	155	189	168
Velocity gradient at wire surface, sec.$^{-1}$	4500	2130	2130

the zone it has reached 1600°C. As the *D* lines are not observable in front of the inner boundary, the temperature gradient at the beginning of the combustion zone must be exceedingly steep.[16]

Figure 33 shows the isotherms for a very rich flame. Here the temperature distribution is modified by combustion with secondary air, hence the upper part represents a broad region of more or less constant temperature. The effect of secondary combustion is noted in the inward bending of the isotherms toward the base of the cone. This causes an increase in the burning velocity just above the base of the cone in agreement with the high gas flow required to blow off flames of rich mixtures. An interesting feature is the concentration of high temperature within the closed isotherms at the sides.

Figure 34 shows the isotherms of a lean natural gas-oxygen flame. Such flames differ from air mixtures, in that the highest temperature is found to border immediately on the luminous combustion zone. Here *D*-line emission is exceptionally brilliant. In the luminous combustion zone no bands of C−C and C−H appear, the radicals evidently reacting rapidly with oxygen; only a continuous spectrum is visible, which also appears in the combustion zone of air flames but much weaker. *D*-line emission in the envelope is not as strong as in air flames, for the same NaCl concentration, although the temperature may be the same. This points to a decrease of the equilibrium concentration of sodium atoms on increasing the oxygen concentration. In accord with this is the observation that the most brilliantly colored flames are those that do not contain excess oxygen. The validity of the line-reversal method is independent of the sodium-atom concentration, the advantage of high concentration being the ease of determining the point of reversal. The maximum temperature in the flame of Fig. 34 exceeds the theoretical temperature by about 120°C.[17] A discussion of this effect, for which there is also evidence from explosion-pressure measurements in excess oxygen mixtures, has been given elsewhere upon the basis of time lag of vibrational excitations.[18]

The difference between oxygen- and air-flames evidently is that in the former the combustion reaction is virtually completed in the combustion zone. A possible explanation is the burning of carbon monoxide which survives the reactions within the zone.

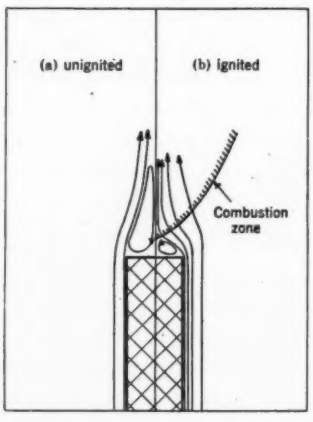

FIG. 36. Stream lines above wire with flat end, showing vortex. Wire diameter, 0.211 cm.

[16] See also F. A. Smith and S. F. Pickering, J. Res. Nat. Bur. Stand. **17**, 7 (1936).

[17] See also H. H. Kaveler and B. Lewis, Chem. Rev. **21**, 421 (1937).

[18] Reference 7, pp. 306–344.

(b) Inverted Flames

The flow pattern of an inverted flame is illustrated by Fig. 17. The flow lines in the unburned gas are deflected outward by back pressure of the expanding flame gas and become parallel again on passing through the combustion zone. At the base of the cone where, in this example, the gas stream becomes turbulent, the combustion zone is always observed to trail because of the decreased burning velocity in the boundary of the stream. In the stagnant space above the wire, an annular vortex is formed that can be made visible with smoke in an air stream. Three such photographs are shown in Fig. 35. The cross section of the vortex is oval because the upward velocity of the outer filaments, which is imparted to them by the adjacent flow lines, exceeds the horizontal velocity of the filaments near the wire, which is decreased by friction. The vortex seems to be unimportant for the attachment of the flame, because it was found that the critical flow for blow-off did not change when the end of the wire was rounded. The presence of the flame, however, greatly reduces the diameter of the vortex as is seen by comparing Fig. 35b with Fig. 17. In the latter the flame tip has compressed the region of vorticity. The original negative of the photograph in Fig. 17 shows particle tracks in vortex motion hugging the end of the wire below the combustion zone. Combustible mixture feeding the combustion zone at the tip is provided by laminar filaments above the vortex. This is illustrated in Fig. 36, which is a sketch of flow lines in the unignited and ignited streams.

Although the experiments described in this paper were performed with natural gas, which has a conveniently low burning velocity for studies in the laminar flow range and satisfactory actinity for photographic exposures, it is evident that the mechanism of flame stabilization and the factors determining flame structure are equally operative for any fuel gas.

FEBRUARY, 1943 JOURNAL OF CHEMICAL PHYSICS VOLUME 11

The Ratio Rule

HERMANN D. NOETHER
Mallinckrodt Chemical Laboratory, Harvard University, Cambridge, Massachusetts

(Received November 28, 1942)

An empirical rule for calculating the frequencies of isotopic groups in molecules is proposed and experimental evidence for it reported.

THE application of the product rule[1] is extremely useful for obtaining an approximate assignment of the fundamental frequencies of isotopic molecules. In the following a rule connected with the product rule will be described.

In the investigation of the isotopic methyl halides it was observed that each frequency of CD_3Cl could be predicted separately, in terms of the corresponding frequency of CD_3X, CH_3X, and CH_3Cl by means of the relation

$$\nu_{nCD_3Cl} = \frac{\nu_{nCD_3X}}{\nu_{nCH_3X}} \nu_{nCH_3Cl},$$

where for ν_n the corresponding frequencies have to be substituted. Table I gives the fundamental frequencies of CD_3Cl[2] calculated by this rule from the CH_3Cl frequencies and those of the isotopic bromides.

Tables II–V give the calculated frequencies for

[1] Teller, cf. C. K. Ingold et al., J. Chem. Soc. London, 971 (1936); O. Redlich, Zeits. f. physik. Chemie **B28**, 371 (1935); E. B. Wilson, Jr., J. Chem. Phys. **9**, 76 (1941).

[2] H. D. Noether, J. Chem. Phys. **10**, 664 (1942).

TABLE I. Frequencies of CD_3Cl calculated by ratio rule. ν=stretch, δ=bending, τ=rocking, π=||, σ=$\perp$.

Frequency	CH_3Br	CD_3Br	CH_3Cl	CD_3Cl Calculated	CD_3Cl Observed
$\nu(\pi)$, $2^2\delta(\sigma)$	2860	2089	2880	2104	2104
	2972	2152	2967	2148	2162
$^2\nu(\sigma)$	3061	2294	3047	2284	2287
$\delta(\pi)$	1305	987	1355	1025	1029
$^2\delta(\sigma)$	1450	1053	1460	1060	1058
$\nu(\pi)$	610	577	732	692	695
$^2\tau(\sigma)$	957	717	1020	764	775

TABLE II. Frequencies of CD_3OH* calculated by ratio rule.

Frequency† class	CH_3OH*	CD_3OH calculated from CD_3Br	CD_3OH calculated from CD_3Cl	Mean value	CD_3OH observed
A_1 $\nu(\pi)$	2845	2078	2078	2078	2094
$\delta(\pi)$	1455	1100	1105	1103	1123
$\nu(\pi)$	1034	981	982	982	990
E $^2\nu(\sigma)$	2978	2232	2235	2233	2232
$^2\delta(\sigma)$	1477	1073	1072	1073	1080?
	1430?	1038	1037	1038	1055?
$^2\tau(\sigma)$	1260	944	957	950	878?
	1209	906	919	912	856?

* For frequencies and assignment of CH_3OH, CH_3OD, CD_3OH, CD_3OD see reference 3.
† ν, δ, τ corresponding frequencies in the methyl halides. (See Table I.)

TABLE III. Frequencies of CD_3OD* calculated by ratio rule.

Frequency† class	CH_3OD*	CD_3OD calculated from CD_3Br	CD_3OD calculated from CD_3Cl	Mean value	CD_3OD observed
A_1 $\nu(\pi)$	2850	2082	2082	2082	2081
$\delta(\pi)$	1459	1103	1108	1106	1121
$\nu(\pi)$	1040	987	987	987	987
E $^2\nu(\sigma)$	2965	2222	2225	2224	2227
$^2\delta(\sigma)$	1480	1075	1075	1075	1075?
	1427	1036	1034	1035	1045?
$^2\tau(\sigma)$	1232	923	936	929	?
	1207	904	917	910	?

* For frequencies and assignment of CH_3OH, CH_3OD, CD_3OH, CD_3OD see reference 3.
† ν, δ, τ corresponding frequencies in halides.

TABLE IV. Frequencies of CD_3NO_2 calculated from ratio rule.

Frequency* class	CH_3NO_2	CD_3NO_2 calculated from CD_3Br	CD_3NO_2 calculated from CD_3Cl	CD_3NO_2 obs.
A_1 $\nu(\pi)$	2965	2166	2166	2195
$\delta(\pi)$	1413	1069	1073	1090
$\nu(\pi)$	921	871	874	879
B_1 $^2\nu(\sigma)$	3048	2284	2288	2290
$^2\delta(\sigma)$	1448	1052	1050	1051
$^2\tau(\sigma)$	1097	822	834	876
B_2 $^2\nu(\sigma)$	3048	2284	2288	2299
$^2\delta(\sigma)$	1488	1081	1078	1050
$^2\tau(\sigma)$	1153	864	876	944

* ν, δ, τ represent the corresponding frequencies in the halides (for notation see Table I).

the isotopic pairs CH_3OH-CD_3OH,[3] CH_3OD-CD_3OD,[3] $CH_3NO_2-CD_3NO_2$ and $C_2H_6-C_2D_6$.[4] The fundamental frequencies of CH_3NO_2 are from the assignment of E. B. Wilson,

TABLE V. Frequencies of C_2H_6 calculated from C_2D_6 by ratio rule.

Frequency* class	C_2D_6	C_2H_6 calc. from CH_3Br	C_2H_6 calc. from CH_3Cl	C_2H_6 exp.
A_1 $\nu(\pi)$, $2^2\delta(\sigma)$	2083	2852	2851	2899
	2147	2965	2946	2955
$\delta(\pi)$	1158	1531	1525	1491 (R) 1538 IR[1]
$\nu(\pi)$	852	901	897	993 (R)
$\bar{A}_2$ $\nu(\pi)$, $2^2\delta(\sigma)$	2088	2859	2858	2896
	2112	2917	2946	2955
$\delta(\pi)$	~1072	~1417	~1412	1380 1380 1414
E $^2\nu(\sigma)$	2237	2985	2980	2980
$^2\delta(\sigma)$	~1102	~1517	~1521	1480
$^2\tau(\sigma)$	601	802	791	820
$\bar{E}$ $^2\nu(\sigma)$	2225	2969	2964	2963
$^2\delta(\sigma)$	1055	1453	1456	1460
$^2\tau(\sigma)$	970	1295	1277	1282, 1216[2]

* ν, δ, τ corresponding frequencies in halides.
[1] Forbidden by selection rules.
[2] See reference 4.

TABLE VI. Frequencies of CD_3F and CD_3I calculated by ratio rule. Values for CH_3F and CH_3I from W. H. Bennett and C. F. Meyer, Phys. Rev. **32**, 888 (1928); E. F. Barker and E. K. Plyler, J. Chem. Phys. **3**, 367 (1935). CD_3F and CD_3I values, average values from CD_3Br and CD_3Cl calculation.

Frequency	CH_3F	Calc.: CD_3F	CH_3I	Calc.: CD_3I
$\nu(\pi)$, $2^2\delta(\sigma)$	2861	2091	2860	2089
	2965	2154	2971	2158
$^2\nu(\sigma)$	2987	2240	3074	2306
$\delta(\pi)$	~1460	~1107	1252	949
$^2\delta(\sigma)$	~1476	~1072	1445	1049
$\nu(\pi)$	1048	995	532	505
$^2\tau(\sigma)$	1200	906	885	668

TABLE VII. Frequencies of D_2S and D_2Se calculated by ratio rule.

Frequency class	H_2O	D_2O	H_2S	D_2S calc.	D_2S obs.	H_2Se	D_2Se from $\frac{D_2O}{H_2O}$	D_2Se obs.	D_2Se from $\frac{D_2S}{H_2S}$
B_1 ν	3654	2666	2611	1905	1892	2260	1649	1630	1638
A_1 ν	3756	2784	2685*	1990	2000*	2350	1740	1696	1750*
			2632*	1950	1940*				1732*
δ	1595	1179	1290*	954	934*	1074	794	745	778*
			1236*	913	898*				780*

* The two values for A_1 ν, δ of H_2S and D_2S originate from two different papers. References see T. Y. Wu (9).

[3] A. Borden and E. F. Barker, J. Chem. Phys. **6**, 553 (1938); E. F. Barker and G. Bosschieter, J. Chem. Phys. **6**, 563 (1938); H. D. Noether, J. Chem. Phys. **10**, 693 (1942).

[4] The H−C−H angle bending in A_1 is usually reported somewhere around 1480 cm^{-1}. In a recent paper Avery and Ellis, J. Chem. Phys. **10**, 10 (1942), detect a band at 1538 in the infra-red which is not assigned. It could be connected with the H−C−H bending in A_1, but this is not certain since A_1 bands are forbidden in the infra-red by selection

TABLE VIII. Comparison of frequency and corresponding diagonal G-matrix coefficient ratios for isotopic methyl compounds.

Frequency class	$\left(\frac{G_{ii}\,CH_3Cl}{G_{ii}\,CD_3Cl}\right)^{\frac{1}{2}}$	$\frac{\nu_{CH_3Cl}}{\nu_{CD_3Cl}}$	$\left(\frac{G_{ii}\,CH_3Br}{G_{ii}\,CD_3Br}\right)^{\frac{1}{2}}$	$\frac{\nu_{CH_3Br}}{\nu_{CD_3Br}}$	$\left(\frac{G_{ii}\,CH_3OH}{G_{ii}\,CD_3OH}\right)^{\frac{1}{2}}$	$\frac{\nu_{CH_3OH}}{\nu_{CD_3OH}}$
A_1 $\nu(\pi)$, $2^2\delta(\sigma)$	1.39	1.37 1.37	1.39	1.37 1.38	1.39	1 36
$\delta(\pi)$	1.30	1.32	1.30	1.32	1.30	1.30
$\nu(\pi)$	1.06*	1.05	1.08*	1.06	1.047*	1.044
E $^2\nu(\sigma)$	1.34	1.33	1.34	1.33	1.34	1.33
$^2\delta(\sigma)$	1.35	1.38	1.35	1.38	1.35	~1.38
$^2\tau(\sigma)$	1.33	1.32	1.34	1.33	1.30	?

* The diagonal element for this frequency is $(\mu_x+\mu_c)$ where for μ_c the reciprocal of the mass of CH_3 and CD_3, respectively, has been used proving simultaneously that the methyl group vibrates as a unit in this motion.

Jr. and A. J. Wells.[5] The frequencies for CD_3NO_2 have been measured by T. P. Wilson.[6] The frequencies of C_2H_6 have been calculated from Stitt's[7] assignment for C_2D_6. The calculation allows one to fix the approximate range of some frequencies the assignment of which has still been doubtful.

Finally the frequencies of CD_3F and CD_3I are calculated by the rule (Table VI). There is already some experimental evidence for the correctness of the calculated CD_3F frequencies. In all the methyl halides $\delta(\pi)$ is lower than $^2\delta(\sigma)$, $\delta(\pi)$ increasing in frequency from CH_3I to CH_3F where it becomes nearly equal to $^2\delta(\sigma)$. In CD_3F $\delta(\pi)$ is calculated to be higher than $^2\delta(\sigma)$. This is substantiated by the corresponding frequencies in CD_3NO_2 where the polarized line is found at 1090 cm^{-1}, higher than the depolarized line at 1051 cm^{-1},[3] the polarization data determining their assignment. In CD_3OD and CD_3OH intensity considerations of the bands in the infra-red lead to the assignment $\delta(\pi)>{}^2\delta(\sigma)$. Also in C_2D_6 the symmetrical bendings are in both cases higher than the asymmetric ones. Calculations of the dependance of the frequencies of the CD_3X molecule on the mass of X using Linnett's[8] set of force constants and C–X distances show also qualitatively that $\delta(\sigma)$ becomes smaller than $\delta(\pi)$ in the CD_3X series, if the mass of X decreases below a definite value ($X\approx 25$ from experimental evidence).

Another series H_2O-D_2O, H_2S-D_2S, H_2Se-D_2Se[9] was also investigated. Here the agreement is not as good as in the case of the isotopic methyl compounds. But considering that the structure of the three pairs of molecules of the series is quite different the H_2O angle being ~105° while the H_2S and the H_2Se angles are found to be ~90°, the agreement is quite remarkable (Table VII).

There is no theoretical derivation of the rule at the present time. A comparison of the ratio of the G-matrix determinants[1] of the different methyl halides reveals the approximate constancy of these ratios. The square roots of the ratios of the diagonal terms of the G-matrix coefficients (in symmetry coordinates) are in good agreement with the experimentally observed ratios (Table VIII) of the frequencies, in spite of the fact that the calculation of frequencies from diagonal G- and F-matrix terms is usually rather crude and inaccurate.

rules. The C–C stretch is the only band which really differs from the calculated frequency. Since the calculation applies to isotopic pairs where the remaining masses stay unchanged, the calculation gives the C–C stretch for D_3C-CH_3. Assuming this C–C stretch approximately as $(C_2D_6+C_2H_6)/2=(852+993)/2=923$, we get much closer to the calculated value. The rocking in $\bar{E}$ at 1282 cm^{-1} is taken from Avery and Ellis, who assign this frequency to a combination tone. Stitt, reference 7, assigns 1170 cm^{-1} for the band. The agreement for the rocking frequency is usually the least accurate, but an error by ~100 cm^{-1} is far outside the limit; thus the band at 1216 or the low temperature band at 1282 can be suggested for this frequency if it is in agreement with heat capacity data.

[5] A. J. Wells and E. B. Wilson, Jr., J. Chem. Phys. **9**, 314 (1941).

[6] I am very grateful for the permission to use these data prior to publication.

[7] F. Stitt, J. Chem. Phys. **7**, 297 (1939).

[8] J. W. Linnett, J. Chem. Phys. **8**, 91 (1940).

[9] Ta-You Wu, *Vibrational Spectra and Polyatomic Molecules* (National University of Peking, Kun-Ming, China, 1939), p. 159 ff. Original references there.

THE AMERICAN INSTITUTE OF PHYSICS

INCORPORATED

ADMINISTRATIVE STAFF

HENRY A. BARTON, *Director*

MADELINE M. MITCHELL, *Publications Manager*

JOHN T. TATE, *Adviser on Publications*

Office: 175 Fifth Avenue, New York, New York

JOURNALS

THE PHYSICAL REVIEW
REVIEWS OF MODERN PHYSICS
JOHN T. TATE, *Editor (on leave)*
J. W. BUCHTA, *Acting Editor*

JOURNAL OF THE OPTICAL SOCIETY OF AMERICA
GEORGE R. HARRISON, *Editor*

THE JOURNAL OF THE ACOUSTICAL SOCIETY OF AMERICA
FLOYD A. FIRESTONE, *Editor*

AMERICAN JOURNAL OF PHYSICS
DUANE ROLLER, *Editor*

THE REVIEW OF SCIENTIFIC INSTRUMENTS
GAYLORD P. HARNWELL, *Editor*

THE JOURNAL OF CHEMICAL PHYSICS
JOSEPH E. MAYER, *Editor*

JOURNAL OF APPLIED PHYSICS
ELMER HUTCHISSON, *Editor*

GOVERNING BOARD

PAUL E. KLOPSTEG, *Chairman*
Central Scientific Company

GEORGE B. PEGRAM, *Secretary*
Columbia University

For the American Physical Society:

L. A. DUBRIDGE
University of Rochester

GEORGE B. PEGRAM
Columbia University

JOHN T. TATE
University of Minnesota

For the Optical Society:

R. C. GIBBS
Cornell University

A. C. HARDY
Massachusetts Institute of Technology

K. S. GIBSON
National Bureau of Standards

For the Acoustical Society of America:

FLOYD A. FIRESTONE
University of Michigan

HARVEY FLETCHER
Bell Telephone Laboratories

WALLACE WATERFALL
The Celotex Corporation

For the Society of Rheology:

R. B. DOW
Aberdeen Proving Ground

HERMANN MARK
Brooklyn Polytechnic Institute

N. W. TAYLOR
The Pennsylvania State College

For the American Association of Physics Teachers:

GEORGE R. HARRISON
Massachusetts Institute of Technology

PAUL E. KLOPSTEG
Central Scientific Company

A. G. WORTHING
University of Pittsburgh

The American Institute of Physics is a membership corporation of which five societies are the founding members. These five societies are the principal national societies devoted to pure and applied physics in America. Their names, and those of their representatives who form the Governing Board of the Institute, are given above. The principal work of the Institute is the publication of journals sponsored by the societies or by itself. The names and the editors of the journals are also listed above.

The broad purpose of the Institute is to represent, in all matters of wide or common interest, the five thousand or more members and subscribers associated with the Founder Societies and the journals. It aims to advance the science and profession of physics, and to promote cooperation between pure research, the applied sciences and the industries. To achieve these aims, it is greatly in need of an endowment and is empowered by law to administer grants and funds of any kind.

CONTENTS

THE JOURNAL OF CHEMICAL PHYSICS VOL. 11, No. 2 FEBRUARY, 1943

Theory of Molecular Size Distribution and Gel Formation in Branched-Chain Polymers . . . . . WALTER H. STOCKMAYER 45

Direct Experimental Determination of the Electron Affinity of Chlorine . . . . . KENNETH JAMES MCCALLUM AND JOSEPH E. MAYER 56

Relation between ζ-Potential and the Electrical Capacity of the Double Layer . . . . . W. G. EVERSOLE AND CHARLES R. ESTHER 63

Statistical Lengths of Rubber-Like Hydrocarbon Molecules . . . . . FREDERICK T. WALL 67

Variation in the Structure of Water in Ionic Solutions. II . . . . . G. W. STEWART 72

Stability and Structure of Burner Flames . . . . BERNARD LEWIS AND GUENTHER VON ELBE 75

Ratio Rule . . . . . HERMANN D. NORTHER 97

LANCASTER PRESS, INC., LANCASTER, PA.